GEORGIA INSTITUTE OF TECHNOLOGY
OFFICE OF RESEARCH ADMINISTRATION

RESEARCH PROJECT INITIATION

Date: ~~September 19, 1975~~

Project Title: NCSL Omnibus R&D Program

Project No: E-21-A00

Principal Investigator: Dr. D. T. Paris

Sponsor: Naval Coastal Systems Laboratory; Panama City, Florida

Agreement Period: From ~~6/11/75~~ Until ~~6/10/76~~

Type Agreement: Contract No. N61339-75-C-0122

Amount: $300,000 Note: Research to be conducted under tasks issued by NCSL, Sub-projects (i.e. A01, A02, etc.) will be initiated via Budget Forms.

Reports Required:

As requested

E-19-A02 is a Sub-project of this

Sponsor Contact Person (s):

Technical Matters

Mr. Al Simmons
Code 712
Naval Coastal Systems Laboratory
Panama City, FL 32401

Administrative Matters thru GTRI

Mr. R. J. Whitcomb
ONR RR

Assigned to: Electrical Engineering

COPIES TO:

Principal Investigator	Library ✓
School Director	Rich Electronic Computer Center
Dean of the College	Photographic Laboratory
Director, Research Administration	Project File
Director, Financial Affairs (2)	
Security-Reports-Property Office	
Patent Coordinator	Other _____

RA-3 (6-71)

E-19-A02

GEORGIA INSTITUTE OF TECHNOLOGY
ATLANTA, GEORGIA 30332

SCHOOL OF
CHEMICAL ENGINEERING

September 29, 1976

Naval Coastal Systems Laboratory
Attn: Mr. Max Weber
Minesweeping Division - Code 721
Panama City, Florida 32401

Subject: Monthly Letter Report No. 2, Task HR-18 and NCSL Omnibus R&D Program Contact N61339-75-C-0122, "A High Current Minesweeping Electrode Investigation" covering the period 20 Aug 1976 to 24 Sept 1976

Gentlemen:

Further, more comprehensive tests, have been conducted, primarily on the carbon filled polyethylene cable jacket. One of the problems in initial studies was contact resistance and various methods have been used to reduce the resistance between the jacket and the core. In addition electrochemical tests in actual and simulated sea water were conducted. The following information provides a summary of the studies to date:

1. Electrical Property Measurements

Resistivity measurements were made on a 2.0" x 2.0" x 0.069" thick piece of jacket material clamped tightly between two flat base copper electrodes. Measured voltages between the electrodes were in the range 0.155 - 1.04 volts as currents in the range 0.5 to 3.0 amperes were impressed. The resulting values of resistivity were in the range 45.8 to 51.2 ohm-cm. The average value of resistivity of the jacket material is thus 49.1 ohm-cm. The 3.0 ampere current corresponds to a current density of 0.11623 amps/cm^2.

Measurements were also made using a 3.0" long coaxial electrode cell composed of inner and outer electrodes of aluminum separated by 3.5% NaCl solution (r_i = 0.5", r_o = 0.57"). Currents in the range 0.5 - 3.0 amperes were impressed, yielding an apparent (linear resistance of 0.21 ohm with a constant overpotential of 0.8 volt. The 60.8049 cm^2 surface area of the inner electrode and the 3.0 ampere current results in a current density of 0.04934 A/cm^2.

Further tests were also made using the same coaxial electrode cell but with the conducting jacket material covering a smaller diameter aluminum electrode (radius of jacket material = 0.525"). Currents in the range 0.5 - 3.0 amperes were impressed. After stabilizing, the cell exhibited an apparent resistance of 1.80 ohms at an overpotential of 5.8 volts. The surface current density on the jacket material was 0.047 A/cm^2 at 3.0 amperes impressed current. No agitation or circulation of the NaCl (~600 ml) was employed, and the cell became noticeably warm. Efforts are underway to perform this test with flowing NaCl solution.

2. Polarization Tests

Measurements of anodic and cathodic current densities were made in slowly stirred 3.5% sodium chloride, and preliminary tests of electrode performance in sea water flowing at velocities of up to 30 knots. The test program also includes microscopic examination of the samples following the exposures.

Samples of the jacket of the size 1 cm^2 were attached to copper holders using Engelhard flexible silver coating #3 or Emerson & Cuming Eccobond solder 66C. The contact resistance was found to be about 100 ohms for Eccobond 66C when allowed to harden without pressure, and about 2 ohms for Eccobond 66C hardened under pressure and for the Engelhard coating. Samples with the 2 ohm resistance were used in all but the initial tests.

Samples have been tested by passing current between the sample and a platinum electrode in a polarization cell containing slowly stirred, aerated 3.5% sodium chloride solution at room temperature. The current was limited to a maximum of 50 mA. The maximum available source voltage was 34 volts. The voltage drop in the solution was found to be about 1 volt at maxiumum current. Summary of results:

In anodic polarization tests the current density was 50 mA/cm^2 at the beginning of the test; the source voltage increased slowly and reached the maximum available (34 V) in about 45 minutes. Because of the limited voltage the current density then slowly decreased with time. Some deterioration of the sample surface was observed after 24 hours of performance.

Tests of the behavior of the samples as cathodes are in progress.

A system for testing under controlled flow velocity has been constructed for laboratory tests of samples of electrodes in sea water. The system consists of a variable flow pump, a flowmeter, a flow-through cell with the samples, and connecting tubing, fittings and valves. The maximum flow velocity is 30 knots at 20 GPM. The samples tested at this time are in the form of a short length of the cable jacket attached to a copper tube. The copper tube not covered with the sample is insulated by an acrylic tubing. The surface area of the sample is 20 cm^2.

In the initial tests two samples have been placed in-line (separation about 0.8 in.), and current was passed between them; thus, the two samples performed one as an anode and the other as a cathode. The current and voltage were monitored as a function of time and flow velocity. Only preliminary data is available at this time. Results will be reported next month when significant information is available.

Respectfully submitted,

Robert F. Hochman
Project Co-director

E-19A02

A LABORATORY TESTING AND ELECTRO-MAGNETIC ANALYSIS PROGRAM FOR CARBON POLYMER JACKETED AND PLATINUM PLATED ELECTRODES

By

R. F. Hochman, M. Marek, J. G. Rinker, and K. J. Bundy
Metallurgy Department, School of Chemical Engineering

And

E. B. Joy, G. K. Huddleston, and W. M. Leach
School of Electrical Engineering

GEORGIA INSTITUTE OF TECHNOLOGY
Atlanta, Georgia

FINAL RESEARCH REPORT
TASK HR-18
CONTRACT N61339-75-C-0122
20 July 1976 – 31 January 1977

1977

Prepared for

NAVAL COASTAL SYSTEMS LABORATORY
MINESWEEPING DIVISION
PANAMA CITY, FLORIDA 32401

A LABORATORY TESTING AND ELECTROMAGNETIC ANALYSIS PROGRAM FOR CARBON POLYMER JACKETED AND PLATINUM PLATED ELECTRODES

By

R. F. Hochman, M. Marek, J. G. Rinker, and K. J. Bundy
Metallurgy Department
School of Chemical Engineering

And

E. B. Joy, G. K. Huddleston, and W. M. Leach
School of Electrical Engineering

Georgia Institute of Technology
Atlanta, Georgia 30332

January 1977

FOREWORD

This final report was prepared by the Metallurgy Department of the School of Chemical Engineering, and the School of Electrical Engineering, Georgia Institute of Technology, Atlanta, Georgia 30332 in fulfillment of the requirements of Task HR-18 under NCSL Omnibus R & D Program Contract N61339-75-C-0122 for the Naval Coastal Systems Laboratory, Panama City, Florida.

The period of performance covered by Task HR-18 and this report is 20 July 1976 to 31 January 1977.

Report authors are R. F. Hochman, M. Marek, J. G. Rinker, and K. J. Bundy from the Metallurgy Department of the School of Chemical Engineering and E. B. Joy, G. K. Huddleston, and W. M. Leach from the School of Electrical Engineering.

The authors acknowledge the assistance and expert guidance of Mr. Miller Epps and Mr. Max Weber of the Naval Coastal Systems Laboratory in providing operational and historical insight concerning the minesweeping problem and for their direction and concern.

The views and conclusions contained in this document are those of the authors and should not be interpreted as necessarily representing the official policies, either expressed or implied, of the Naval Coastal Systems Laboratory or the U.S. Government.

TABLE OF CONTENTS

TITLE PAGE i

FOREWORD ii

Chapter

I. BACKGROUND 1

II. TEST PROGRAM 3

A. Introduction 3
B. Resistivity Measurements 4
C. Potentiostatic and Galvanostatic Polarization Measurements 8
D. Static Measurements in a Small Coaxial Cell. 13
E. Testing Flowing in Sea Water 16
F. Microscopic Examination 25
G. Miscellaneous Coaxial Cell Tests 28
H. Discussion 33

III. PRELIMINARY DESIGN OF NOBLE METAL ELECTRODE. 36

A. General Design Features 36
B. Temperature Distribution 40
C. Stiffness Considerations 41
D. Cost Estimate and Life Expectancy. 45

IV. ELECTROMAGNETOSTATIC ANALYSIS 46

A. Electrode Current Calculation. 46
B. Voltage Produced by Horizontal Lines of Current 54
C. Solution for N Conductors 61
D. Interconnection of Conductors 65
E. Longitudinal Impedance 71
F. Electrical Model for Cable 75
G. Solution for Unknown Radial and Load Currents 78
H. Two Electrode Solution 80
I. Preliminary Results 85

V. MAGNETIC FIELD CALCULATIONS 88

A. Introduction 88
B. The Magnetic Field Due to the Current in the Water 88
C. The Magnetic Field Due to the Current in the Electrodes 97
D. The Magnetic Field Due to the Current in the S-Cable 98
E. Numerical Results 100
F. The Three-Dimensional Field 109

TABLE OF CONTENTS (concluded)

Chapter

VI. CONCLUSIONS AND RECOMMENDATIONS 118

A. Conclusions 118
B. Recommendations 121

APPENDIX I 123

APPENDIX II 128

CHAPTER I

BACKGROUND

The initial investigation on this program, "A High Current, Minesweeping Electrode Investigation," carried out at Georgia Tech, proposed two major alternatives for replacing the existing high current aluminum minesweeping electrodes. The first alternative was a cross linked carbon-impregnated polyethylene jacket electrode, and the second, was a platinum-plated (platinized) niobium electrode with a configuration to be designed. Basically, the first program indicated the design contents were feasible and raised hopes that long life, low drag, and a cost effective high current electrode would be possible.

The purpose of this program was to initiate a test phase to evaluate the basic characteristics of the carbon impregnated polymer-conductive materials and platinized niobium. These materials showed the best properties for operating with the current densities and potentials desired. Studies in this program include basic electrochemical electrode evaluations as well as studies in flowing sea water, simulating speeds up to 30 knots. In addition, continuing programs in the evaluation of the electromagnetic characteristics of the general electrode system (in sea water) and the magnetic field calculations of these electrical systems in sea water were continued to provide a more definite precise evaluation of the characteristics of the system.

This report will provide an in-depth summary of the test program to date as well as conclusions and recommendations regarding the continuation and completion of the test phase of the program. In addition, the fundamental characteristics of the noble metal system design, including thermal and

mechanical characteristics, will be provided as well as in initial mockup of the general configurations proposed for the noble-metal electrodes to be evaluated.

Extended studies in electro-magnetic field evaluations for the mine-sweeping configurations are extended further. General conclusions and recommendations on the present data and electrode design configurations for the high current minesweeping electrodes will be discussed.

Chapter II

TEST PROGRAM

A. Introduction

The test program was designed to evaluate the most promising electrode materials in a variety of laboratory tests. Resistivity measurements (Section B) were performed on samples of the carbon-impregnated polyethylene jacket to obtain data required in the mathematical analysis of the system. Initial galvanostatic tests of the electrode materials (Section C) were performed on small samples in a standard laboratory cell using a simple salt solution; they provided basic information on the electrode behavior of the materials under static conditions. Other static electrode tests (Section D) were performed on samples of the carbon-impregnated polyethylene jacket using a coaxial electrode cell to obtain data on resistances in such cells. Tests in flowing sea water (Section E) provided the most important data on the performance of the various materials under conditions simulating the field conditions. Following the sea water tests, the polyethylene samples were examined in a scanning electron microscope (Section F) to evaluate the extent of deterioration. Tests of several combinations of materials (Section G) were performed to explore the possibility of modifying the basic materials to improve their performance.

B. Resistivity Measurements

Test Conditions: A 2.0"x2.0"x0.06875" (avg.) thick piece of jacket material was placed between two flat, bare copper electrodes and clamped tightly as shown in Figure 1. The copper electrodes and the sample were cleaned with soap and water and dried thoroughly just prior to measurement. The sample was clamped tightly to ensure good contact. Clamping pressure was applied until minimum electrical resistance was indicated; additional pressure would indicate an increased resistance due presumably to deformation. Copper electrodes were found by experiment to give the lowest contact resistance.

Results: The results are shown in Table I. The average value of resistivity of the jacket material is 49.1 ohm.cm. The range of values obtained was 45.8 to 51.2 ohm.cm.

The variability of results due to electrode contact resistance is illustrated in Figure 2. Note that aluminum does not appear to be a good choice of electrode due to the high contact resistance between it and the jacket material.

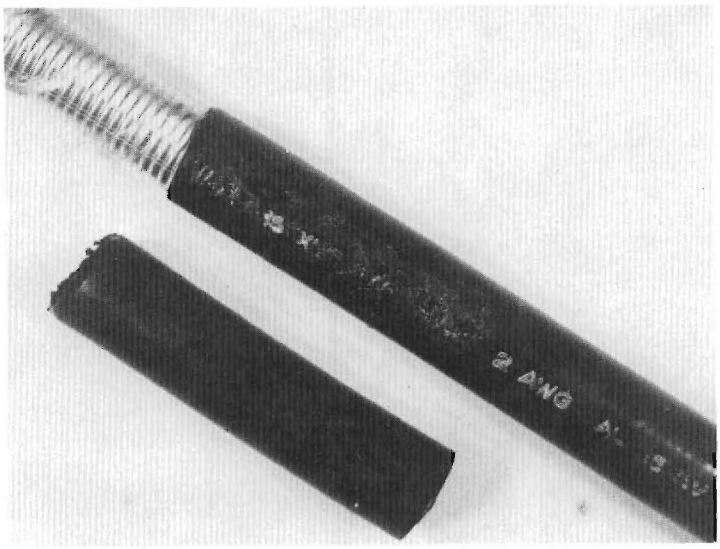

(a) Cable from which samples were taken.

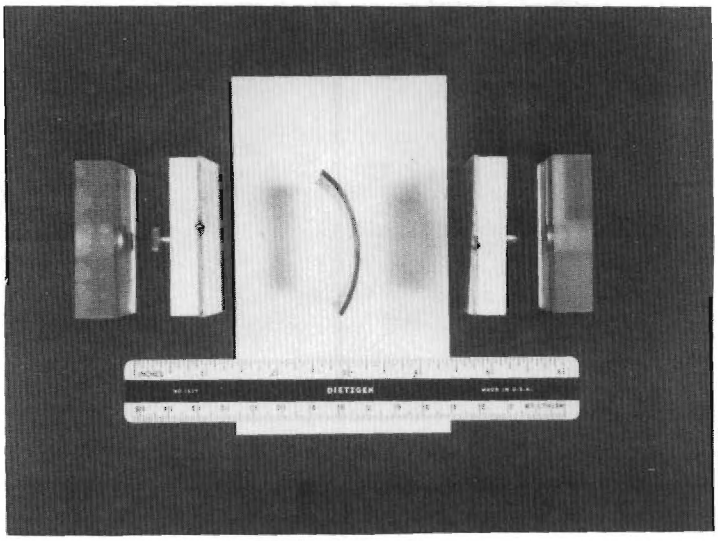

(b) Electrode arrangement (from left to right: plexiglas, aluminum, copper, sample, copper, aluminum, plexiglas.)

Figure 1. Conducting Plastic Jacket Material and Measurement Apparatus

TABLE I. MEASUREMENT RESULTS - RESISTIVITY OF JACKET MATERIAL[1]

Sample #2: 2.0" x 2.0" x 0.06875" thick

MEASURED CURRENT (A)	MEASURED VOLTAGE (V)	CALCULATED RESISTANCE (Ω)[2]	CALCULATED[3] RESISTIVITY (Ω.cm)
0.5	.164	.328	48.47
1.0	.335	.335	49.51
1.5	.500	.333	49.26
2.0	.680	.340	50.25
2.5	.860	.344	50.84
3.0[4]	1.04	.347	51.23
2.5	.845	.338	49.95
2.0	.660	.330	48.77
1.5	.490	.327	48.27
1.0	.320	.320	47.29
.50	.155	.310	45.81
			ρavg.=49.06

NOTES:

1. General Cable Co. samples provided by E. B. Joy with jacket markings "HS XLP MILS 2 AWG AL 15 KV 1975."

2. Calculated Resistance = (Measured V)/(Measured I) = R_Ω.

3. Resistivity calculated according to

$$\rho\Omega.cm = \frac{R_\Omega Area}{thickness} = 147.78\ R_\Omega$$

4. 3.0 amperes corresponds to 0.11623 amps/cm^2 current density.

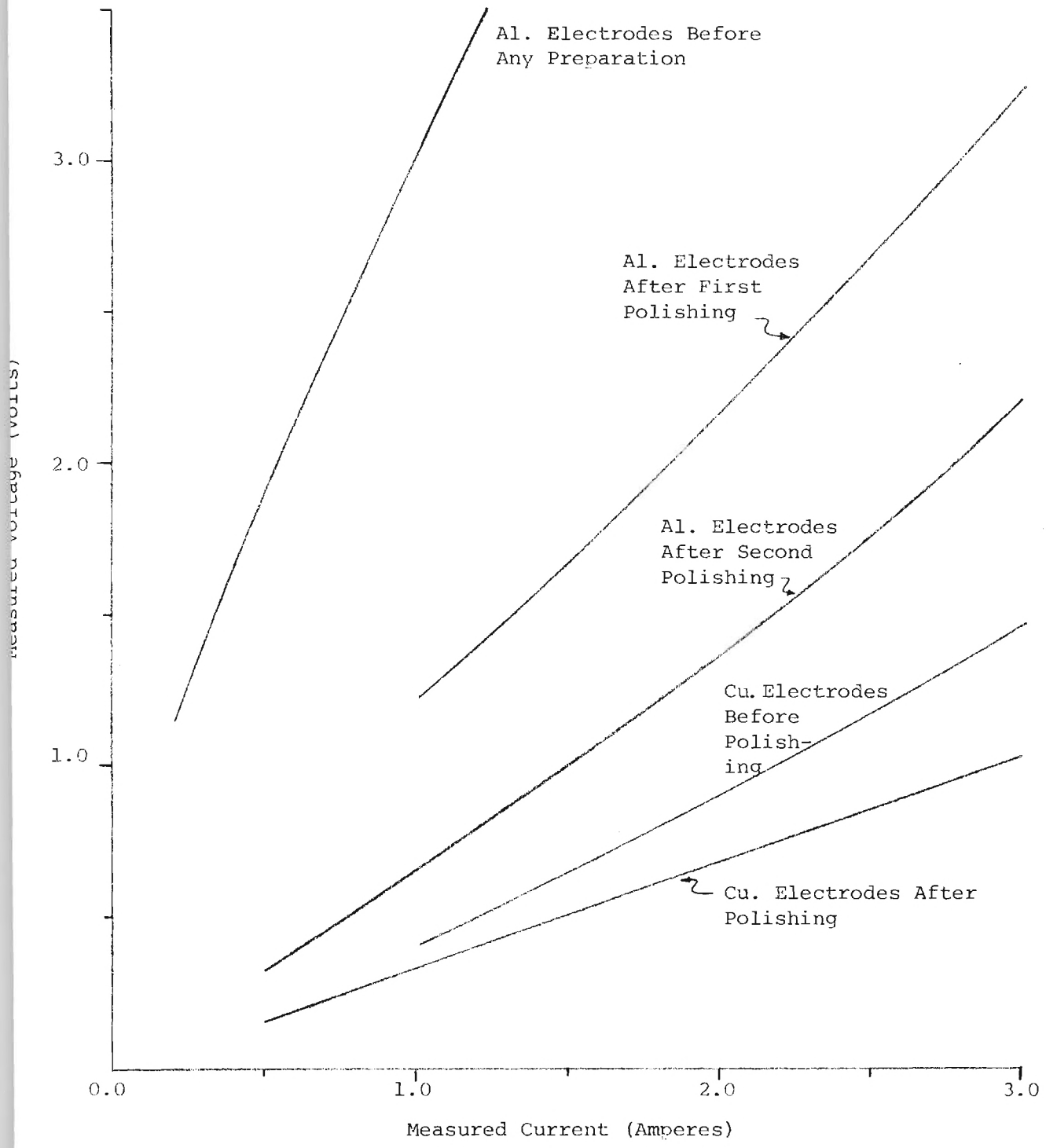

Figure 2 . Measured Results for Parallel Plate Electrodes Showing Variability of Results Due to Electrode Material and Surface Preparation.

C. Potentiostatic and Galvanostatic Polarization Measurements Test Conditions: Samples of the electrode materials were prepared with a surface area of 1.0 cm^2. The samples of the carbon-filled polyethylene were cut out of a cable jacket supplied by General Cable Company (cable markings "HS XLP MILS 2 AWG AL 15 KV 1975"); they were attached to copper supports using a silver-filled electrically conducting glue (Engelhard flexible coating #13). The samples of a noble metal electrode were short lengths of platinized niobium wire dia. 0.093", supplied by Engelhard Industries, Inc. (Part. No. 37975-4). For the test, the sample was placed in a 3-electrode polarization cell filled with about 500 ml of air-saturated, mildly stirred, 3.5% sodium chloride solution. Current was passed between the sample and an auxiliary platinum electrode. The potential difference across the boundary layer at the sample electrode was measured by means of a reference electrode probe placed close to the surface of the sample. The reference electrode was a standard commercial saturated calomel electrode.

In the potentiostatic tests, the samples were polarized from the natural potential to progressively higher overpotentials, anodic or cathodic; the potential scanning speed was 1.0 volt/hr. The test was terminated when the design current density was reached or exceeded, or when the maximum controlled potential was reached (±10 volts). The current density versus potential curve was continuously recorded on a X-Y recorder.

The polarization setup consisted of the Wenking Electronic Potentiostat Model 68TS3, Wenking Potential Meter Model PPT69, and Wenking Stepping Motor Model SMP69.

In the galvanostatic tests, the current was controlled; both current and the potential of the sample with respect to the reference electrode were continuously recorded as a function of time.

Results and Discussion: The potentiostatic polarization curves for both tested materials, i.e., the carbon-impregnated polyethylene and the platinized niobium, are presented in Figures 3 and 4. The result of the anodic galvanostatic test on the carbon-impregnated polyethylene is shown in Figure 5. The galvanostatic results for platinized niobium are not shown in graphical form because both current and potential remained constant during the 24-hour test; at the current density of 0.5 A/cm^2, the potential was 3.5 volts (SCE).

The potentiostatic and galvanostatic results for platinized niobium show the expected behavior, i.e., high efficiency as an electrode in both the anodic and cathodic regimes. Passivation is indicated on the anodic polarization curve, but it did not seriously affect the performance of the electrode. The overpotential remained low (3.5 volts) even for the high design current density (0.5 A/cm^2).

The potentiostatic polarization curves show that the tested type of carbon-impregnated polyethylene is a rather inefficient electrode material. At the potential limit of the potentiostat (±10 volts), the current density was only about 3.3 mA/cm^2 in the anodic regime and about 11.5 mA/cm^2 in the cathodic regime. The galvanostatic results (Figure 5) show that the full voltage of the potentiostat (34 volts) was reached in about 40 minutes to maintain the current density of 50 mA/cm^2. At longer times this voltage was insufficient to maintain the current density and the current decreased continuously with time. Exploratory measurements on the tested samples showed that the average resistivity increased by two to three orders of magnitude by the end of the anodic test.

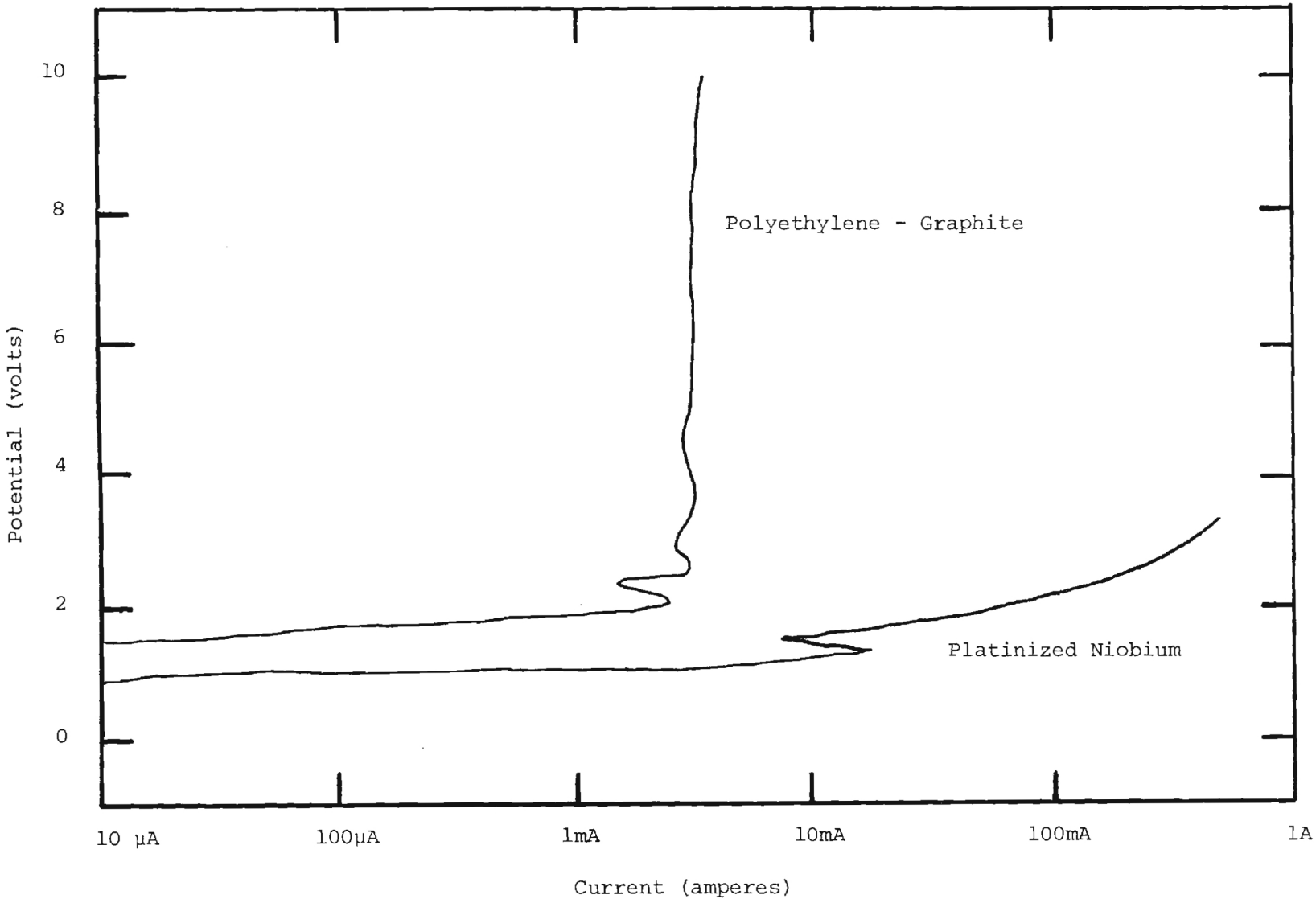

Figure 3. Anodic Polarization Curves.

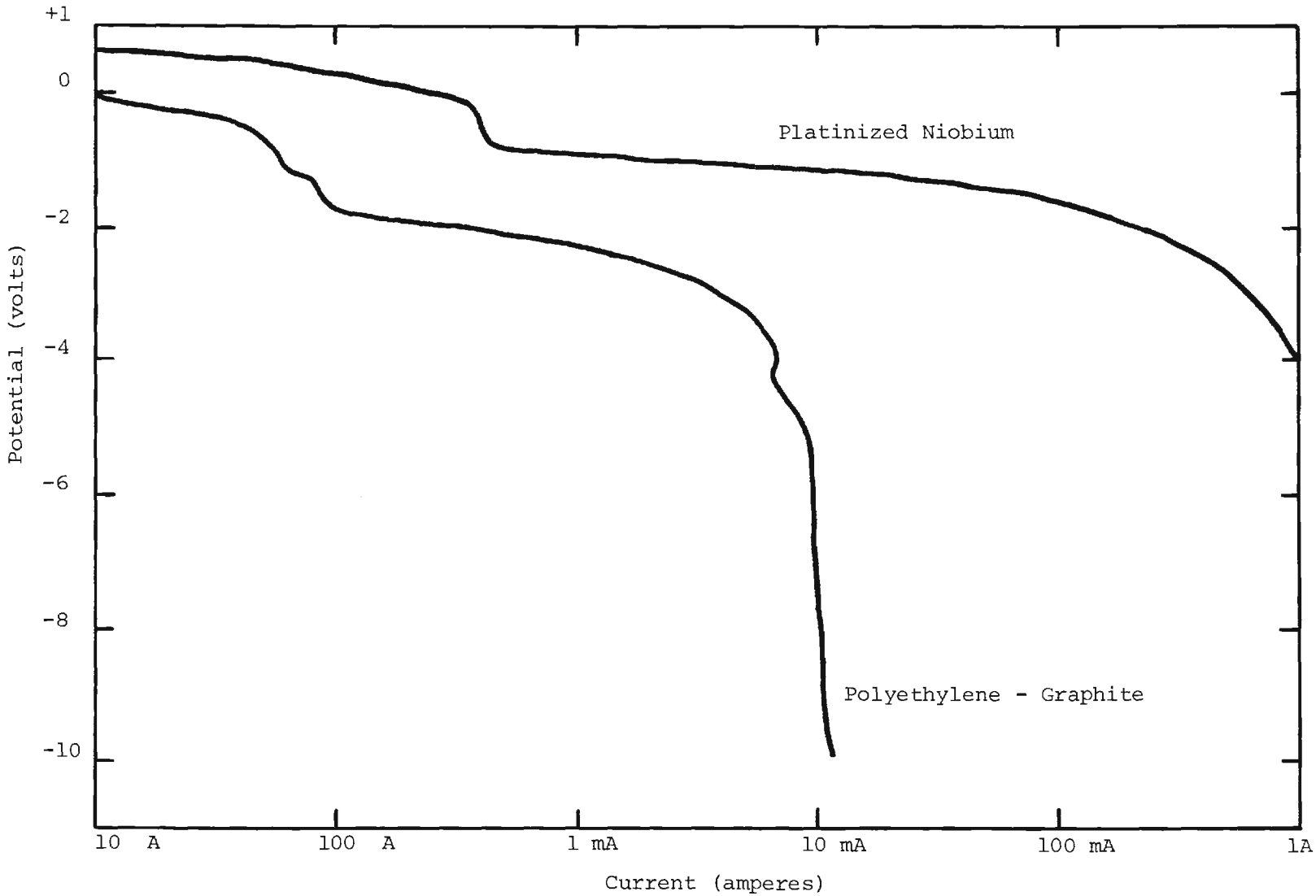

Figure 4. Cathodic Polarization Curves.

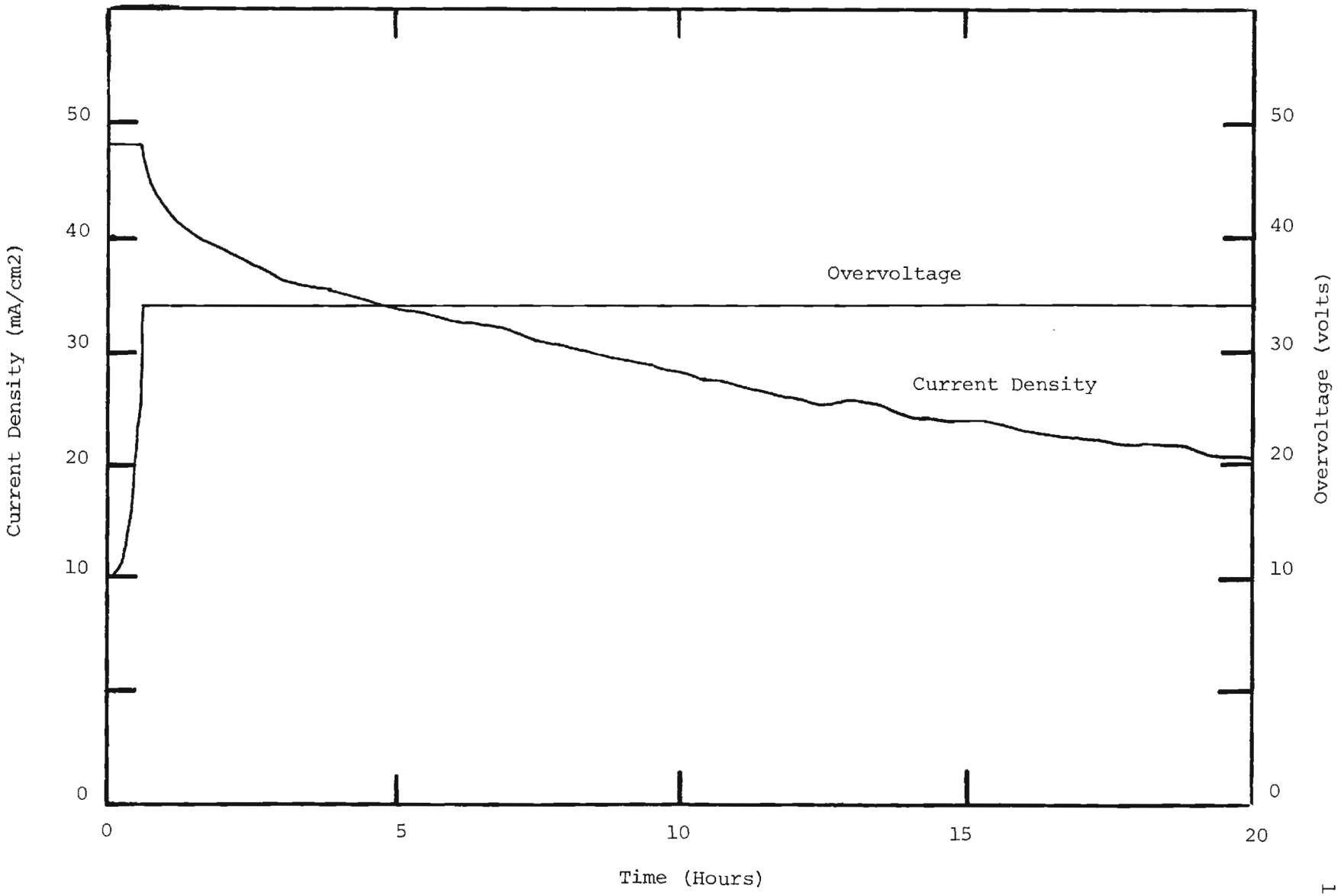

Figure 5. Results of Galvanostatic Polorization Measurements on the Carbon-Impregnated Polyethlene (supply voltage limit = 34V)

D. Static Measurements in a Small Coaxial Cell Test Conditions:

A coaxial cell was constructed for testing the jacket material in a configuration similar to that anticipated in the actual application. The outer electrode was made from 1.25" O.D. aluminum tube (1.14" I.D.). Two inner electrodes were constructed: (1) a 1.0" O.D. aluminum tube electrode; and (2) a jacketed electrode consisting of a length of conducting jacket material forced tightly over a length of 0.92" O.D. aluminum rod. The inner and outer electrodes were held in the coaxial configuration by plexiglas end caps. The space between the inner and outer electrodes was filled with simulated sea water (3.5% NaCl) for testing. The inner electrode was used as the anode. With the end caps in place, the length of electrode exposed to the brine was 3.0 inches. Approximately 10 cc of NaCl solution was used to fill the space between the coaxial electrodes. No stirring or other agitation was used during the tests. A significant amount of NaCl solution was "bubbled out" through the small filling hole during the tests. This loss was most significant for the jacketed electrode tests wherein the cell became too hot to handle.

Results: Figure 6 shows the results of measurements made using coaxial electrodes separated by simulated sea water (3.5% NaCl solution). The lower curve shows the results for aluminum anode and cathode; the apparent resistance is

$$R = \frac{1.42 - 0.9}{3.0 - 0.5} = 0.21\Omega$$

with a constant overpotential estimated to be 0.8 volts. The cell is 3.0" long, resulting in an anode surface area of 60.8 cm^2. The 3.0 ampere cell current thus corresponds to a current density of $0.049/Acm^2$. Fringing effects are assumed small to yield uniform electric field distributions.

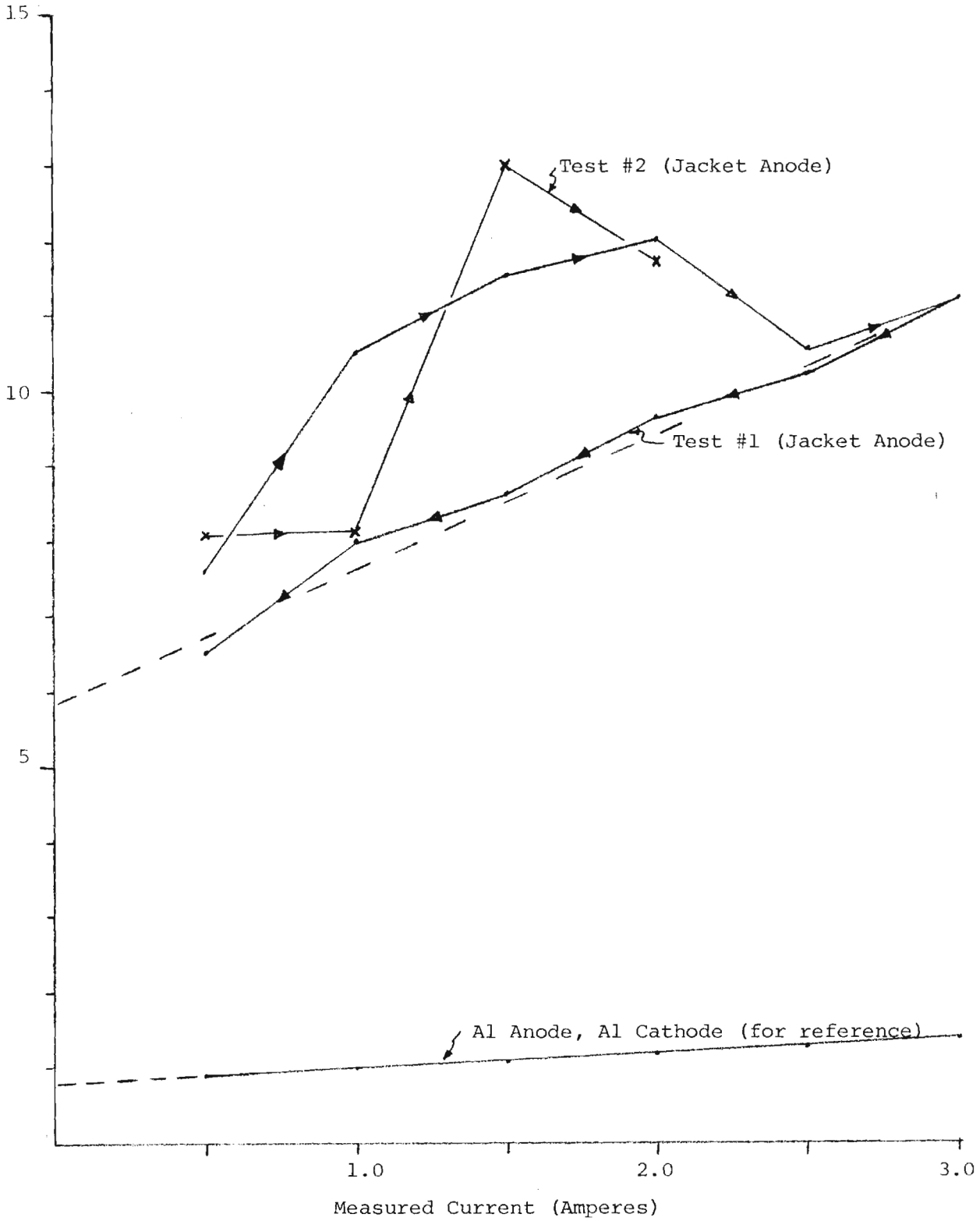

Figure 6 . Measured Results for Coaxial Electrodes and 3.5% NaCl (Non-circulating) Solution.

The upper curves of Figure 6 show the results when an inner aluminum anode is encased in the conducting plastic jacket ($\rho_{jacket} \simeq 50\ \Omega$ cm).

In Test #1, the apparent cell resistance appears to decrease at 2.5 amperes so that the minimum cell resistance is given by

$$R = \frac{11.2 - 5.8}{3.0} = 1.80\ \Omega$$

at an estimated overpotential of 5.8 volts. For the cell length of 3.0 inches, 3.0 amperes corresponds to a surface current density on the outer periphery of the jacket of 0.047 A/cm^2.

Test #2 was performed using the same arrangement as in Test #1. New NaCl solution was used. The curve in Figure 6 indicates that the behavior was approaching that of Test #1.

In Tests #1 and #2, the cell became very warm due to the electrical power dissipated.

E. Tests in Flowing Sea Water

Test Conditions: A special flow-through cell with coaxial electrodes was designed and made for the tests. The final design is shown in Figure 7a. In principle, a cylindrical sample was placed along the axis of the cell, and sea water was pumped at high speed through the annular passage between the sample and a concentric auxiliary electrode. For anodic test the auxiliary electrode was made of copper; for cathodic tests the copper electrode was lined with platinum foil.

The nominal O.D. of the samples was one inch and they were one inch long. For tests of the carbon-impregnated polyethylene the samples were made from jackets cut from cable samples supplied by the General Cable Company. The one-inch-long segment of the jacket was forced tightly over a copper rod, and insulating acrylic rods were attached on both ends. The samples of the platinized niobium were made by winding platinized niobium wire dia. 0.093" into grooves machined in a polyethylene rod 1.0" in diameter on a length of one inch. Both types of specimens are shown in Figure 7b. The electrode surface area of both types of samples was close to 20 cm^2.

Initially, the distance between the sample and the auxiliary electrode was about 0.04", and the sea water velocity at full pump capacity was about 50 ft/sec. The cell was then re-designed and the distance between the electrodes was increased to 0.125"; the test velocity was then about 16 ft/sec.

The final design of the testing setup is shown in Figure 8. The sea water was pumped by means of a centrifugal pump from a holding tank, through the cell, through a flowmeter, and back into the tank. A cooling coil was installed in the tank to keep the water temperature constant. The tests were run at approximately room temperature. The sea water was supplied by

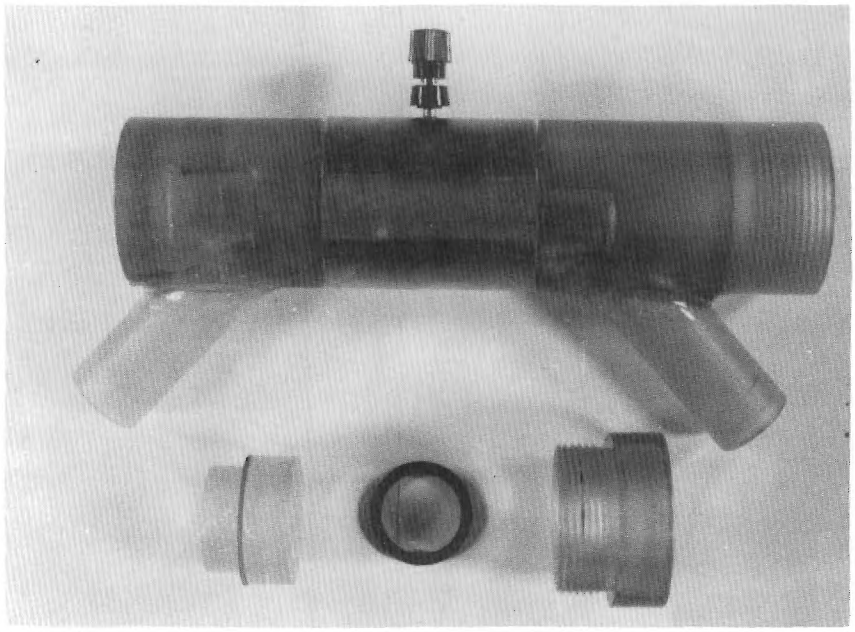

a

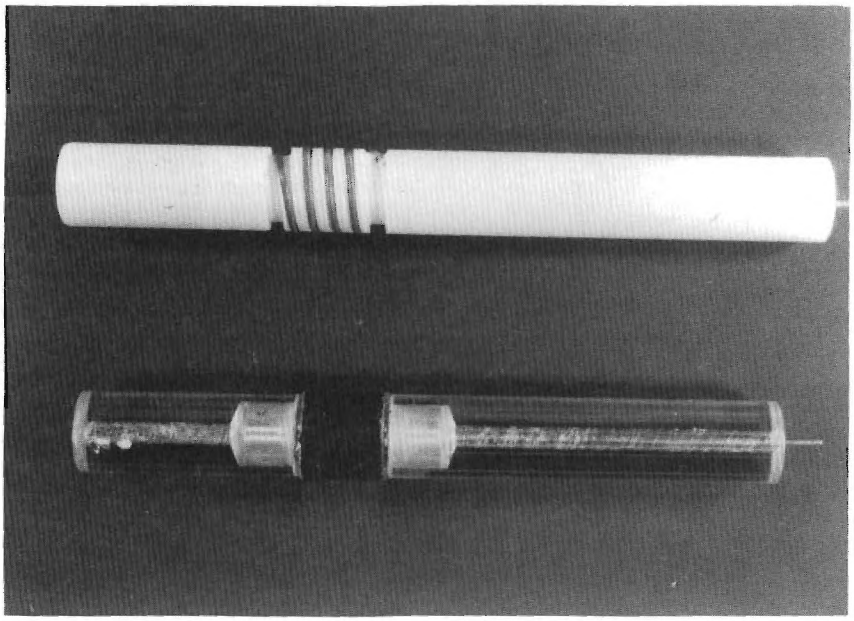

b

Figure 7. (a) Cell for Flowing Sea Water Tests, (b) Platinized Niobium and Conductive Polymer Samples.

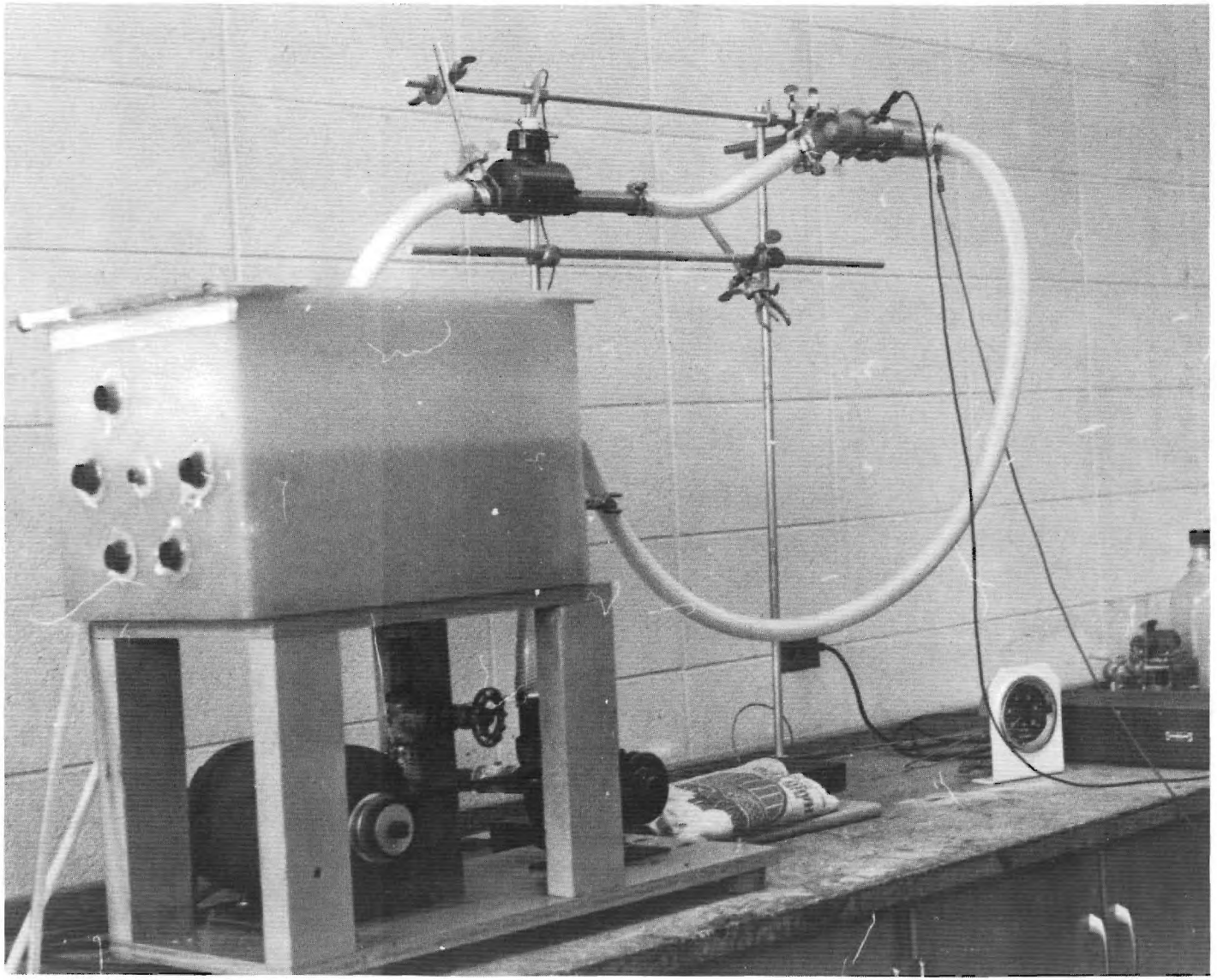

Figure 8. Apparatus for Flowing Sea Water Tests.

Naval Coastal Systems Laboratory. The current between the electrodes was kept constant by means of a regulated power supply, and the required voltage was recorded as a function of time on a strip-chart recorder. Table II summarizes the test conditions.

TABLE II

TEST CONDITIONS IN FLOWING SEA WATER TESTS

Sample	Water Velocity ft/sec	Current Density A/cm^2	Total Test Period hrs:min
Platinized Niobium	16.3	0.5	24:00
Carbon Impregnated PE jacket	15.8	0.072	2:00
"	16.0	0.036	5:10
" sample "A"	16.3	0.036	5:30
" sample "D"	16.0	0.036	2:00
" sample "H"	16.0	0.036	3:00

Results and Discussion

The results of the tests are presented in Figures 9 and 10, which show the cell voltage as a function of time at a constant cell current. The cell voltage is a sum of the overvoltages at the two electrodes and the voltage drop in the sea water. For the higher current density in tests of the platinized niobium, the overvoltage on the auziliary electrode and the voltage drop in the water had to be taken into account. Polarization tests with the copper electrode showed that the overvoltage at 0.5 A/cm^2 was about 3 volts, and the voltage drop in the sea water was calculated to be about 2.9 volts. Thus, for the measured cell voltage of 10.4 volts, the corrected overvoltage on the tested platinized niobium electrode was about 4.5 volts.

For the samples of carbon-impregnated polyethylene jacket, which were tested at a current density of 70 mA/cm^2 or lower, the overvoltage on the auxiliary electrode and the voltage drop in the water could be neglected, especially in view of the high measured overvoltages on the samples. Basically, all cable jacket samples exhibited similar anodic behavior: the overvoltage first increased rapidly to a moderate to high value, then decreased, and increased again. Samples examined after the second increase started, which was usually in less than 3 hours, invariably showed signs of deterioration. Continuation of the test resulted in further deterioration and high overvoltage, and eventual perforation of the jacket.

Both types of electrode materials were tested as cathodes in short exposures at about 18 ft/sec. The platinized niobium exhibited a steady overvoltage (corrected) of 2.4 volts at the end of a 3-hour exposure at 0.3

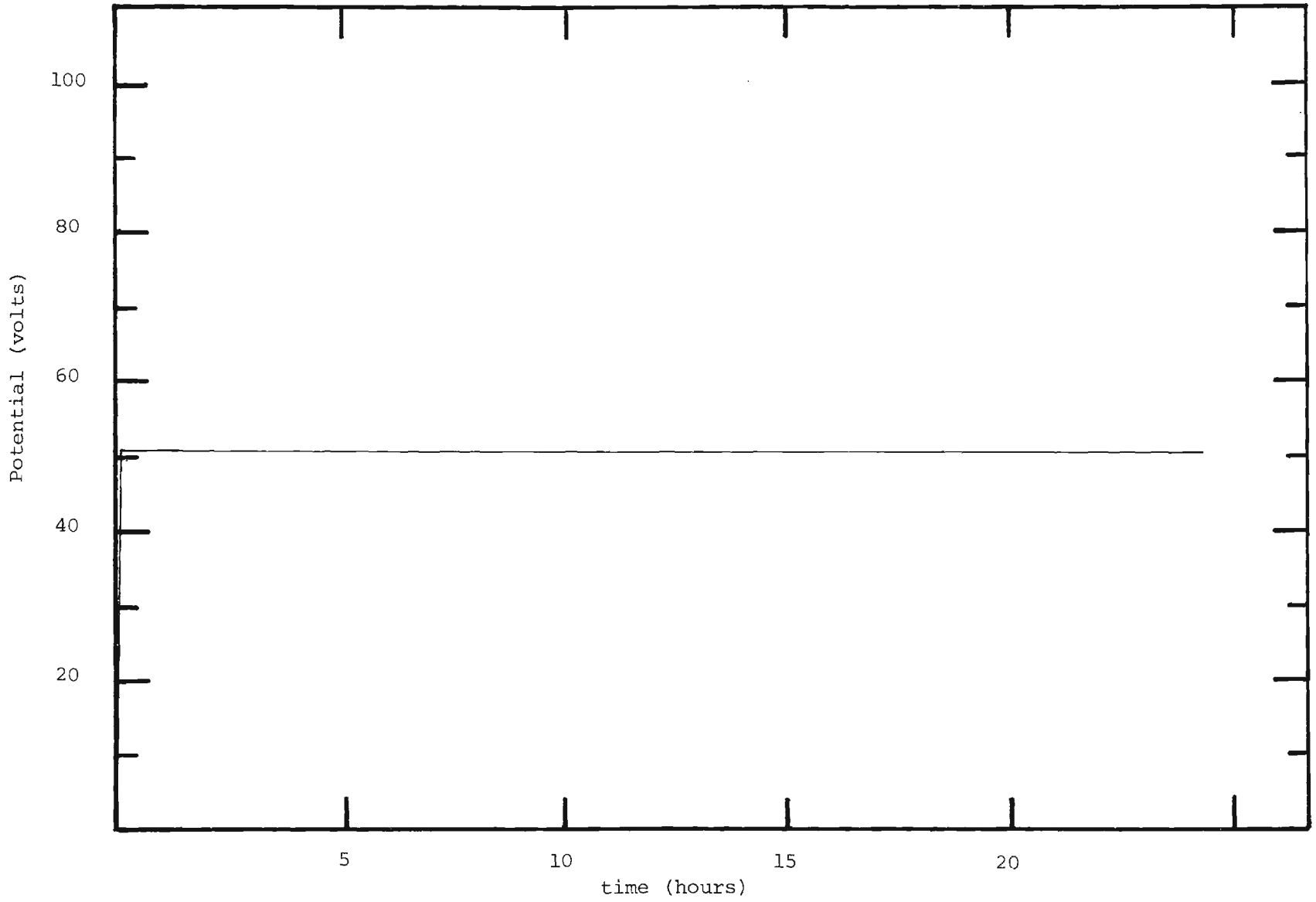

Figure 9. Flowing Sea Water Test of Platinized Niobium at 500 $^{ma}/cm^2$.

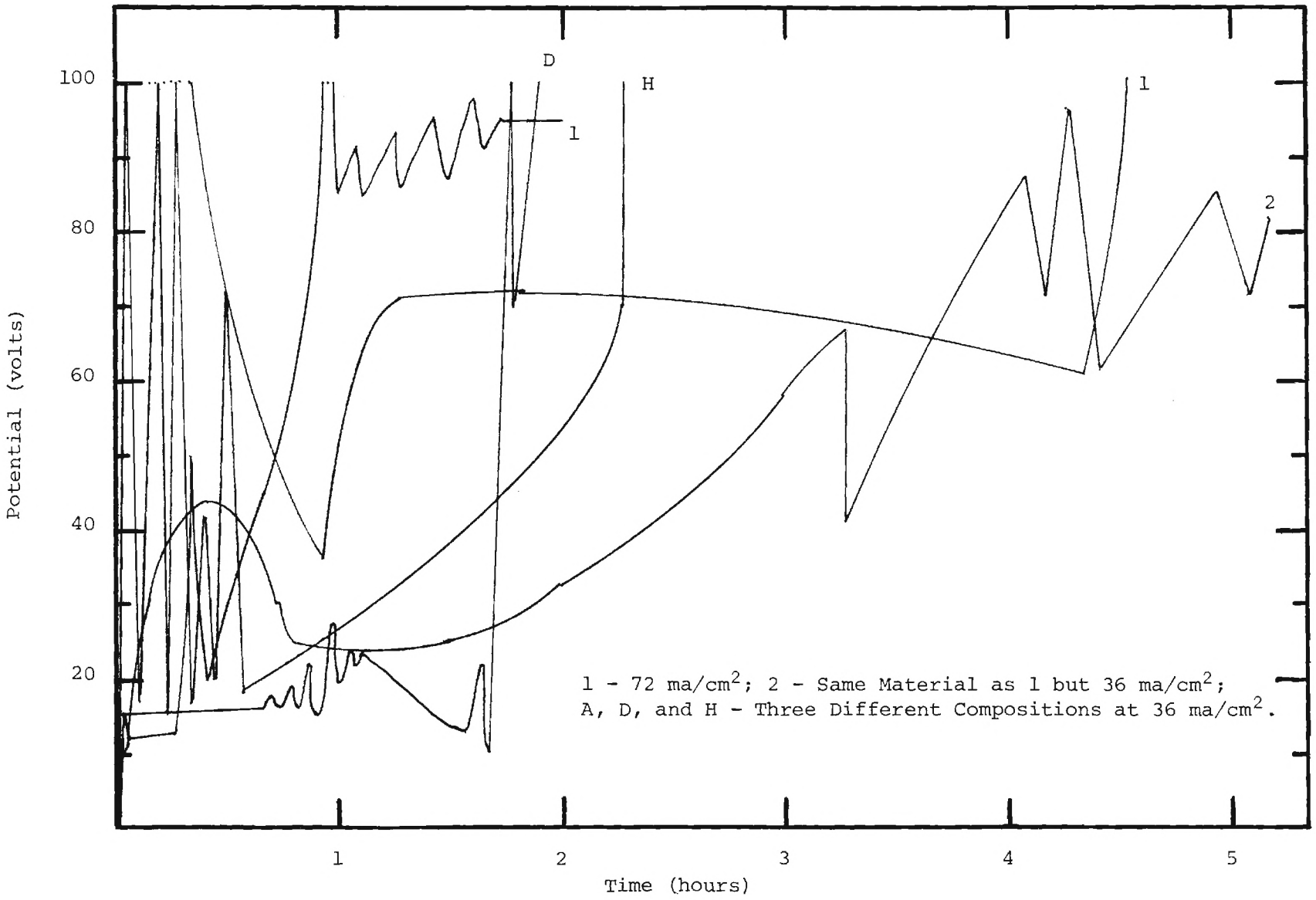

Figure 10. Flowing Sea Water Tests of Carbon Impregnated Polymer Samples.

A/cm^2. The carbon-impregnated polyethylene sample exhibited an overvoltage increasing from the initial value of 7.8 volts to a steady value of 9.4 volts at 50 mA/cm^2 after 2 hours.

F. Microscopic Examination

The samples of the carbon-impregnated polyethylene jacket were examined visually following each test. Several samples were also examined in a scanning electron microscope (SEM). Figure 11 shows low magnification SEM photographs of the surface following a galvanostatic test. The surface is blistered and cracks can be observed. High magnification photographs of the surface before and after the exposure (Figure 12) show some changes in the structure, but do not show enough detail to allow interpretation. No changes were observed on the platinized niobium electrodes after a 24-hour exposure at $0.5A/cm^2$.

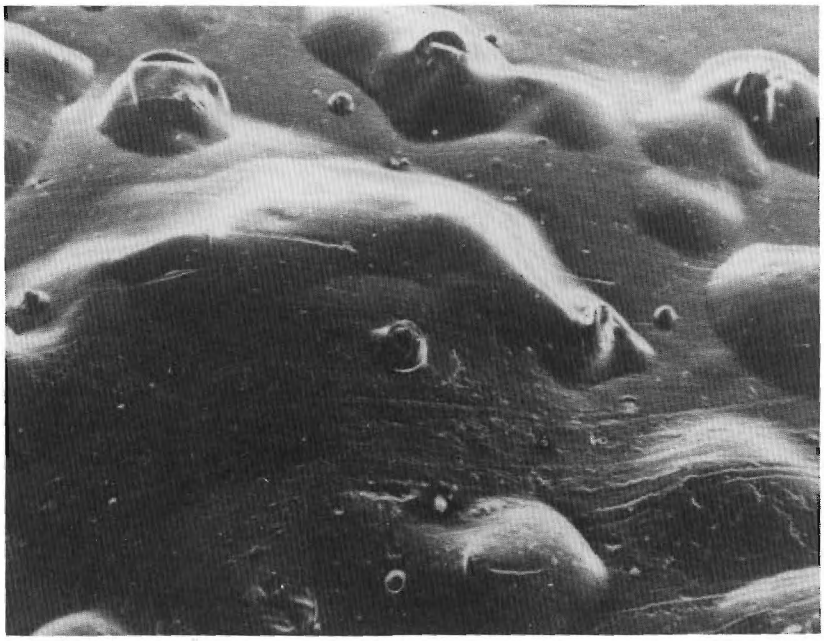

a

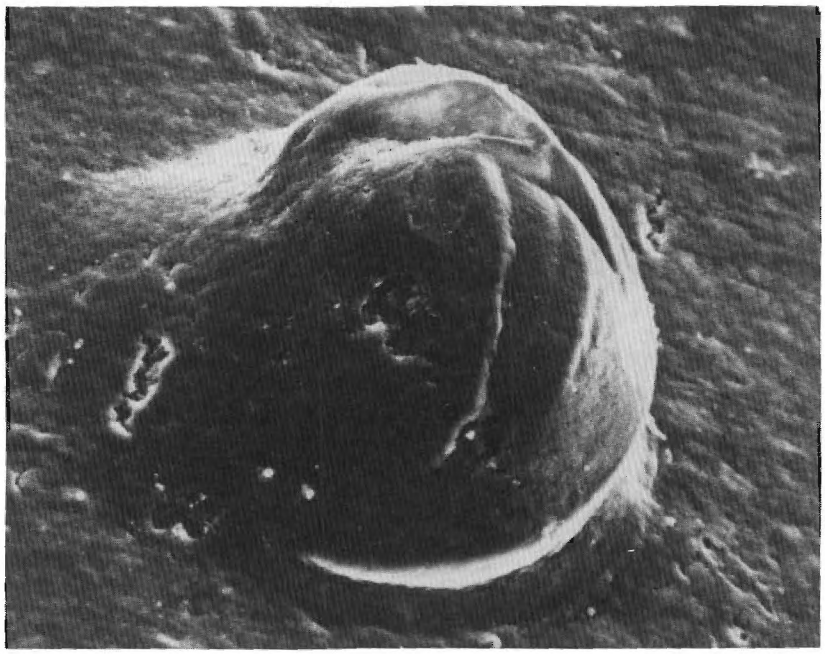

b

Figure 11. Scanning Electron Micrographs of of a Conductive Polymer Sample; (a) 30X, (b) 300X.

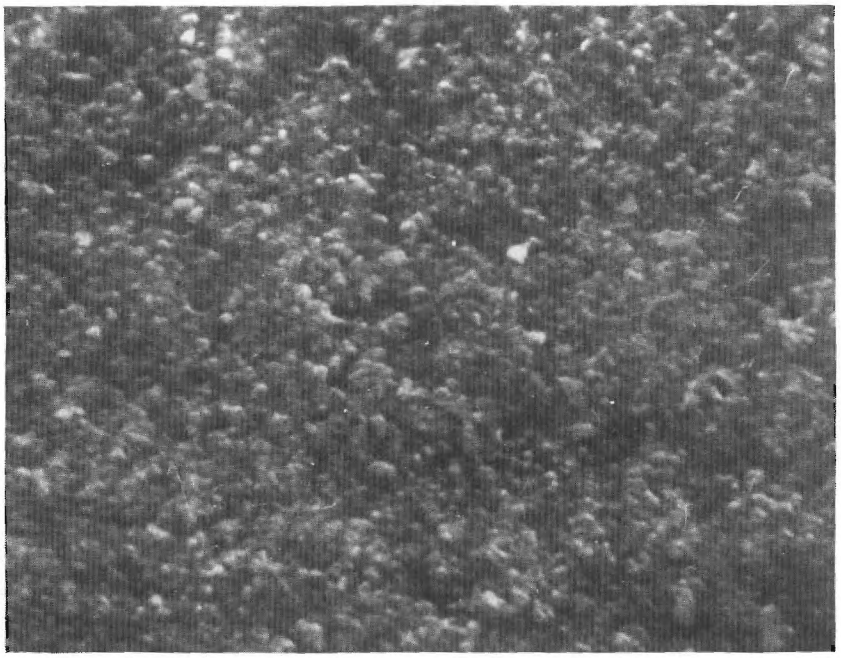

a

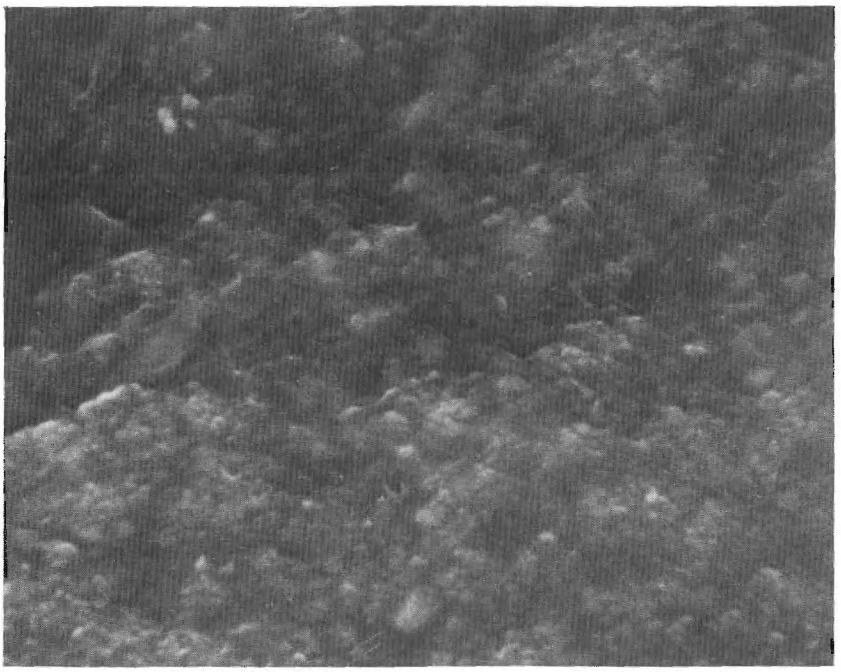

b

Figure 12. Scanning Electron Micrographs of Conductive Polymer Samples Showing the Surface Topography at 7500X; (a) Before Testing, (b) After Testing.

G. Miscellaneous Coaxial Cell Tests

Test Conditions: A large coaxial cell was constructed which allowed circulation of salt water between the inner and outer electrodes. The outer electrode was made from 1.5" copper tube (1.52" I.D.). A copper inner electrode (0.92" O.D.), identical in dimensions to the aluminum electrode made earlier for the small coaxial cell, was also constructed. Plexiglas end caps with O-rings were used to hold the electrodes in the coaxial configuration with waterproof joints. The electrical length of the cell was 3.0 inches.

The cell is shwon in Figure 13. The small peristaltic pump and speed controller also shown were used to circulate 3.5% NaCl solution through the cell from a 2000 ml reservoir (not shown). The flow rate used was 15.4 cm^3/sec, which corresponds to approximately 0.05 mph towing speed.

Results and Discussion: Figure 14 shows the salient results of the important tests performed using the cell. Curve 1 is a plot of cell voltage versus time for a jacketed copper inner electrode for impressed currents of 1.0 ampere and 2.0 amperes. Note the large increase in voltage when the current was increased from 1.0 A to 2.0 A. Note also the steady decline of cell voltage to a minimum of approximately 11 volts at $\sim$ 50 min followed by a steady increase to 13.3 volts at 130 minutes (not shown) when the test was terminated.

Curve 2 shows the cell voltage obtained using a jacketed copper inner electrode with a 14" length of platinized niobium wire spiralled tightly around the jacket. The dramatic decrease in cell voltage is evident when comparing curves 1 and 2.

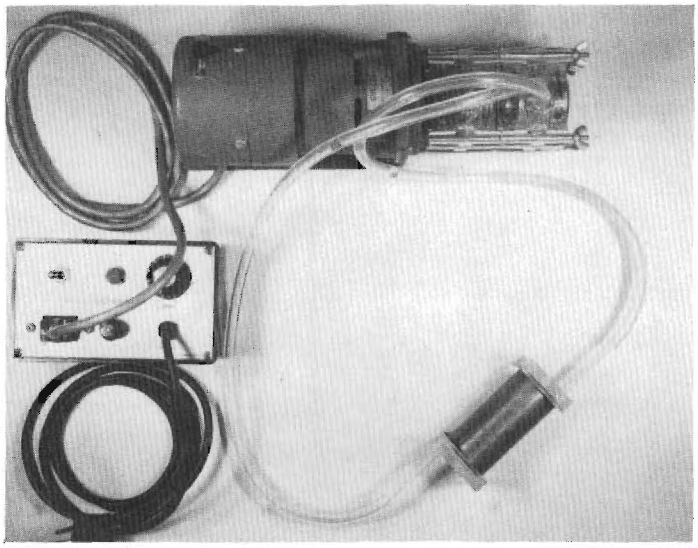

Figure 13. Illustration of Large Coaxial Cell and Pump Used for Dynamic Testing

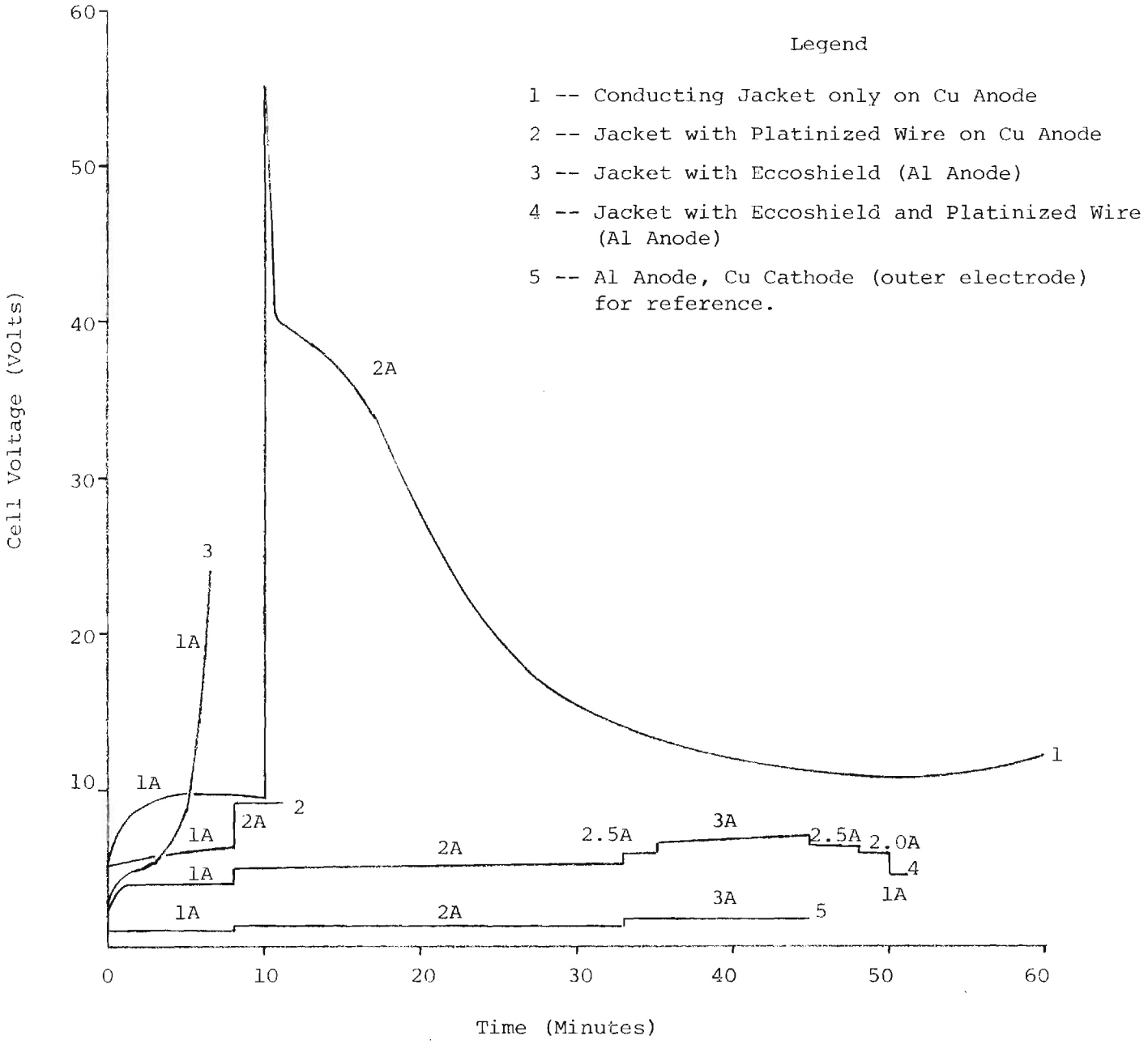

Figure 14 . Salient Results of Tests Using the Large Coaxial Cell and Circulating NaCl Solution.

Curve 3 was obtained by painting the inner and outer surfaces of the conducting jacket with conducting silver paint*. When the paint was removed from the very ends of the cylindrical jacket, there resulted a coaxial resistor with a dc resistance of $\sim$ 0.9 ohm. This value of resistance corresponds to a resistivity of 320 ohm.cm for the jacket material. The painted jacket was then forced onto the aluminum inner electrode for testing. In Figure 14, the steady increase in cell voltage (curve 3) indicates that the inner electrode became less conducting with time. This behavior is attributed to the fact that as the silver was removed by electrolysis from the paint on the jacket, the lacquer film left behind formed an insulator which inhibited the flow of current.

Curve 4 of Figure 14 shows the most promising results obtained. In this case, the jacket material was painted inside and out with Eccoshield ES and then forced onto the aluminum electrode. A 14" length of platinized niobium wire was then spiralled tightly around the painted electrode as indicated in Figure 15a. The dc resistance between inner aluminum electrode and the platinized wire was approximately 0.5 ohm.

Curve 5 shows the results obtained when the inner electrode was an aluminum tube with outer diameter equal to that of the jacketed electrode. This curve is provided as a reference curve and is a standard for any other electrode configuration.

---

*Emerson and Cuming, Inc., Eccoshield ES in aerosol spray can.

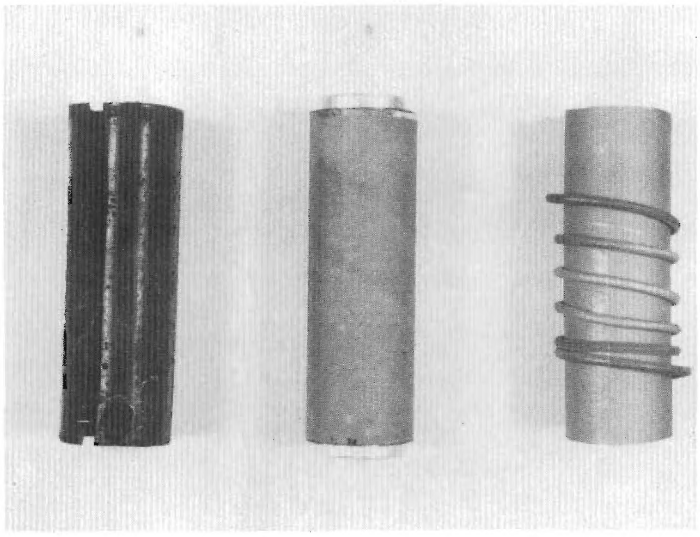

a) Anodes Corresponding to Curves 1, 3, and 4 (left to right).

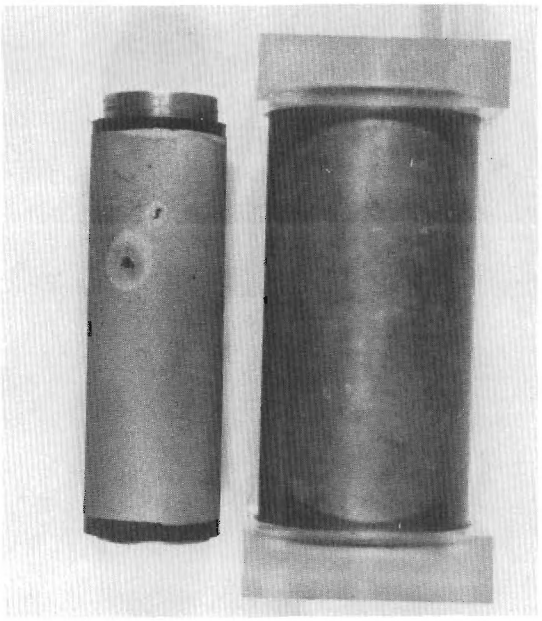

b) Anode 3 after failure (cell on right).

Figure 15 Photographs of Anode Configurations Used in Large Coaxial Cell

H. Discussion

In a two-electrode, open-loop system operating in sea water, an electronic current flows through the metallic conductors, and an ionic current through the water. On the electrode surfaces electrochemical reactions take place, the sum of the reaction rates being equal to the total current flowing in the circuit. If the electrodes are inert, the main reactions on the anode in sea water are electrolytic evolution of oxygen and chlorine:

$$2H_2O = O_2 + 4H^+ + 4e^-$$

$$2Cl = Cl_2 + 2\,e^-$$

A certain overvoltage is needed to maintain the required current density; it depends on the polarization characteristics of the electrode material.

If the electrode is not inert, anodic dissolution and/or electrochemical formation of various compounds may take place. resulting in deterioration. All the electrochemical reactions are potential-dependent, and the rates of the individual reactions depend on the overvoltage which is needed to maintain the required current density. The lower the overvoltage, the more efficient is the electrode, and less power is dissipated in the surface reactions. Although the sea water path resistance is the major term in the total circuit resistance and thus in the total power dissipation, the term due to the electrode overvoltage can also be significant and create unacceptable demand on the power supply unless an efficient electrode is used.

The tests have shown that platinized niobium is a very efficient and almost inert anode. The overvoltage at the current density of 0.5 A/cm^2 was in the range of only 3.5 to 4.5 volts. No deterioration was observed in

tests of up to 24 hours duration and the industrial experience with this type of anode in cathodic protection systems gives confidence in a long life-expectancy.

The carbon-impregnated polyethylene exhibited considerably higher overvoltages and rapid deterioration. Although the mechanism was not investigated in detail, the following general mechanism can be suggested to explain the observations: the amount of carbon in the surface layer is relatively low, and a high local current density must exist on the exposed particles to maintain the current. The high current density can be achieved only at a high overvoltage; the high overvoltage allows other reactions to occur, such as

$$C + 2\ H_2O = CO_2 + 4H^+ + 4\ e^-$$

Carbon in the surface layer is thus depleted by conversion into carbon dioxide or other compounds; this results in a further increase in current density and overvoltage. As more and more carbon is exhausted, the reaction occurs deeper and deeper in the material, the average resistivity increases, and the gaseous products of the reactions cause blistering. Eventually, the deterioration causes a local perforation of the jacket.

In the cathodic regime the main reaction is expected to be the electrolytic evolution of hydrogen,

$$2H^+ + 2e^- = H_2,$$

but electrolytic deposition of various compounds from sea water may play a significant role. Platinum group metals are excellent electrodes for the hydrogen reduction reaction, and the tests with the platinized niobium confirmed this. However, niobium is highly susceptible to hydrogen embrittle-

ment, and the durability of this type of cathode is questionable. Platinizing of another substrate material may be the solution, but the stability of the platinum layer under the condition of high rate hydrogen evolution would have to be carefully examined.

The carbon-impregnated polyethylene jacket has shown promising behavior in short-term cathodic tests. Although carbon can suffer cathodic deteroration by formation of methane,

$$C + 4H^{+} + 4e^{-} = CH_4$$

which would result in a damage similar to the one observed under anodic conditions, the efficiency in the cathodic regime was higher and may be sufficient to keep the rate of the methane reaction low. Further tests of both types of materials will be needed to determine the life expectancy.

CHAPTER III

PRELIMINARY DESIGN OF A NOBLE METAL ELECTRODE

A. General Design Features

Platinized niobium anodes can be used at high current densities (up to 7A/in^2); therefore, the electrodes can be made quite small even for high current demands. For the application in minesweeping, however, a reduction in size is limited by the consideration of the sea water path resistance, which is primarily a function of the electrode length. The length of the electrode is thus in effect fixed. The length of 150 feet was considered in the proposed design.

Because of the high cost and weight of niobium, it cannot be used to conduct the full current flowing to all the electrode surfaces. Aluminum conductors are a natural choice for this function. Since they have to be insulated from the sea water by a jacket, and the electrode must have a certain buoyancy, the basic design specifications of a noble metal electrode are almost identical to those of the "S" cable, except for the addition of platinized niobium electrodes connected to the conductors of the cable. Therefore, the proposed design calls for a modification of the new "S" cable and the electrode will have essentially same physical characteristics.

Platinized niobium products are commercially available in a variety of forms, such as wires, rods, mesh, etc. To keep the drag and stiffness of the electrode as low as possible, it is proposed to use thin niobium strips platinized on one side. Niobium strips are readily available and so is platinizing on strips of up to 50 ft. in length. The present design uses 10 strips 50 ft. in lenth each, 0.5x0.0626 in. cross section. Each strip

will be wrapped around the cable on a length of 15 ft. and connected to the aluminum conductors at both ends. More frequent connection can be made if necessary. The average current density on a 10,000 A electrode will be about 3.33 A/in^2, $0.52A/cm^2$. The strips will be connected to the aluminum conductors by means of simple open collars and the joints will be sealed by means of heat shrinkable polyethylene tubing combined with either adhesives or ultrasonic welding. The total added weight will be about 58 lb.

The procedure of modification of the "S" cable will be basically as follows:

a. Rings of the polyethylene jacket will be cut out from the cable every 15 ft. to expose the aluminum conductors. The width of the rings will be about one to two inches.

b. Open collars of the same width, made of preformed strips of a suitable metal of the same thickness as the polyethylene jacket will be attached to the aluminum conductors by welding, soldering or conductive adhesives.

c. Ends of the platinized niobium strips will be attached to the collars by spot welding at the proper angle of the spiral, the strips being tightly wound around the cable between the collars.

Note: It may be necessary to weld the strips to the collars before they are connected to the conductors.

d. Short lengths of expanded, heat shrinkable polyethylene tubing will be placed over each collar, overlapping about one inch on each side over the cable jacket. The jacket and the inside surface of the tubing will have been chemically treated to improve adhesion. An adhesive for polyethylene will be applied on the overlapping surfaces, and the polyethylene tubing will

be heated to shrink it tightly over the joint.

Note: Several segments of the heat shrinkable tubing with graduated lengths may be used to improve the tightness of the joint and the flow of sea water along the electrode. Instead of using adhesives, the polyethylene tubing can be ultrasonically welded to the cable jacket.

The material and size of the collars, the methods of joining, and other design details have not been decided at this time, since they require further design analysis.

Two models have been constructed based on the preliminary design. One is a scale model using a section of the same underground power distribution cable from which conductive jacket samples were taken. Aluminum strip and connecting collars were used and heat shrinkable tubing was applied over the collars. It was found that the addition of the strip did not impair the flexibility of the cable. Figure 16a shows this model bent to a radius of about five times the cable diameter. In Figure 16b, a full scale mock-up is shown along with a section drawing of the proposed design.

A theoretical analysis has been performed of two factors which are important in evaluating the proposed design:

1. Dissipation of the heat produced by the flow of electrical current;
2. Stiffness of the electrode, which in large measure determines the ease of handling.

The basic theory and the results of the calculations are given in the following two sections; Appendices 1 and 2 contain further information about the mathematical details.

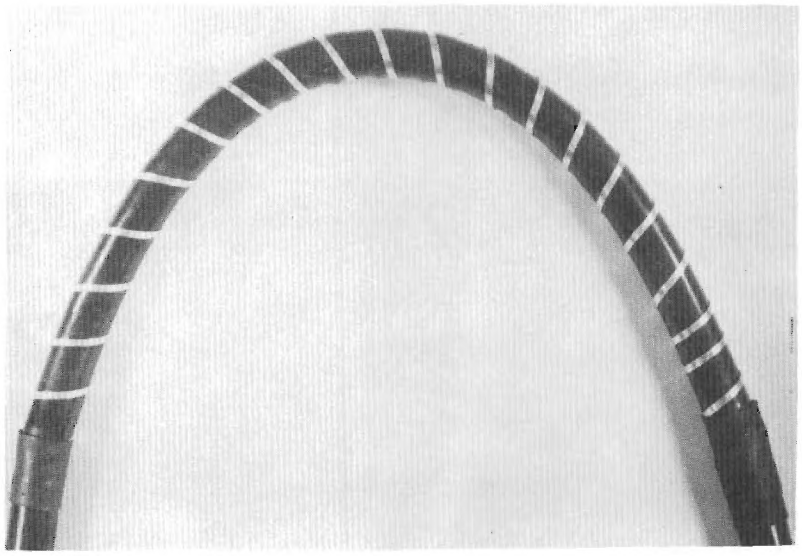

a

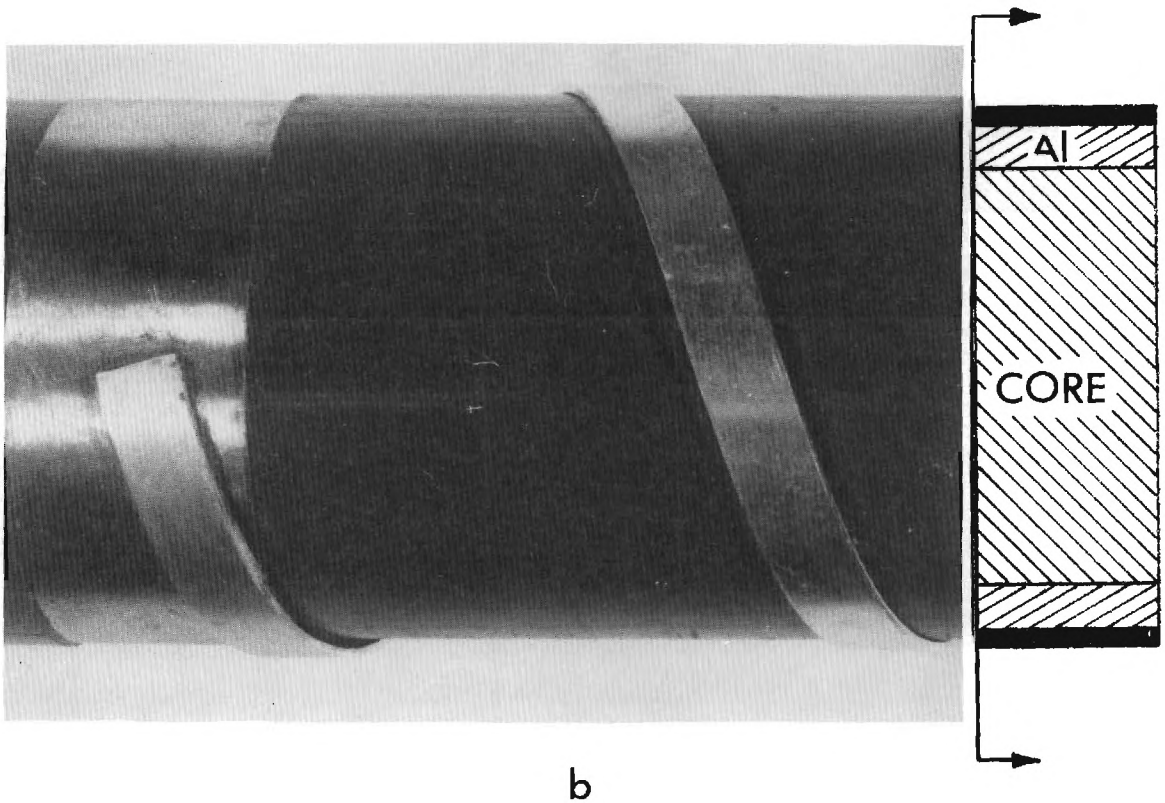

b

Figure 16. Models of Preliminary Design of a Platinized Niobium Electrode;
(a) Scale Model Flexion Test,
(b) Full Size Mock-up and Section Drawing.

The helical geometry of the Nb strip produces analytical complications for both the stiffness and heat transfer problems. The latter is, in addition, complicated by the non-uniform distribution of current. To facilitate solution of the two problems, simplifying assumptions have been made as to geometry and current distribution which result in postulation of more severe operating conditions for the electrode than it would ever actually encounter in practice. Hence, these are "worst case" analyses.

Since the S-cable material which forms the basis of the platinized Nb electrode design has undergone a prolonged development program and thus can be presumed to function adequately under the conditions which will be imposed on it, the aim of the calculations discussed here was to compare temperature distribution and stiffness of a cable with and without a Nb strip so as to determine the magnitude of the strip's influence.

B. Temperature Distribution

Two simplifications were made to obtain a one-dimensional problem: (1) the spiral Nb strip was replaced by a Nb tube of the same thickness and rate of heat production per unit volume, and (2) the currents in the Al and Nb conductors were assumed to be uniform and equal to the maximum values which occur in the real electrode. Both result in overestimation of the temperature rise since, for assumption 1, the polymer jacket surface is not in contact with the heat sink of the sea, and for assumption 2, since the axial heat flow (which results from non-uniform heating by non-uniform currents causing temperature gradients) which would tend to produce a more even temperature distribution is neglected.

Under these conditions, the differential equation governing the steady-state temperature distribution in media which have heat sources is the one-dimensional Poisson equation:

$$\frac{dT^2}{dr^2} + \frac{1}{r}\frac{dt}{dr} + \frac{q'''}{k} = 0$$

where T = temperature, r = radial coordinate, q''' = rate of heat production per unit volume, and k = thermal conductivity.

The temperature distribution T(r) for an electrode with and without the Nb layer is shown graphically in Figure 17 (see Appendix 1 for a discussion of how this solution is obtained). Since, in general, polymer-based materials are much less stable at elevated temperatures than are metals, the basic reason for calculating temperature distributions is to determine the maximum temperature use above the ambient sea temperatures which will occur in the polymer regions of the electrode (i.e., central core and cable jacket). The central core temperature is 41.13°C without the Nb outer layer and 43.80°C with the outer layer. The maximum temperature of the cable jacket will be 41.05°C without a Nb layer and 43.74°C with the layer. The increase in the maximum temperature rise in the polymeric portions of the cable will be 6.5% for this "worstcase" analysis, so it can be concluded that the presence of the Nb strips will have only a slight influence on the temperature rise of the electrode.

C. Stiffness Considerations

The ease of handling an electrode when it is being coiled or uncoiled is related to the ease with which it can be bent. For a beam whose axis is

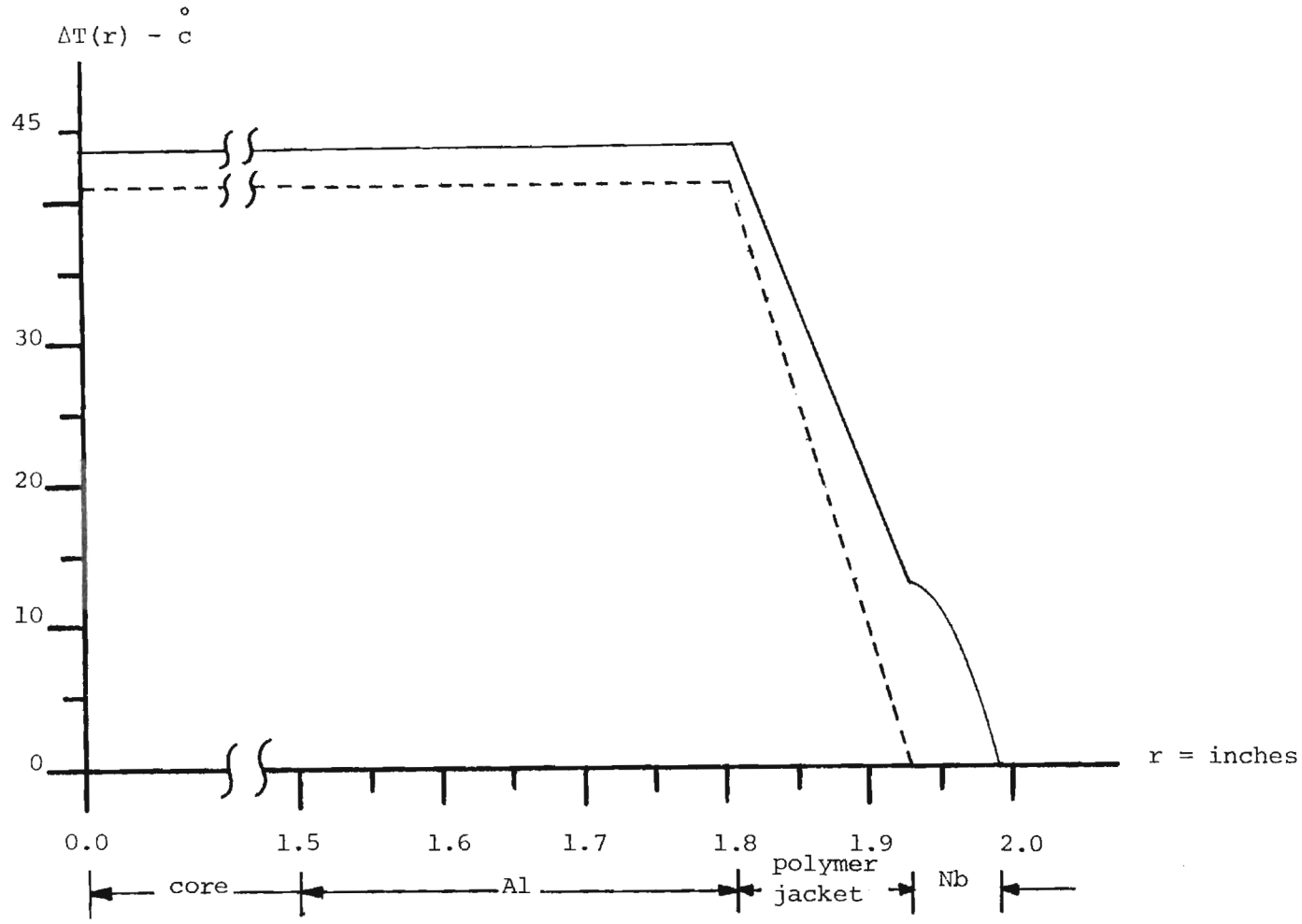

Figure 17. Comparison of the temperature rise ΔT(r) vs. r for electrodes without (----) and with (———) platinized Nb strips.

directed along the x-axis and which undergoes bending in the xy plane, the beam deflection, y, is given by:

$$y = (1/EI) \cdot f(x)$$

where E = Young's modulus of the beam, and

I = second moment of area of the beam cross-section about the z-axis.

The function f(x) depends upon the applied loads and the boundary conditions (assumed to be the same for an electrode with and without Nb strips).

Let the subscripts e and eps respectively stand for the electrode without the strips and the electrode plus strips. Then, for the same loads on both, the ratio of the deflections is:

$$y_e/y_{eps} = (EI)_{eps}/(EI)_e \tag{1}$$

The bending stiffnesses (i.e., the EIs) are given by:

$$(EI)_{eps} = E_{sc}I_{sc} + E_{str}I_{str} \tag{2}$$

$$(EI)_e = E_{sc}I_{sc} \tag{3}$$

where subscript sc stands for S Cable material and str denotes the Nb strip.

Substitution of (2) and (3) into (1) yields:

$$y_e/y_{eps} = 1 + \frac{E_{str}I_{str}}{E_{sc}I_{sc}} \tag{4}$$

As was the case for the thermal analysis, a simplifying assumption is made to avoid dealing with the spiral geometry of the strip. The strip is

assumed to lie on the S-cable with its axis straight and parallel to that of the cable. Bending occurs in the plane defined by the two axes. This again constitutes a "worst case" calculation, since here a greater portion of the strip provides resistance to bending than would be the case for a helically wrapped strip.

Using this assumption, I_{sc} and I_{str} are straight forwardly calculated (see Appendix 2). E_{str} is known ($E_{str} = E_{Nb} = 15 \times 10^6$ psi); however, we do not know the value of E_{sc}. Thus, at this time, the ratio y_e/y_{eps} given by (4) cannot be determined with precision numerically, but it is expressible in terms of the ratio of the Young's moduli:

$$y_e/y_{eps} = 1 + 1.1 \times 10^{-2} \cdot \frac{E_{str}}{E_{sc}}$$

Even for $E_{str}/E_{sc} = 10$ (which is probably higher than the true value), the decline in deflection due to the strip is only 10%. Considering that this was a "worst case" analysis, it can be concluded that it is most unlikely that placing Nb strips on the S-cable material will result in more than a very modest increase in bending stiffness.

D. Cost Estimate and Life Expectancy

The cost of the noble metal electrode of the proposed design can be estimated as the cost of the "S" cable + conversion cost. The conversion cost is a sum of the costs of materials + labor. The cost of materials, based on the 1976 quotations from Kawecki Berylco Industries and Engelhard Industries for the niobium strips and platinizing, respectively, is estimated for one electrode as follows:

500 ft niobium strip 0.5x0.0625 in, 56 lb @ $51.15/lb	$2,864
Platinizing 100 μ inch Pt, 0.5 in x 500 ft	2,370
Heat shrinkable PE tubing, 4 in. ID, 10 ft	41
Collars and miscellaneous	225
TOTAL	$5,500

The cost of materials in larger quantities will be lower by at least 5%. Considering the expected increases in prices, it is estimated that the total conversion cost (including labor) will be $10,000 or less.

At the current density of 3.33 A/in^2 the life-expectancy of commercial platinized niobium electrodes with 100 μ in Pt is about one year. At the high towing speed of the minesweeping electrodes, the life will be shortened due to erosion. It is estimated that the life will not be less than 1,000 hours of operation.

CHAPTER IV

ELECTROMAGNETOSTATIC ANALYSIS

A method for the calculation of electrode currents is presented which combines integrals of Green's function solutions, superposition and the method of moments to yield accurate current densities for resistive electrodes in sea water of finite depth. The method allows for submergence of the electrodes and includes specification of sea bottom conductivity, electrode physical and electrical properties. The solution is restricted such that each electrode is composed of N subsections, each of which are equal length conducting cylinders with an outer cylindrical layer of conducting jacket.

A. Electrode Current Calculation

The starting point for the development of this method is the solution for the voltage in a three region media generated by a point of current I_p located in the middle medium. This solution is called the Green's Function for the problem. Figure 18 shows the three region media, the point of current, and the reference coordinate system for this point problem. The three regions are characterized by their conductivities and planar boundries at z'=b and z'=-a. The solution to the problem is obtained from Laplace's Equation in cylindrical coordinates independent of the angle Φ. In cylindrical coordinates the solution for the voltage is separable into functions of z', Z(z') and cylindrical r, R(r) for the case of no Φ dependence as

$$V(r,z') = R(r)Z(z')$$

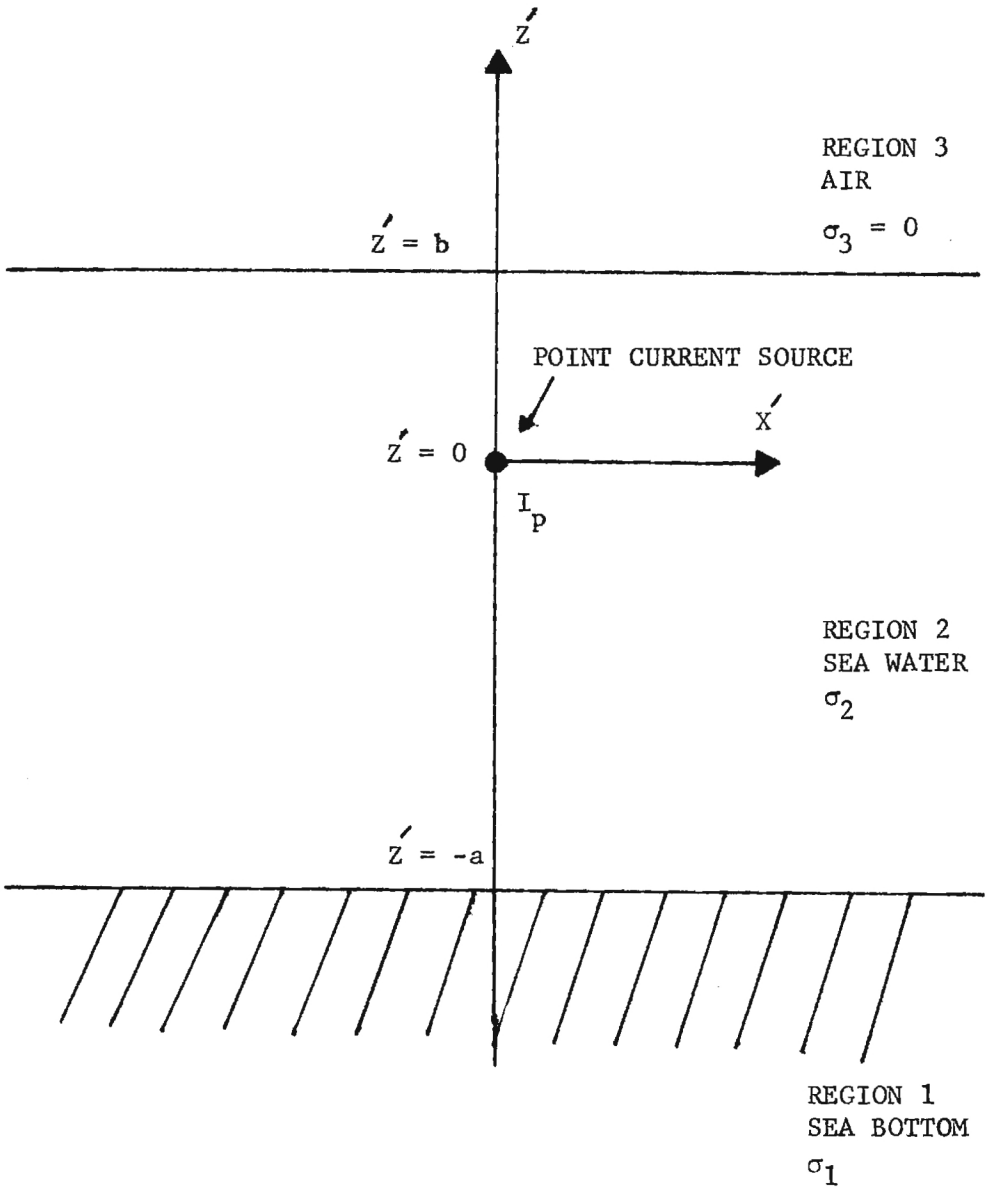

Figure 18

Three region media and coordinate system for point source problem.

Laplace's Equation for this case reduces to

$$\nabla^2 V(r,z') = \frac{r}{R(r)} \frac{\partial}{\partial r} \left(r \frac{\partial R(r)}{\partial r}\right) + \frac{r^2}{Z(z')} \frac{\partial^2 Z(z')}{\partial z'^2} = 0.$$

The general solution to the equation is given as

$$V(r,z') = \frac{I_p}{4\pi\sigma} \int_o^\infty \theta(k) J_o(kr) e^{\pm kz'} dk$$

where $\theta(k)$ is an arbitrary function of k. The general solution is seen to have two possible functional forms with respect to z' and in general both forms must be employed.

The general solution for region three can now be written as follows:

$$V_3(r,z') = \frac{I_p}{4\pi\sigma_2} \int_o^\infty \Omega(k) J_o(kr) e^{-kz} dk, \quad z' \geq b \tag{1}$$

where the +kz' solution must have a zero coefficient, for $z' = +\infty$ the voltage $V_3(r,\infty)=0$. The conductivity σ_2 is used instead of σ_3 in the multiplier to keep the coefficients for all regions identical. The missing multiplying factor $\frac{\sigma_2}{\sigma_3}$, if needed, is absorped in the unknown function $\Omega(k)$.

The general solution for region 2 is written as

$$V_2(r,z') = \frac{I_p}{4\pi\sigma_2} \left[\int_o^\infty J_o(kr) e^{-k|z'|} dk + \int_o^\infty \psi(k) J_o(kr) e^{-kz'} dk + \int_o^\infty \theta(k) J_o(kr) e^{+kz'} dx \right], \quad -a \leq z' \leq b . \tag{2}$$

The solution for region two is seen to contain both the +kz' and -kz' general solutions. In addition, the first term of this solution is a forcing solution in the form of the known solution for a point current of magnitude I_p in an infinite region of conductivity σ_2. The unknown functions $\psi(k)$ and $\theta(k)$ must then compensate for the forcing function.

The general solution for region one is written as

$$V_1(r,z') = \frac{I_p}{4\pi\sigma_2} \int_o^\infty \Phi(k) J_o(kr) e^{+kz'} dk \qquad z' \leq -a. \tag{3}$$

As seen in this solution, the multiplying function for the -kz' solution was set to zero in order that the voltage at $z' = -\infty$ would be zero.

The above set of three equations is seen to possess four unknown functions $\Omega(k)$, $\psi(k)$, $\theta(k)$ and $\Phi(k)$ which must be determined to solve for the voltages in the three regions. Four equations can be generated by applying boundary conditions to the solutions at the two boundries z'=b and z'=-a. At each planar boundary the voltage on each side of the boundary must be continuous at the boundary (i.e.)

$$V_3(r,b) = V_2(r,b) \tag{4}$$

and

$$V_2(r,-a) = V_1(r,-a) \tag{5}$$

Also at each boundary the current normal to the boundary must be continuous as it crosses the boundary (i.e.)

$$\sigma_3 \frac{\partial V_3(r,b)}{\partial z'} = \sigma_2 \frac{\partial V_2(r,b)}{\partial z'} \tag{6}$$

and

$$\sigma_2 \frac{\partial V_2(r,-a)}{\partial z'} = \sigma_1 \frac{\partial V_1(r,-a)}{\partial z'} \tag{7}$$

The solution to the four unknown functions as determined from the four boundary conditions is aided by the fact [1] that for equality of integral equations of this type, the integrands must be equal. Also, as differentiation is not performed with respect to r in any of the four equations all terms have the common factor $J_o(kr)$ which may be divided out of each side of the equations. Boundary condition equations (4) and (5) result in the following algebraic equations:

$$\Omega(k)e^{-kb} = e^{-kb} + \psi(k)e^{-kb} + \theta(k)e^{kb}$$

$$\Phi(k)e^{-ka} = e^{-ka} + \psi(k)e^{ka} + \theta(k)e^{-ka}$$

Likewise, boundary condition equations (6) and (7) result in the following algebraic equations

$$-\sigma_3\Omega(k)e^{-kb} = -\sigma_2 e^{-kb} - \sigma_2\psi(k)e^{-kb} + \sigma_2\theta(k)e^{kb}$$

$$\sigma_1\Phi(k)e^{-ka} = \sigma_2 e^{-ka} - \sigma_2\psi(k)e^{ka} + \sigma_2\theta(k)e^{-ka}$$

The solution of the four equations for the four unknown functions is straight forward but tedious. The results are given as:

$$\Omega(k) = \frac{2\sigma_2}{\sigma_3+\sigma_2}\left[\frac{1-K_{12}e^{-2ka}}{1-K_{12}K_{32}e^{-2kc}}\right]$$

$$\theta(k) = -K_{32}\left[\frac{e^{-2kb}-K_{12}e^{-2kc}}{1-K_{12}K_{32}e^{-2kc}}\right]$$

$$\psi(k) = -K_{12}\left[\frac{e^{-2ka}-K_{32}e^{-2kc}}{1-K_{12}K_{32}e^{-2kc}}\right]$$

$$\Phi(k) = \frac{2\sigma_2}{\sigma_1+\sigma_2}\left[\frac{1-K_{32}e^{-2kb}}{1-K_{12}K_{32}e^{-2kc}}\right]$$

where:

$$K_{12} \triangleq \frac{\sigma_1-\sigma_2}{\sigma_1+\sigma_2} \quad ,$$

$$K_{32} \triangleq \frac{\sigma_3-\sigma_2}{\sigma_3+\sigma_2} \quad ,$$

and

$$c \triangleq a+b$$

Substitution of these functions into the voltage equations (1), (2), and (3) yields integrals of the following form

$$M = \int_o^\infty \left[\frac{e^{-2kd}}{[1-K_{12}K_{32}e^{-2kc}]}\right] J_o(kr)e^{\pm kz'}dk$$

where d takes on the positive values a, b, c, or zero. The denominator

of the integrand may be recognized as the sum of a power series of the form

$$\frac{1}{1-x} = x + x^2 + x^3 + x^4 + x^5 + \ldots$$

where $|x| < 1$.

It can be seen from the definition of K_{12} and K_{32} that each has a magnitude of one or less and that because both c and k are positive, the magnitude of e^{-2kc} is always less than one except when k=0. The k=0 point is integrable in this form and therefore does not present a problem and may be ignored. Expanding the denominator of the integrand of integral M in its power series representation, yields integrals of the following form

$$M_N = (K_{12}K_{32})^N \int_o^\infty J_o(kr)e^{\pm k(z'\bar{+}2d\bar{+}2Nc)}dk$$

where N is any non-negative integer and d is as defined previously. It is known that integrals of this form have the following value

$$M_N = \frac{(K_{12}K_{32})^N}{[r^2+(z'\bar{+}2d\bar{+}2Nc)^2]^{\frac{1}{2}}}$$

Applying the above procedure of substituting the solution for the four unknown functions into the three voltage equations, expanding the denominators of each integral in a power series and integrating term by term, yields the following infinite series for the voltages in the three regions:

$$V_3(r,z') = \frac{I_p}{2\pi(\sigma_3+\sigma_2)}\left[\sum_{i=o}^{\infty}\frac{(K_{12}K_{32})^i}{[r^2+(z'+2ic)^2]^{\frac{1}{2}}} - K_{12}\sum_{i=o}^{\infty}\frac{(K_{12}K_{32})^i}{[r^2+(z'+2a+2ic)^2]^{\frac{1}{2}}}\right] \quad \text{for } z \geq b \tag{8}$$

$$V_2(r,z') = \frac{I_p}{4\pi\sigma_2}\left[\frac{1}{[r^2+z'^2]^{\frac{1}{2}}} - K_{12}\sum_{i=o}^{\infty}\frac{(K_{12}K_{32})^i}{[r^2+(z'+2a+2ic)^2]^{\frac{1}{2}}} + \sum_{i=1}^{\infty}\frac{(K_{12}K_{32})^i}{[r^2+(z'+2ic)^2]^{\frac{1}{2}}} - K_{32}\sum_{i=o}^{\infty}\frac{(K_{12}K_{32})^i}{[r^2+(z'-2b-2ic)^2]^{\frac{1}{2}}} + \sum_{i=1}^{\infty}\frac{(K_{12}K_{32})^i}{[r^2+(z'-2ic)^2]^{\frac{1}{2}}}\right] \tag{9}$$

for $-a \leq z' \leq b$

and

$$V_1(r,z') = \frac{I_p}{2\pi(\sigma_1+\sigma_2)}\left[\sum_{i=o}^{\infty}\frac{(K_{12}K_{32})^i}{[r^2+(z'-2ic)^2]^{\frac{1}{2}}} - K_{32}\sum_{i=o}^{\infty}\frac{(K_{12}K_{32})^i}{[r^2+(z'-2b-2ic)^2]^{\frac{1}{2}}}\right] \tag{10}$$

for $z' \leq -a$

The above three equations are called the Green's function solution for each medium and in the next section will be integrated to find the voltages due tc lines of currents.

B. Voltage Produced by Horizontal Lines of Current

In this section the Green's function solutions (point source solutions) are used in the determination of the voltages produced in the three regions due to a horizontal line of current. A different coordinate system (coordinates x,y,z) will be used in this development. The coordinate system is the same as defined in Figure 18 except that Z = 0 is located at the air-sea interface surface.

The superposition theorem is employed to find the voltage in the three regions as a summation of the voltages due to a distribution of point currents which are located on a horizontal line. The line is assumed to be parallel to the x axis with a length 2L, and center located at the rectangular coordinates (xI, yI, and zI). Let the total current, I, be uniformly distributed along the length of the line, resulting in a current density of

$$p = \frac{I}{2L} \quad \text{(amps/meter)}$$

Now, let the line be segmented into infinitesimal segments of length dx_s. The current associated with each segment is $pdx_s = \frac{I}{2L} dx_s$. Then the contribution to the voltage at a point in (x,y,z) in any of the regions due to the segment with x-coordinate x_s can be obtained by the use of equation (8) (9), or (10) with I_p replaced by $\frac{I}{2L} dx_s$, r replaced with $\sqrt{(x-x_s)^2 + (y-yI)^2}$ and z replaced by (z-zI). The incremental voltage contributions can then be integrated to yield the total voltage due to the line current. For example, if we let $V_{L3}(x,y,z)$ be the voltage at a point (x,y,z) in region three due to a line of current, we have

$$V_{L3}(x,y,z) = \int_{xI-L}^{xI+L} \frac{I}{2L2\pi(\sigma_s+\sigma_2)} \left[\sum_{i=o}^{\infty} \frac{(K_{12}K_{32})^i}{\sqrt{(x-x_s)^2+(y-yI)^2+(z-zI+2ic)^2}} \right.$$

$$\left. - K_{12} \sum_{i=o}^{\infty} \frac{(K_{12}K_{32})^i}{\sqrt{(x-x_s)^2+(y-yI)^2+(z-zI+2ic)^2}} \right] dx_s \ .$$

Similar expressions are obtained for $V_{L2}(x,y,z)$ and $V_{L1}(x,y,z)$. Thus each voltage expression is an infinite series of terms of the form

$$P = K \int_{xI-L}^{xI+L} \frac{\frac{I}{2L}}{\sqrt{(x-x_s)^2+(y-yI)^2+(z-zI\pm 2E)^2}} dx_s$$

where K and E are constant for each integration. The evaluation of this integral is straightforward for all points (x,y,z) not colinear with the line current. For points colinear with the line current but not on the line of current, the denominator reduces to the $|x-x_s|$ when the constant E is zero. The evaluation of this integral for points on the line current will be presented later. In all cases, except for points on the line current, the evaluation of this integral is determined as

$$P = K \frac{I}{2L} \ell n \left[\frac{\sqrt{(|x-xI|+L)^2+(y-yI)^2+(z-zI+E)^2}+|x-xI|+L}{\sqrt{(|x-xI|-L)^2+(y-yI)^2+(z-zI\pm E)^2}+|x-xI|-L} \right]$$

Applying the above integral evaluation to each term in the voltage equations yields:

$$V_{L3}(x,y,z) = \frac{I}{4\pi L(\sigma_3+\sigma_2)} \left[\sum_{i=o}^{\infty} (K_{12}K_{32})^i \right.$$

$$\ell n \left[\frac{\sqrt{(|x-xI|+L)^2+(y-yI)^2+(z-zI+2ic)^2} + |x-xI|+L}{\sqrt{(|x-xI|-L)^2+(y-yI)^2+(z-zI+2ic)^2}+|x-xI|-L} \right]$$

$$\left. -K_{12} \sum_{i=o}^{\infty} (K_{12}K_{32})^i \ell n \left[\frac{\sqrt{(|x-xI|+L)^2+(y-yI)^2+(z-zI+2a+2ic)^2}+|x-xI|+L}{\sqrt{(|x-xI|-L)^2+(y-yI)^2+(z-zI+2a+2ic)^2}+|x-xI|-L} \right] \right]$$

for $z \geq 0$

and

$$V_{L2}(x,y,z) = \frac{I}{8\pi L\sigma_2} \left[\ell n \left[\frac{\sqrt{(|x-xI|+L)^2+(y-yI)^2+(z-zI)^2}+|x-xI|+L}{\sqrt{(|x-xI|-L)^2+(y-yI)^2+(z-zI)^2}+|x-xI|-L} \right] \right. \tag{11}$$

$$-K_{12} \sum_{i=o}^{\infty} (K_{12}K_{32})^i \ell n \left[\frac{\sqrt{(|x-xI|+L)^2+(y-yI)^2+(z-zI+2a+2ic)^2}+|x-xI|+L}{\sqrt{(|x-xI|-L)^2+(y-yI)^2+(z-zI+2a+2ic)^2}+|x-xI|-L} \right]$$

$$+ \sum_{i=1}^{\infty} (K_{12}K_{32})^i \ell n \left[\frac{\sqrt{(|x-xI|+L)^2+(y-yI)^2+(z-zI+2ic)^2}+|x-xI|+L}{\sqrt{(|x-xI|-L)^2+(y-yI)^2+(z-zI+2ic)^2}+|x-xI|-L} \right]$$

$$-K_{32} \sum_{i=o}^{\infty} (K_{12}K_{32})^i \ell n \left[\frac{\sqrt{(|x-xI|+L)^2+(y-yI)^2+(z-zI-2b-2ic)^2}+|x-xI|+L}{\sqrt{(|x-xI|-L)^2+(y-yI)^2+(z-zI-2b-2ic)^2}+|x-xI|-L} \right]$$

$$\left. + \sum_{i=1}^{\infty} (K_{12}K_{32})^i \ell n \left[\frac{\sqrt{(|x-xI|+L)^2+(y-yI)^2+(z-zI-2ic)^2}+|x-xI|+L}{\sqrt{(|x-xI|-L)^2+(y-yI)^2+(z-zI-2ic)^2}+|x-xI|-L} \right] \right]$$

and

for $-c \le z \le 0$ and (x,y,z) not on the line of current

$$V_{L1}(x,y,z) = \frac{I}{4\pi L(\sigma_1+\sigma_2)}\left[\sum_{i=o}^{\infty}(K_{12}K_{32})^i \ell n\left[\frac{\sqrt{(|x-xI|+L)^2+(y-yI)^2+(z-zI-2ic)^2}+|x-xI|+L}{\sqrt{(|x-xI|-L)^2+(y-yI)^2+(z-zI-2ic)^2}+|x-xI|-L}\right]\right.$$

$$\left.-K_{32}\sum_{i=o}^{\infty}(K_{12}K_{32})^i \ell n\left[\frac{\sqrt{(|x-xI|+L)^2+(y-yI)^2+(z-zI-2b-2ic)^2}+|x-xI|+L}{\sqrt{(|x-xI|-L)^2+(y-yI)^2+(z-zI-2b-2ic)^2}+|x-xI|-L}\right]\right]$$

for $z \le -c$

where $b = -ZI$ and $a = C + ZI$

The equations for the voltage in region two were restricted, in that the voltage could not be evaluated on the line of current. It will be necessary in what follows to be able to evaluate this voltage. Examination of the expressions for V_{L1}, V_{L2}, and V_{L3} show that only the first term of $V_{L2}(x,y,z)$ becomes undefined for a point on the conductor (i.e. $y=yI$, $z=zI$, $xI-L \le x \le xI+L$). Define this term to be $V'_{L2}(x,y,z)$. It is also noted that $V'_{L2}(x,y,z)$ has physical significance. This term is recognized as the voltage at (x,y,z) which would have been produced had the problem been composed only of an <u>infinite</u> medium of homogenous conductivity σ_2 with a line of current of length 2L, directed parallel to the x axis and having a center at (xI,yI,zI). The solution of this problem is now obtained with an alternate method and will be substituted for the undefined term in V_{L2} whenever the point of solution lies on the current line.

For the purposes of calculating the potentials on the line of current in an infinite medium, the line of current may be replaced

with a tube of current of length 2L and diameter 2d, with a total current I leaving from the surface of the tube, uniformly distributed over the surface area of the tube with current density ρ given by

$$\rho = \frac{I}{(2\pi d)(2L)} = \frac{I}{4\pi dL}$$

The equation for the potential in an infinite medium of homogeneous conductivity σ_2 is given by the surface integral of the current distribution weighted by $1/4\pi r\sigma_2$, where r is the distance measured from each current element to the point of voltage evaluation. For a current tube parallel to the x-axis centered at (xI,yI,zI) the voltage on the tube center line (y=yI, z=zI) is

$$V(x,yI,zI) = \frac{1}{4\pi\sigma_2} \int_0^{2\pi} \int_{xI-L}^{xI+L} \frac{\frac{I}{4\pi dL}}{\sqrt{(x-x_s)^2+d^2}} \, dx_s \, d\alpha$$

where α is defined in Figure 19.

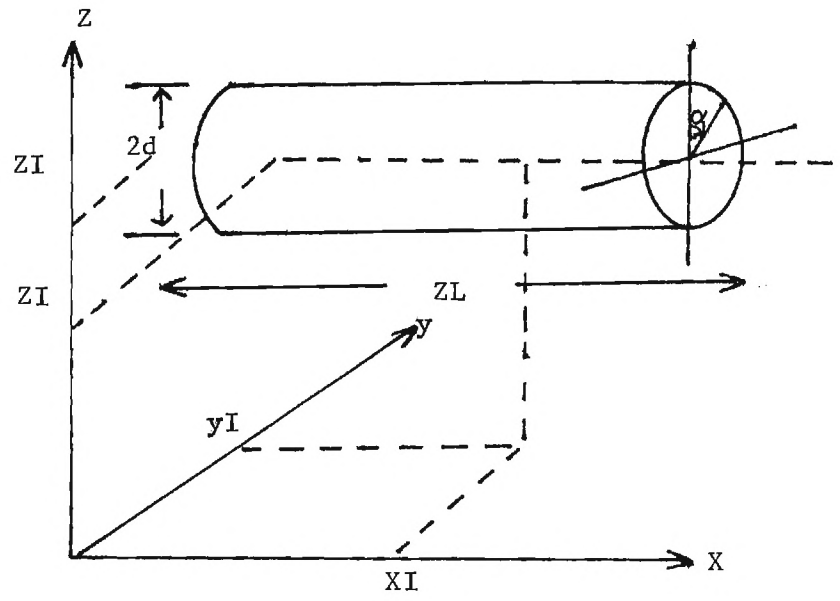

Figure 19

Geometry of Current Tube

Evaluating the integral yields

$$V(x,yI,zI) = \frac{1}{8\pi\sigma_2 L} \ell n \left[\frac{\sqrt{(|x-xI|+L)^2+d^2}+|x-xI|+L}{\sqrt{(|x-xI|-L)^2+d^2}+|x-xI|-L} \right] \qquad (12)$$

Thus for cases in which the voltage of the line current must be evaluated on the line current, the first term of equation (11) is replaced with equation (12). When the voltage is evaluated at the center of the line current (center of tube current) the resulting voltage is known as the self-potential of the tube. For self-potential evaluation, equation (12) becomes

$$V'_{L2}(xI,yI,zI) = \frac{I}{8\pi\sigma_2 L} \ell n \left[\frac{\sqrt{L^2+d^2}+L}{\sqrt{L^2+d^2}-L} \right] \qquad (13)$$

Comparison of equation (12) with the first term of equation (11) shows that they are identical when d=0 and that the two results become asymptotically equal as $|x-xI|$ increases beyond L. As an example, let $|x-xI|$ be greater than L by 10 radii, 10d; the voltage equation derived above for the tube of current becomes:

$$V(10d+ xI +L, yIzI) = \frac{I}{8\pi\sigma_2 L} \ell n \left[\frac{\sqrt{400d^2+d^2}+20d}{\sqrt{100d^2+d^2}+10d} \right]$$

$$= \frac{I}{8\pi\sigma_2 L} \ell n \left[\frac{\sqrt{401d^2}+20d}{\sqrt{101d^2}+10d} \right]$$

$$\simeq \frac{I}{8\pi\sigma_2 L} \ell n \left[\frac{\sqrt{400d^2}+20d}{\sqrt{100d^2}+10d} \right]$$

The last expression is seen to be equal to the first term of equation (11) when evaluated on a line colinear with the line source.

The above analysis has shown that the voltage equations for lines of currents are the same as the equations of tubes of currents with finite diameter as long as the evaluation of the voltages is performed many diameters from the tube. The analysis concludes having developed voltage equations in all three regions of space for a tube of current located at (xI,yI,zI). The self-potential was defined as the voltage at the center of the tube. The next section is devoted to solving for the currents leaving N tubes of current all located in the middle region of a three region conducting space.

C. SOLUTION FOR N CONDUCTORS

The development up to this point has been devoted to the calculation of the voltage due to a single tube of current in the middle region of a three region space. In this section a method will be presented for the calculation of the voltage in all three regions due to N current tubes each with a different potential. This procedure requires that the currents from each tube be computed first and their effects combined by superposition to obtain the voltages in the three regions.

From the superposition theorem, the voltage at any point is space is equal to the sum of the voltages due to all sources in the space. The equation for the voltage in region two due to N tubes of current in region two is given by:

$$V_{LN2}(x,y,z) = \sum_{i=1}^{N} V_{L2i}(x,y,z,xI_i,yI_i,zI_i,LENGTH_i,DIA_i,I_i)$$

where, for clarity, the voltage V_{L2i}, the voltage due to the i^{th} tube of current, is shown explicitly to be a function of the coordinates of the center of the tube (xI_i,yI_i,zI_i), the length LENGTH, and diameter DIA_i of the tube and the total current leaving the tube I_i. With the location, length and diameter of the conductor specified V_{L2} becomes a function of only the coordinates of the point of evaluation (x,y,z) and the current I_i. Examination of all voltage equations derived thus far, V_{L2i} is seen to be linearly dependent on the current I_i leaving the tube. A new function is now defined to emphasize the linear dependence of I. The function is called the mutual resistance between the i^{th} current tube and the point of evaluation, the current tube being parallel to the x axis with center at (xI_i,yI_i,zI_i) with length 2L and diameter 2d.

The function is defined as

$$R_{LM2i}(x,y,z) = \frac{V_{L2i}(x,y,z,I)}{I}$$

The mutual resistance is seen to be just the voltage at the point of evaluation due to the i^{th} tube divided by the total current of the i^{th} tube. When the evaluation point is the center of the conductor itself, the mutual resistance becomes the self-resistance of the conductor and the special first term of the V_{L2} equation (Equation (13)) must be employed. It is noted that the mutual and self-resistances are only functions of geometry and the electrical properties of the media. The equation for the voltage at any point (x,y,z) due to N conductors (current tubes) may be written utilizing the newly defined resistances as

$$V_{LN2}(x,y,z) = \sum_{i=1}^{N} I_i R_{LM2i}(x,y,z) \qquad (14)$$

Thus, the values of the currents, I_i, must be obtained. This is done by the following procedure. If the self-potentials of the N current conductors are known, N voltage equations may be written and the N unknown currents solved for. Let the voltage at the center of each conducting tube be given by $V_i \equiv V_{LN2}(xI_i, yI_i, zI_i)$, $i = 1,2, \ldots ,N$. Also define $R(i,j) \equiv R_{LM2i}(xI_j, yI_j, zI_j)$, the mutual resistance $R_{LM2i}(xI_j, yI_j, zI_j)$ between the i^{th} and j^{th} current tubes. Then one can write equation (14) for the i^{th} tube voltage as

$$V_i = \sum_{j=1}^{N} I_j R(i,j), \quad j = 1,2, \ldots ,N.$$

The self potential equations for all N conductors can be written in matrix form as:

$$\begin{bmatrix} V_1 \\ V_2 \\ \cdot \\ \cdot \\ \cdot \\ V_N \end{bmatrix} = \begin{bmatrix} R(1,1) & R(1,2) & \cdots & R(1,N) \\ R(2,1) & R(2,2) & & \cdot \\ & & & \cdot \\ & & & \cdot \\ & & & \cdot \\ R(N,1) & & & R(N,N) \end{bmatrix} \begin{bmatrix} I_1 \\ I_2 \\ \cdot \\ \cdot \\ \cdot \\ I_N \end{bmatrix}$$

If the voltages are specified, the matrix equation is then solved for the N currents I_i. The resulting I_i's are used in equation (14) to solve for the voltage at any point in region two. Voltages in region one and three are calculated using equations similar to equation (14) as

$$V_{LN1}(x,y,z) = \sum_{i=1}^{N} I_i R_{LM1i}(x,y,z)$$

and

$$V_{LN3}(x,y,z) = \sum_{i=1}^{N} I_i R_{LM3i}(x,y,z)$$

where

$$R_{LM1i}(x,y,z) \triangleq \frac{V_{L1i}(x,y,z)}{I_i}$$

and

$$R_{LM3i}(x,y,z) \triangleq \frac{V_{L3i}(x,y,z)}{I_i}$$

and $V_{Lli}(x,y,z)$ is the voltage produced in region one at (x,y,z) due to the i^{th} current tube. A similar definition holds also for $V_{L3i}(x,y,z)$.

In summary, a method has been presented for the calculation of the voltage at any point in space due to N tubular conductors of finite length and diameter, each with a known voltage and each embedded in the middle region of a three-layered conducting media, and each parallel to the x axis. The N conductors were considered to be independently located within the middle region and the conductors are assumed to be electrically disconnected. The next section will consider the problem of supplying the conductors from a power source, connecting the N conductors together and allowing current flow from one conductor to the next.

D. INTERCONNECTION OF CONDUCTORS

The current leaving each of the N conductors must be supplied by an external power source or by interconnection of the N electrodes to external power at some point of the interconnected network. The tubular conductors up to this point have not been physically defined other than by their physical dimensions (length 2L and diameter 2d), by their location (xI,yI,zI) within the middle region and by the fact that they are assumed to be conducting such that current can leave them and enter the conducting media. The tubular conductors are now given a physical form containing some general properties. The cross section of the subsection conductors is shown in Figure 20 where the conductors are seen to have a hollow, non-conducting core of radius r_1, a cylindrical metallic tube of conductivity σ_c, with outer radius r_2, and a semi-conducting jacket of outer radius r_3 and conductivity σ_J. The physical description is general to the extent that r_1 may have a minimum value of zero, and σ_c, σ_J, r_2, and r_3 may be variable over wide ranges. The primary restrictions as will be seen later, are that the longitudinal impedance of the subsections be predominantly determined by the metallic conductor and that the radial impedance be determined primarily by the semiconducting jacket.

Most metallic conductors used for high current transmission such as aluminum or copper have conductivities on the order of 5×10^7 mhos/meter, whereas typical cable semiconducting carbon impregnated jackets have conductivities on the order of 2 mhos/meter, thus the above restrictions are easily met as long as the cross-sectional area of the jacket is not 2.5×10^7 times greater than the cross-sectional area of the conductor. Under these conditions, a resistive circuit model for a small conducting segment is given as shown in Figure 21. The current leaving the small

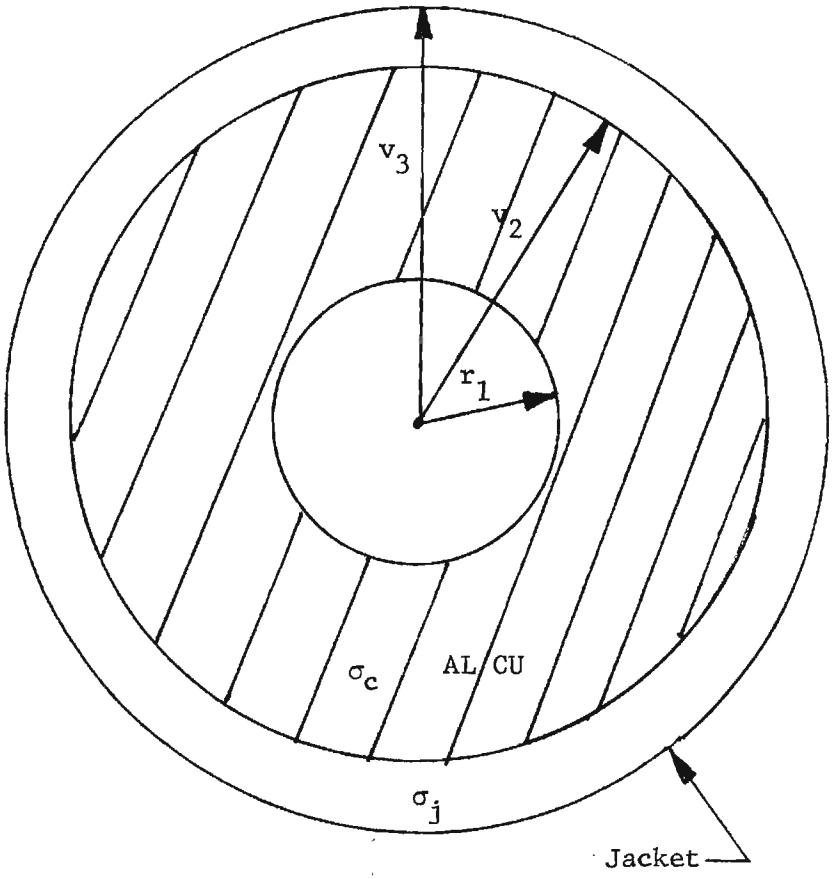

Figure 20

CROSSECTION OF CONDUCTOR

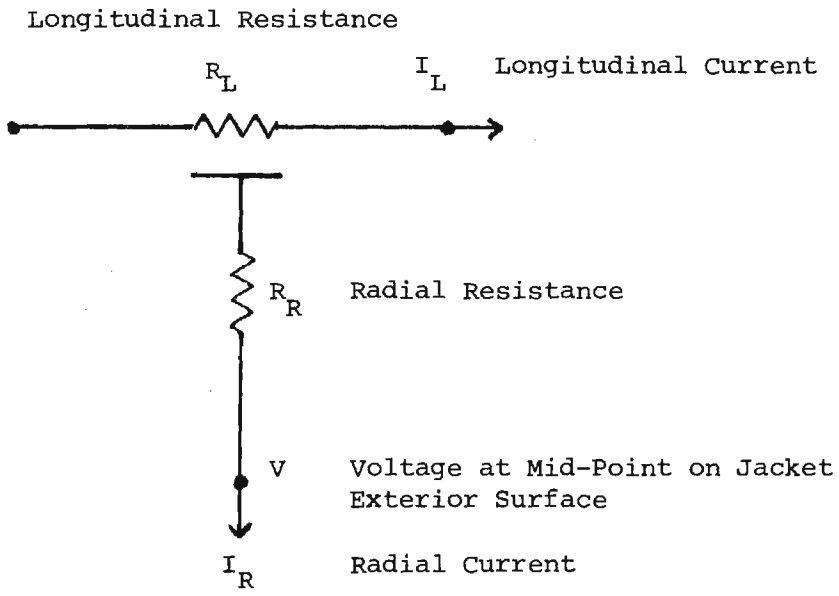

FIGURE 21. Distributed Circuit Model of the Conducting Segment.

section of cable is divided into two components, a longitudinal current I_L and a radial current I_R. The longitudinal current produces a voltage drop of

$$V_{dL} = I_L R_L$$

over the length of the section. The radial current is assumed to be distributed uniformly over the length of the conductor with a radial current density given by

$$\rho_r = \frac{I_R}{L} \quad .$$

Associated with the radial density is a longitudinal current which has a value of I_R at the beginning of the section and zero at the end, this longitudinal current is given by

$$I_{LR} = I_R(1 - \frac{x}{L})$$

where x is the longitudinal distance along the conductor length. The longitudinal voltage drop, as a function of distance x along the section, is given by

$$V_L = \int_o^x I_R(1 - \frac{y}{L})R \, dy$$

$$V_L = I_R[x - \frac{x^2}{2L}]R$$

where R is the longitudinal resistance per unit length.

Evaluation at x=L gives the total longitudinal voltage drop across the section due to radial currents as

$$V_L(L) = I_R R \frac{L}{2} = \frac{I_R R_L}{2}$$

where $R_L = R \cdot L$ is the longitudinal resistance of a length L of cable section.

Evaluating $x = \frac{L}{2}$ gives the longitudinal voltage drop at the center of the cable section due to radial currents as

$$V_L(\tfrac{L}{2}) = I_R[\frac{L}{2} - \frac{L^2}{8L}]R = \frac{3\ I_R RL}{8}$$

$$= I_R R_L \frac{3}{8}$$

The radial voltage drop is given by

$$V_R = I_R R_R$$

In summary, the total longitudinal voltage drop across the length of the cable is given by

$$V_L(L) = I_L R_L + \frac{1}{2} I_R R_L$$

and the total longitudinal voltage drop at the center of the cable is given by

$$V_L(\tfrac{L}{2}) = \frac{1}{2} I_L R_L + \frac{3}{8} I_R R_L$$

The total radial voltage drop is given by

$$V_R = I_R R_R$$

The voltage on the outer surface of the cable evaluated at L/2 would involve both the longitudinal and radial voltage drops as given by

$$V(L/2) = V_I - V_L(\frac{L}{2}) - V_R$$

$$= V_I - \frac{1}{2} I_L R_L - \frac{3}{8} I_R R_L - I_R R_R$$

where V_I is the voltage on the inner conductor at x=0.

E. LONGITUDINAL IMPEDANCE

The longitudinal impedance of aluminum or copper conductors at DC is purely resistive and dependent on cross-sectional area and temperature of the conductors as given below. The longitudinal resistance per meter of an aluminum conductor is given by

$$R_L = \frac{1}{AREA} \left[\frac{1 + .0056(t-20°)}{\sigma_{AL20°}} \right]$$

where:

$\sigma_{AL20°}$ = 3.536×10^7 mhos/meter, the conductivity of aluminum at 20° celsius

t = temperature in degrees celsius

The longitudinal resistance per meter of copper conductor is

$$R_L = \frac{1}{AREA} \left[\frac{1 + .004(t-20°)}{\sigma_{CV20}} \right]$$

where:

σ_{CV} = 5.8×10^7 mhos/meter, the conductivity of copper at 20° celsius

The area in the above equations has the units of meters squared. However, cable conductor area is often given in circular mills. The diameter in inches of a round conductor with area of CM circular mills is given by

$$\text{Dia}'' = \frac{\sqrt{CM}}{1000}$$

The area in meters squared of that conductor is given by

$$\text{Area}(m)^2 = \frac{\pi}{4}\left[\frac{CM\ (2.54)^2}{10^{10}}\right]$$

$$\text{Area}(m)^2 = CM\left[\frac{5.067075}{10^{10}}\right]$$

As an example, an aluminum conductor with 1,250,000 circular mill area at 75°C has a resistance per meter of

$$R_L = \frac{1}{1.25\text{x}10^6\left[\frac{5.067075}{10^{10}}\right]}\left[\frac{1 + .0056(75-20)}{3.537\text{x}10^7}\right] = \frac{1.308}{2240.28}$$

$$R_L = .00058386\ \Omega/\text{meter}$$

RADIAL IMPEDANCE

The radial impedance of L meters of a cylindrical tube of conducting material with inner radius r_o and outer radius r_1, a conductivity σ_1, and a permeativity of ϵ_1 can be modeled as a parallel resistor and compacitor with the following values:

$$R_1 = \frac{\ell n(r_1/(r_1-r_o))}{2\pi L\sigma_1} \qquad C_1 = \frac{2\pi L\epsilon_1}{\ell n(r_1/(r_1-r_o))}$$

This circuit model of radial impedance can be extended to the multi-layered concentric cylindrical tube as shown in Figure 22. The corresponding circuit model, the resistor, and capacitor values are given in the same figure. At DC the capacitances have no effect on the electrical

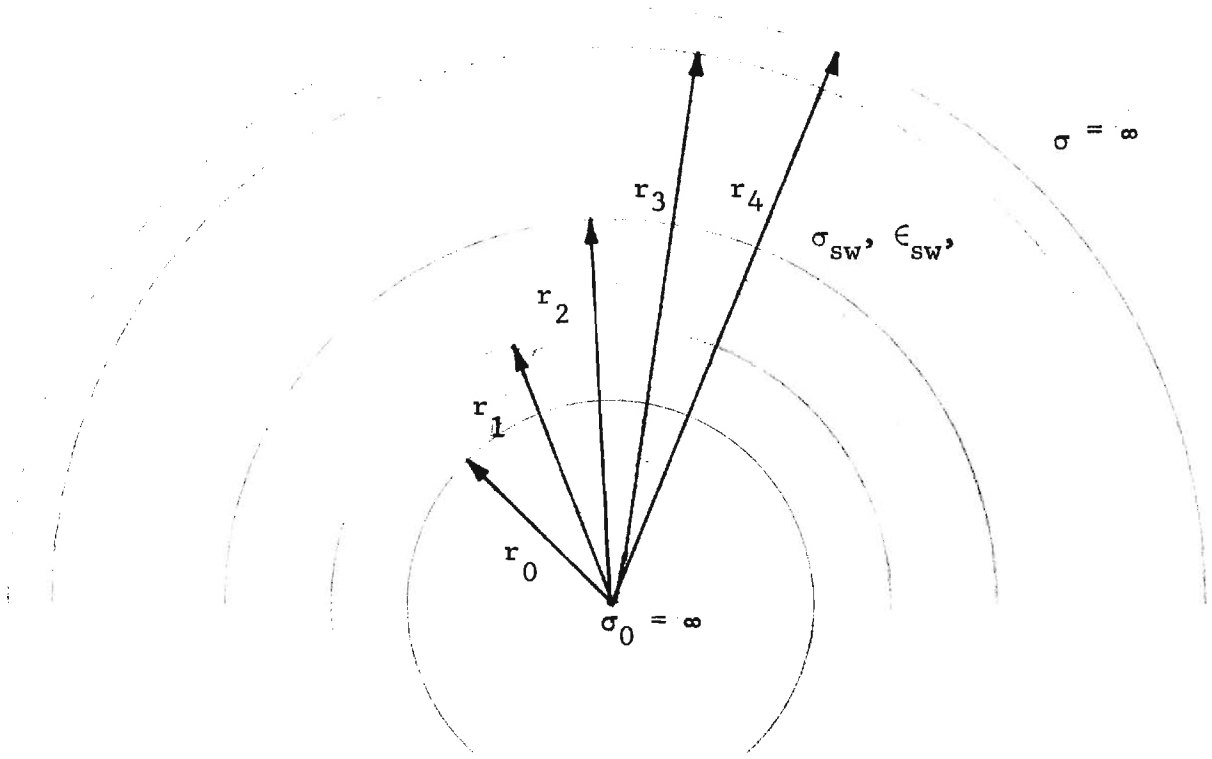

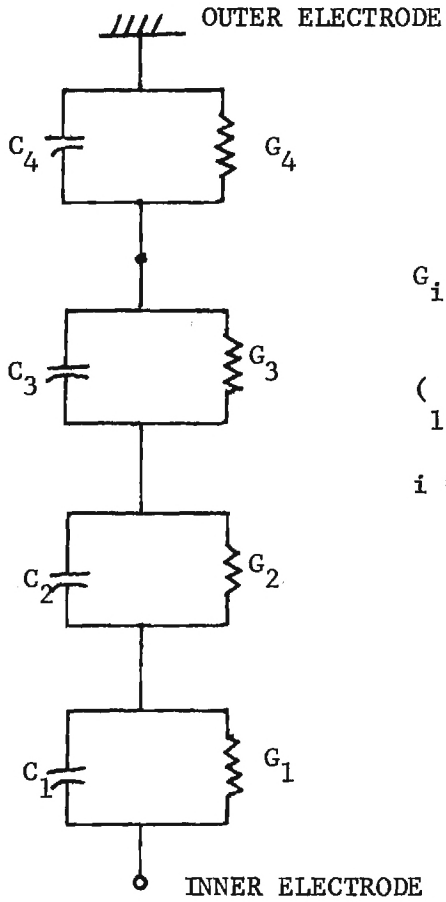

$$C_i = \frac{2\pi L \epsilon_i}{\ln(r_i / r_{i-1})}$$

(farads for L meters of length)

i = 1,2,3,4

$$G_i = \frac{2\pi L \sigma_i}{\ln(r_i / r_{i-1})}$$

(for L meters of length)

i = 1,2,3,4

Figure 22

Multi-layered semiconductor cylinder models

behavior of the cable and the coaxial impedance is purely resistive. The radial resistance of a 3.51 inch outer diameter jacket of thickness 0.1 inch and a conductivity of 2 mhos/meter for a one meter length is given by

$$R_R = \frac{\ell n(\frac{3.51}{2}/\frac{3.31}{2})}{2\pi(1)(2)} = .0046686 \text{ ohm}$$

F. ELECTRICAL MODEL FOR CABLE

A length L_c of cable can be modeled as N sections of cable in series, each with length $L_{c/N}$. On each subsection the assumption is made that the radial current is uniformly distributed over the surface area of the subsection. The magnitude of the radial current of each subsection is unknown and is to be determined by the method presented. What is needed at this point is a relationship between the various currents and voltages on such a cable including the exciting source voltage and its internal resistance and any load resistance at the far end of the cable.

The electrical model for such a cable is shown in Figure 23 where it is seen to be composed of N subsections electrical models as derived previously.

Using the equations derived previously for the voltage at the surface of the cable jacket mid point of each subsection, the equation for the voltage at the i^{th} subsection is given by

$$V_i = V_s - \sum_{j=1}^{i-1} I_j \left[R_s + R_L\left(j-\tfrac{1}{2}\right)\right] - I_i\left[R_s + R_L(i-1) + RL\,\frac{3}{8} + RR\right] \qquad (15)$$

$$- \sum_{j=i+1}^{N} I_j \left[R_s + R_L\left(i-\tfrac{1}{2}\right)\right] - I_L\left[R_s + R_L\left(i-\tfrac{1}{2}\right)\right]$$

A similar equation is written for V_L as

$$V_L = V_s - \sum_{j=1}^{N} I_j \left[R_s + R_L\left(j-\tfrac{1}{2}\right)\right] - I_L\left(R_s + NR_L\right)$$

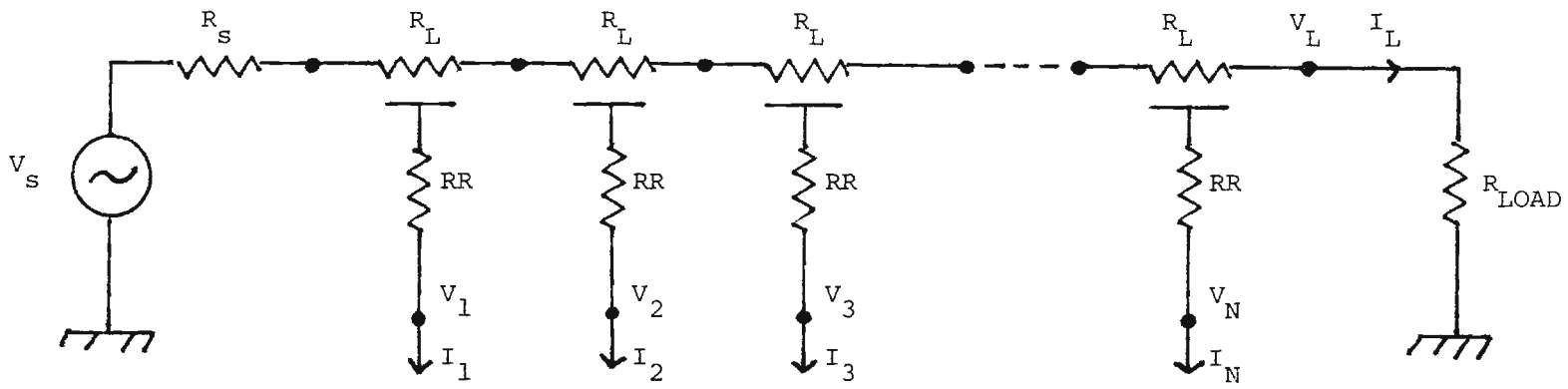

FIGURE 23. Distributed Circuit Model for N Subsection Electrode.

Another equation may be written for V_L which includes the resistance of the load R_{LOAD} as

$$V_L = I_L R_{LOAD}$$

Subtracting the two equations for V_L and rearranging yields:

$$0 = V_s = \sum_{j=1}^{N} I_j [R_s + R_L(j-\tfrac{1}{2})] - I_L [R_s + NR_L + R_{LOAD}] \qquad (16)$$

This equation is the auxiliary equation which must be used when a load is attached to the cable.

G. SOLUTION FOR UNKNOWN RADIAL AND LOAD CURRENTS

The two sets of voltage equations, one from the solution of Laplace's equations for cylindrical conductors, and one from the circuit model for the cable can now be equated and unknown currents solved for. The Laplace equation solution yields a linear set of N equation relating the N cylindrical subsection mid point voltages to the N uniform radial currents for each subsection as:

$$\begin{bmatrix} V_1 \\ V_2 \\ \cdot \\ \cdot \\ \cdot \\ V_N \end{bmatrix} = \begin{bmatrix} R(1,1) & R(1,2) & \cdots & R(1,N) \\ R(2,1) & R(2,2) & \cdots & \\ \cdot & & & \\ \cdot & & & \\ \cdot & & & \\ R(N,1) & & & R(N,N) \end{bmatrix} \begin{bmatrix} I_1 \\ I_2 \\ \cdot \\ \cdot \\ \cdot \\ I_N \end{bmatrix}$$

where the R(i,i) terms are the self-resistances of each cylindrical subsection and the R(i,j) terms are the mutual resistances between the subsections.

The ohms law solution of the cable circuit model yielded as a set of N+1 equations relating the N radial currents plus the load current to the N subsection mid point voltages plus the load voltage. This set of equations is written

$$\begin{bmatrix} V_1 \\ V_2 \\ \cdot \\ \cdot \\ \cdot \\ V_N \\ 0 \end{bmatrix} = \begin{bmatrix} V_s \\ V_s \\ \cdot \\ \cdot \\ \cdot \\ V_s \\ V_s \end{bmatrix} - \begin{bmatrix} \bar{R}(1,1) & \bar{R}(1,2) & \cdots & \bar{R}(1,N) & \bar{R}(1,N+1) \\ \bar{R}(2,1) & \bar{R}(2,2) & \cdots & & \\ \cdot & & & & \cdot \\ \cdot & & & & \cdot \\ \cdot & & & & \cdot \\ \bar{R}(N,1) & & & \bar{R}(N,N) & \cdot \\ \bar{R}(N+1,1) & & & & \bar{R}(N+1,N+1) \end{bmatrix} \begin{bmatrix} I_1 \\ I_2 \\ \cdot \\ \cdot \\ \cdot \\ I_N \\ I_L \end{bmatrix}$$

where $\bar{R}(i,j)$ $1 \leq i \leq N$, $1 \leq j \leq N+1$ are the resistance terms in equation (15) derived above and $\bar{R}(N+1,j)$ $1 \leq j \leq N+1$ are the resistance terms in equation (16) for the load voltage.

Subtracting these two sets of equations yields:

$$\begin{bmatrix} V_s \\ V_s \\ \cdot \\ \cdot \\ \cdot \\ V_s \\ V_s \end{bmatrix} = \begin{bmatrix} R(1,1)+\bar{R}(1,1) & R(1,2)+\bar{R}(1,2) & \cdots & R(1,N)+\bar{R}(1,N) & \bar{R}(1,N+1) \\ R(2,1)+\bar{R}(2,2) & R(2,2)+\bar{R}(2,2) & & \cdot & \cdot \\ \cdot & & & \cdot & \cdot \\ \cdot & & & \cdot & \cdot \\ \cdot & & & \cdot & \cdot \\ R(N,1)+\bar{R}(N,1) & \cdots & & R(N,N)+\bar{R}(1,N) & \bar{R}(N,N+1) \\ \bar{R}(N+1,1) & & & R(N+1,N) & \bar{R}(N+1,N+1) \end{bmatrix} \begin{bmatrix} I_1 \\ I_2 \\ \cdot \\ \cdot \\ \cdot \\ I_N \\ I_L \end{bmatrix}$$

This set of N+1 simultaneous linear equations may now be solved for the N radial currents and the load current as all other terms in these equations are known. For the case of no load resistance and hence $I_L=0$, this set of equations reduces to the first N equations where the $(N+1)^{th}$ term of each equation is missing.

H. TWO ELECTRODE SOLUTION

The Laplace solution of N electrode subsection currents is not influenced by the electrical connections of the subsections. Thus the N linear equations developed from the Laplace solution remain the same for any connections or location of subsections. The key factor in determining the number of electrodes present is the circuit model which links certain subsections together, such that longitudinal current leaving the i^{th} subsection enters the $i+1^{th}$ subsection. For the case of two electrodes which are each excited by a source: one of voltage + V_s and the other by a source of $-V_s$, the circuit model becomes:

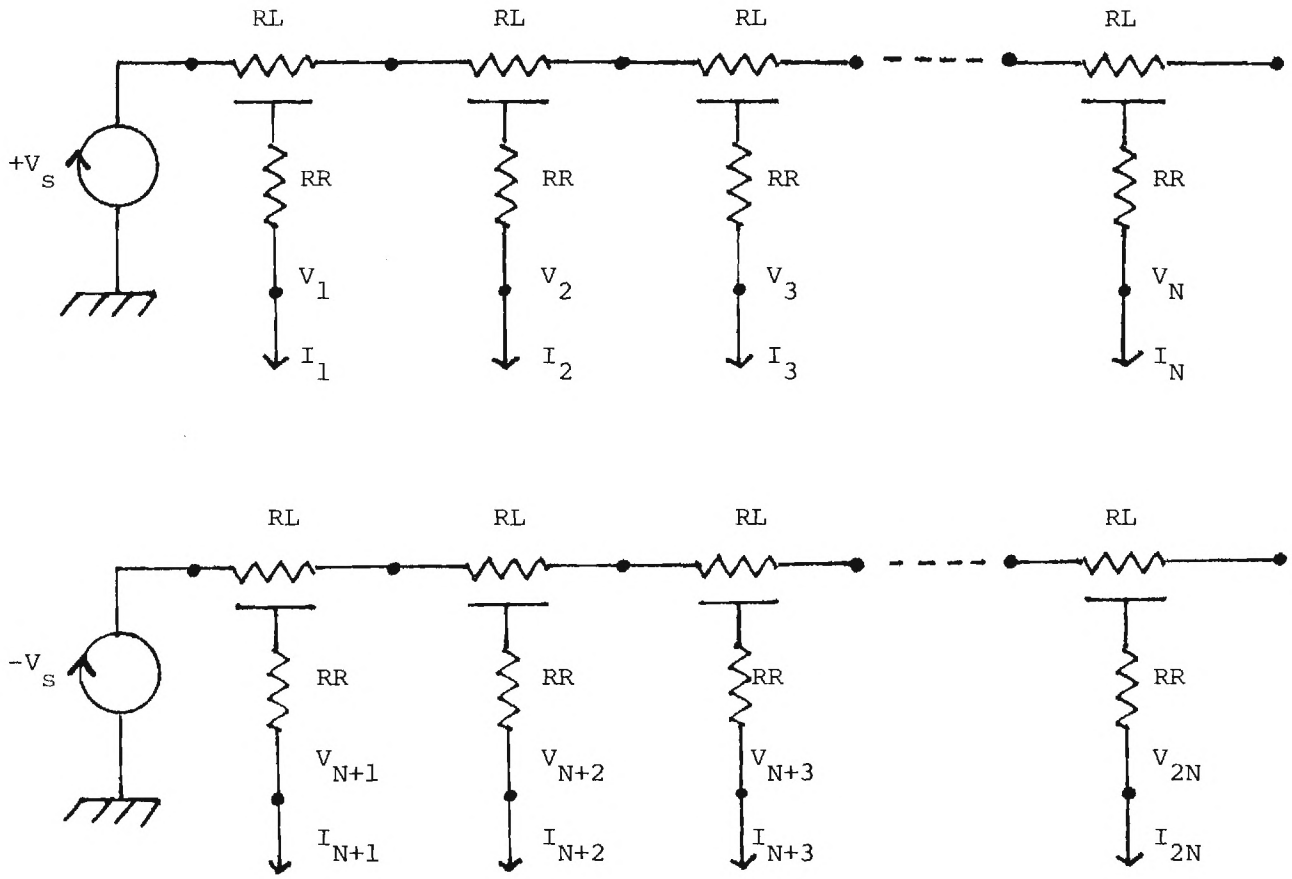

where it can be seen that, for simplicity, the source impedances have been set to zero and there is no load attached to either electrode. Thus, in the two electrode problem subsections 1 through N are connected in series and supplied by $+V_s$ and subsections N+1 through 2N are connected in series and supplied by $-V_s$. The ohms law circuit equations developed previously are written for each electrode. From these equations and from the circuit model it can be seen that V_{N+i} is independent of I_j for $1 \leq i \leq N$ and $1 \leq j \leq N$. The resulting matrix of equations, resulting from the two electrode circuit model is

$$\begin{bmatrix} V_1 \\ \cdot \\ \cdot \\ \cdot \\ V_N \\ V_{N+1} \\ \cdot \\ \cdot \\ \cdot \\ V_{2N} \end{bmatrix} = \begin{bmatrix} V_s \\ \cdot \\ \cdot \\ \cdot \\ V_s \\ -V_s \\ \cdot \\ \cdot \\ \cdot \\ -V_s \end{bmatrix} - \begin{bmatrix} \bar{R}(1,1) & \cdots & \bar{R}(1,N) & & & \\ \cdot & & \cdot & & 0 & \\ \cdot & & \cdot & & & \\ \cdot & & \cdot & & & \\ \bar{R}(N,1) & \cdots & \bar{R}(N,N) & & & \\ & & & \bar{R}(N+1,N+1) & \cdots & \bar{R}(N+1,2N) \\ & 0 & & \cdot & & \cdot \\ & & & \cdot & & \cdot \\ & & & \cdot & & \cdot \\ & & & \bar{R}(2N,N+1) & \cdots & \bar{R}(2N,2N) \end{bmatrix} \begin{bmatrix} I_1 \\ \cdot \\ \cdot \\ \cdot \\ I_N \\ I_{N+1} \\ \cdot \\ \cdot \\ \cdot \\ I_{2N} \end{bmatrix}$$

Subtracting the Laplace solution set of linear equations, which are the same for any set of 2N conductors, yields:

$$
\begin{bmatrix} V_s \\ \cdot \\ \cdot \\ \cdot \\ V_s \\ \\ -V_s \\ \cdot \\ \cdot \\ \cdot \\ -V_s \end{bmatrix} =
\begin{bmatrix}
\begin{matrix} R(1,1)+\bar{R}(1,1) & \cdots & R(1,N)+\bar{R}(1,N) \\ \vdots & & \vdots \\ R(N,1)+\bar{R}(N,1) & \cdots & R(N,N)+\bar{R}(N,N) \end{matrix} &
\begin{matrix} R(1,N+1) & \cdots & R(1,2N) \\ \vdots & & \vdots \\ R(N,N+1) & \cdots & R(N,2N) \end{matrix} \\
\begin{matrix} R(N+1,1) & \cdots & R(N+1,N) \\ \vdots & & \vdots \\ R(2N,1) & \cdots & R(2N,N) \end{matrix} &
\begin{matrix} R(N+1,N+1)+\bar{R}(N+1,N+1) & \cdots & R(N+1,2N)+\bar{R}(N+1,2N) \\ \vdots & & \vdots \\ R(2N,N+1)+\bar{R}(2N,N+1) & \cdots & R(2N,2N)+\bar{R}(2N,2N) \end{matrix}
\end{bmatrix}
\begin{bmatrix} I_1 \\ \cdot \\ \cdot \\ \cdot \\ I_N \\ \\ I_{N+1} \\ \cdot \\ \cdot \\ \cdot \\ I_{2N} \end{bmatrix}
$$

This set of 2N linear equations may be solved for the unknown radial currents. Examination of the terms of the matrix equation shows that the following variables affect the resultant currents:

Source Voltages

Longitudinal Resistance

- Temperature of Conductor
- Area of Conductor
- Conductivity of Conductor

Radial Resistance

- Jacket Conductivity
- Thickness
- Outer Diameter

Length of Cables

Number of Subsections

Head to Tail Separation of Cables

Conductivity of Sea

Electrical Depth of Sea

Submergence of Cable

Conductivity of Sea Bottom

Thus many variables must be considered in the electrical design of the two electrode system.

The resultant currents are used in two ways. First, the current density for each subsection is determined by dividing the subsection current by the surface area of the subsection as follows:

$$\rho_i = \frac{I_i}{\pi\ 2d * \frac{\text{Length}}{N}}$$

The current density is used in electrochemical calculations for the electrode. Second, the total resistance of the two cable circuit

including the combined effects of electrode longitudinal resistance, electrode jacket radial resistance and sea path resistance is determined as follows:

$$R = \frac{2V_s}{\sum_{i=1}^{N} I_i}$$

This resistance plus the resistance of the S cable are used to determine the voltage requirements for a desired total current.

I. Preliminary Results

A computer program has been written and tested to implement the solutions presented above. The following hypothetical two-electrode case, as given in Table III was programmed.

Table III

Analysis Conditions

Sea Parameters:	
Water Conductivity	4.0 mhos/meter
Electrical Depth	100 meters
Bottom Conductivity	5.0×10^{-3} mhos/meter
Anode Parameters:	
Length	45.72 meters
Outer Diameter	0.09 meters
Submergence	3.0 meters
Metallic Conductor	Aluminum
Metal Conductivity (20^{o} C)	3.536×10^{7} mhos/meter
Metal Crossectional Area	1,250,000 cm
Metal Temperature	75^{o} C
Jacket Type	semi-conducting
Jacket Conductivity	2×10^{-3} mhos/meter
Jacket Thickness	0.00254 meters
Longitudinal Resistance	.0000584 ohms/meter
Radial Resistance	.0046235 ohm meters
Cathode Parameters: (Same as anode)	
Electrical Separation:	91.44 meters
Source Voltage	100 volts

The anode was segmented into 10 subsections, each of 4.572 meters in length, and the cathode was likewise segmented into 10 subsections, each of 4.572 meters in length. Segment #1 was the leading subsection of the anode and subsection #10 was the trailing subsection of the anode. Segment #11 was the leading subsection of the cathode and segment #20 was the trailing subsection of the cathode. Table IV gives the results of the computations.

The total current leaving the anode was determined to be 6174.12 amps and the total current entering the cathode from the sea was determined to be 6174.13 amps, in good agreement with the anode current. The total resistance of this electrode configuration less S-cable is

$$R = \frac{100 \text{ volts}}{6174.12 \text{ amps}} = 0.0162 \text{ ohms} .$$

Total power delivered by the source is

$$P = 100 \text{ volts} * 6174.12 \text{ amps} = 617{,}412 \text{ watts} .$$

Total power dissipated in electrodes is 15,330.2 watts.

REFERENCE

Smythe, W.R., "Static and Dynamic Electricity," McGraw-Hill Book Company, 1950, Chapter V.

Table IV

Computer Program Results

Segment Number	Current Entering Sea from Segment (Amps)	Average Current Density on Segment (m Amps/cm^2)	Power Dissipated in Segment Metallic Conductor (Watts)	Power Dissipated in Segment Jacket (Watts)	Total Dissipated Power in Segment (Watts)
1	812.11	62.8	1943.1	145.9	2088.9
2	671.52	51.9	1475.4	99.7	1575.2
3	615.16	47.6	1121.9	83.7	1205.6
4	582.34	45.0	836.3	75.0	911.3
5	562.22	43.5	602.5	69.9	672.4
6	551.40	42.7	411.7	67.2	478.9
7	549.43	42.5	258.7	66.8	325.5
8	558.56	43.2	140.4	69.0	209.4
9	587.17	45.4	55.8	76.3	132.1
10	684.22	52.9	6.8	103.5	110.4
11	-828.04	-64.1	1937.7	151.7	2089.4
12	-681.94	-52.8	1463.0	102.9	1565.9
13	-622.11	-48.1	1106.7	85.6	1192.3
14	-586.37	-45.4	820.8	76.0	896.8
15	-563.55	-43.6	588.3	70.2	658.3
16	-550.09	-42.6	400.0	66.9	466.9
17	-545.42	-42.2	250.1	65.8	315.9
18	-551.62	-42.7	135.1	67.3	202.4
19	-576.74	-44.6	53.4	73.6	127.0
20	-668.24	-51.7	6.5	98.8	105.3

CHAPTER V

MAGNETIC FIELD CALCULATIONS

A. INTRODUCTION

The magnetic field produced by a two electrode system in salt water has three components. These are the field produced by the current in the water, the field produced by the current in the electrodes, and the field produced by the current in the interconnecting cable between the electrodes, i.e. the S-cable. Of these, the calculation of the field due to the current in the water is the most difficult, for the magnetic field at any one point is a function of the current at every point. This dependency makes any numerical solution difficult to implement because of the tremendous number of steps which would be required in the computations. For this reason, it was decided at the beginning of this phase of the project to attempt only a two-dimensional solution to the problem, thus reducing all three-dimensional integrals in the solution to two-dimensional ones. It is well known that the solution to a two-dimensional problem can be used to predict the solution to the equivalent three-dimensional problem if certain symmetries are present. That is the case with the two electrode system.

The major objective of the magnetic field calculations in this phase has been to develop a rapid numerical technique for the calculation of the three components of the magnetic field in the water and their resultant sum. From these calculations, the predominant component of the total magnetic field can be identified and changes in the field can be predicted for different electrode and S-cable geometries. For example, it will be shown in the following that,

under the stated assumptions, the predominant component of the two-dimensional magnetic field is that produced by the S-cable for the assumed geometry. In addition, it will be seen that the magnetic field in this particular case increases by approximately 25% if the length of the S-cable is increased by 50%.

The solution for the three-dimensional field has been obtained, but it has not been implemented numerically. This solution is in a form such that the total magnetic field can be computed from the point source current calculations described in Chapter IV. The three-dimensional solution will be implemented in the next phase of this work. A derivation of the pertinent mathematics is presented in this chapter.

B. THE MAGNETIC FIELD DUE TO THE CURRENT IN THE WATER

Consider the two electrode geometry illustrated in Figure 24. In this figure, the separation between electrodes is 2a and the length of each electrode is b-a. A closed form solution to the electric field in the water, and thus the current in the water, can be obtained if it is assumed that the net charge per unit length on the electrodes is constant. Although this assumption will not permit precise determination of the magnetic field near the electrodes, it will not significantly alter the field in the region far from the electrodes. It can be shown that a uniform line charge has an electric field associated with it that is the same as that produced by an equipotential ellipsoid. Thus the assumption of a uniform line charge is equivalent to that of approximating the electrode by an ellipsoidal conductor which has the shape of a cigar.

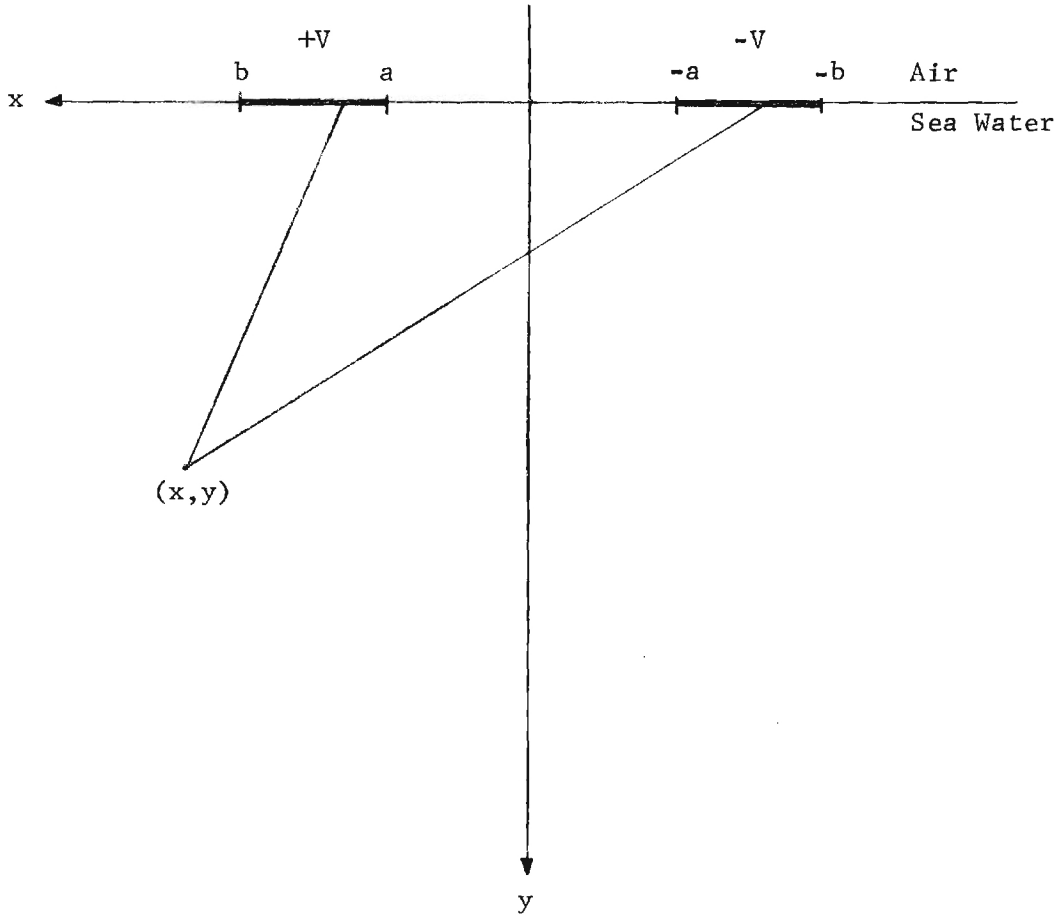

Figure 24. Illustration of the two-dimensional two electrode geometry.

To compute the electric field associated with a uniform line charge, consider the geometry in Figure 25. The two-dimensional radial electric field at the point (x,y) due to the charge element $\rho dx'$ located at x' is given by [1]

$$dE_r = \frac{1}{2\pi\epsilon} \frac{\rho dx'}{r} \tag{1}$$

where ρ is the two-dimensional line charge density with units coulombs per meter, and r is the distance given by

$$r = \sqrt{(x-x')^2 + (y-y')^2} \tag{2}$$

The field component dE_r can be resolved into its x and y components by multiplication by $\cos\theta$ and $\sin\theta$, respectively, where θ is defined in Figure 2. The values for these trigonometric functions are given by

$$\cos\theta = \frac{x-x'}{r} \tag{3}$$

$$\sin\theta = \frac{y}{r} \tag{4}$$

The total x and y electric field components at the point (x,y) can be obtained by summing the differential components due to each charge element ρdx. In the limit, these sums become the following integrals:

$$E_x(x,y) = \frac{\rho}{2\pi\epsilon} \int_{-d}^{d} \frac{(x-x')dx'}{(x-x')^2+y^2} \tag{5}$$

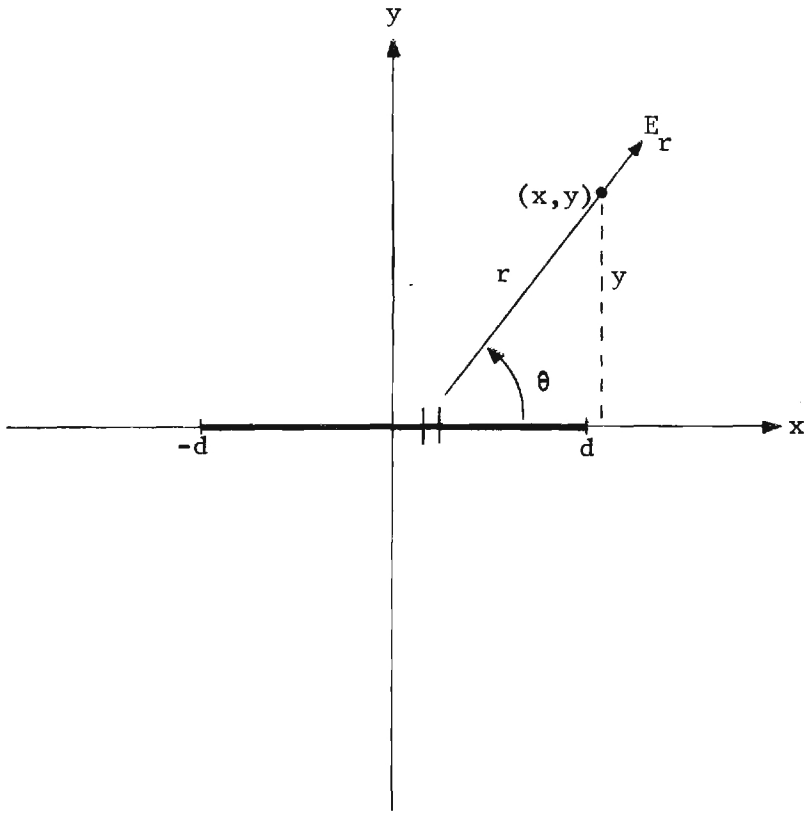

Figure 25. Geometry for the calculation of the electric field associated with a uniform two dimensional charge.

$$E_y(x,y) = \frac{\rho}{2\pi\epsilon} \int_{-d}^{d} \frac{y\,dx}{(x-x')^2+y^2} \tag{6}$$

where the constant charge density ρ has been factored out of the integral. These expressions can be integrated to obtain

$$E_x(x,y) = \frac{\rho}{4\pi\epsilon} \ln \left[\frac{(x+d)^2+y^2}{(x-d)^2+y^2} \right] \tag{7}$$

$$E_y(x,y) = \frac{\rho}{2\pi\epsilon} \left[\tan^{-1}\left(\frac{x+d}{y}\right) - \tan^{-1}\left(\frac{x-d}{y}\right) \right] \tag{8}$$

The expressions for E_x and E_y are not in the desired form, for ρ must be determined as a function of the electrode voltage V. These are related by the capacitance per unit length of the two-dimensional electrode system, or

$$\rho = CV \tag{9}$$

where C has the units of farads per meter. Substitution of (9) into (7) and (8) yields:

$$E_x(x,y) = \frac{CV}{4\pi\epsilon} \ln \left[\frac{(x+d)^2+y^2}{(x-d)^2+y^2} \right] \tag{10}$$

$$E_y(x,y) = \frac{CV}{2\pi\epsilon} \left[\tan^{-1}\left(\frac{x+d}{y}\right) - \tan^{-1}\left(\frac{x-d}{y}\right) \right] \tag{11}$$

The current densities J_x and J_y in the water follow from multiplication of these expressions by the water conductivity σ. They are

$$J_x(x,y) = \frac{\sigma CV}{4\pi\epsilon} \ln\left[\frac{(x+d)^2+y^2}{(x-d)^2+y^2}\right] \tag{12}$$

$$J_y(x,y) = \frac{\sigma CV}{2\pi\epsilon}\left[\tan^{-1}\left(\frac{x+d}{y}\right) - \tan^{-1}\left(\frac{x-d}{y}\right)\right] \tag{13}$$

The above expressions for the current in the water are for the single electrode geometry in Figure 25. The total current in the water for the two electrode geometry of Figure 1 can be obtained by suitable coordinate transformations. For a voltage of +V on the left electrode and -V on the right electrode, these are

$$J_x(x,y) = \frac{\sigma CV}{4\pi\epsilon} \ln\left[\frac{[(x+a)^2+y^2][(x-a)^2+y^2]}{[(x+b)^2+y^2][(x-b)^2+y^2]}\right] \tag{14}$$

$$J_y(x,y) = \frac{\sigma CV}{2\pi\epsilon}\left[\tan^{-1}\left(\frac{x+a}{y}\right)+\tan^{-1}\left(\frac{x-a}{y}\right)-\tan^{-1}\left(\frac{x+b}{y}\right)-\tan^{-1}\left(\frac{x-b}{y}\right)\right] \tag{15}$$

To solve for the magnetic field produced by these currents, we first solve for the two-dimensional magnetic vector potential function. Let the point (x,y) be the field point at which the magnetic vector potentials A_x and A_y are to be found. These are given by

$$A_x(x,y) = \frac{\mu}{2\pi}\int_S J_x(x',y')\ln\left(\frac{r_o}{r}\right)dx'dy' \tag{16}$$

$$A_y(x,y) = \frac{\mu}{2\pi}\int_S J_y(x',y')\ln\left(\frac{r_o}{r}\right)dx'dy' \tag{17}$$

where S is the area over which the currents flow, r_o is the radius of the arbitrary cylinder over which $A_x = A_y = 0$, and r is the distance

between the points (x,y) and (x',y')given by (2). The magnetic field associated with the vector potential is given by

$$\vec{B} = \nabla \times \vec{A}$$

$$= \hat{z}\left[-\frac{\partial Ax}{\partial y} + \frac{\partial Ay}{\partial x}\right] \tag{18}$$

where the ∇ operator operates only on the unprimed coordinates. After a lengthy manipulation, it can be shown that B_z is given by

$$B_z(x,y) = \frac{\mu\sigma CV}{8\pi^2\epsilon}\left[\int_0^\infty\int_{-\infty}^\infty \ell n\left[\frac{[(x'+a)^2+y'^2][(x'-a)^2+y'^2]}{[(x'+b)^2+y'^2][(x'-b)^2+y'^2]}\right]\frac{(y-y')}{(x-x')^2+(y-y')^2}\,dx'dy'\right.$$

$$\left.-2\int_0^\infty\int_{-\infty}^\infty\left[\tan^{-1}\left(\frac{x'+a}{y'}\right)+\tan^{-1}\left(\frac{x'-a}{y'}\right)-\tan^{-1}\left(\frac{x'+b}{y'}\right)-\tan^{-1}\left(\frac{x'-b}{y'}\right)\right]\frac{(x-x')}{(x-x')^2+(y-y')^2}\,dx'dy'\right] \tag{19}$$

This is the desired expression. Although no method has been found to evaluate it in closed form, it can be evaluated numerically as will be discussed in a following section.

A potential problem in the evaluation of (19) is that the integrand in both integrals becomes singular at x=x' and y=y'. However, it can be shown that the integrals are zero over a small region containing this singular point. Thus the singularity can be avoided in any numerical evaluation of B_z. To show this, construct a small circle about the point (x,y) as shown in Figure 26. For d sufficiently small, the only terms in (19) which vary appreciably over this circle are the fractions which have the denominator $(x'-x)^2 + (y'-y)^2$. Thus it is

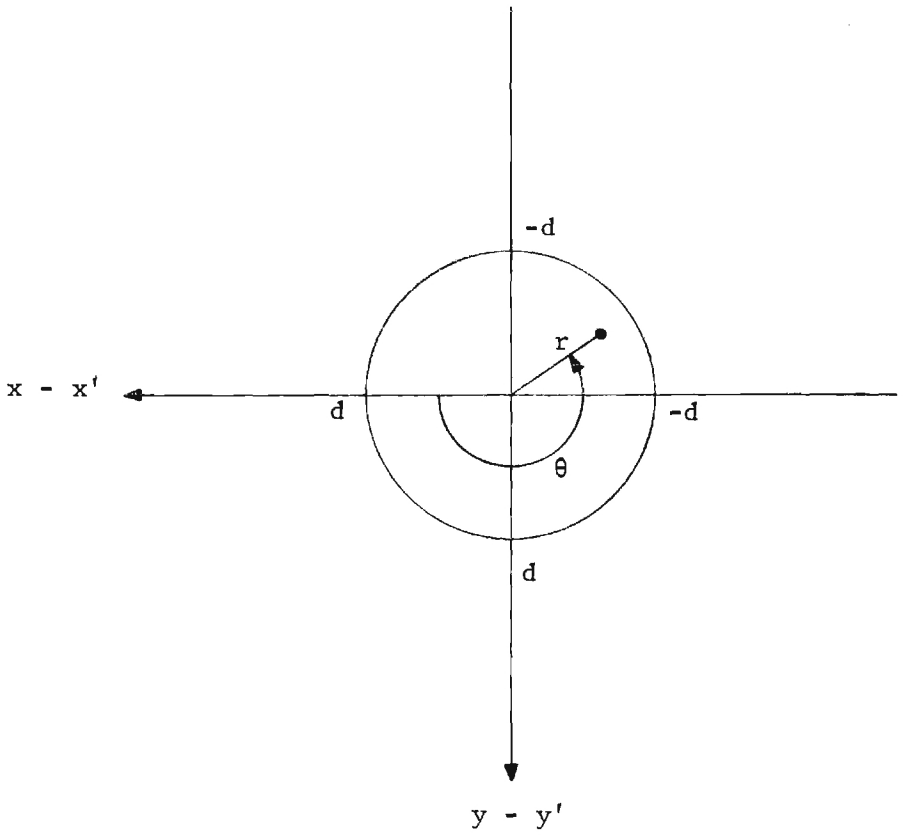

Figure 26. Illustration for calculation of the singular integrals.

only necessary to examine the behavior of the integrals

$$I_1 = \int\int_{\text{circle}} \frac{(y-y')}{(x-x')^2+(y-y')^2}\, dx'dy' \tag{20}$$

$$I_2 = \int\int_{\text{circle}} \frac{(x-x')}{(x-x')^2+(y-y')^2}\, dx'dy' \tag{21}$$

To evaluate I_1 and I_2, we make the substitutions

$$(x-x') = r\cos\theta \tag{22}$$

$$(y-y') = r\sin\theta \tag{23}$$

$$dx'dy' = r\, drd\theta \tag{24}$$

The integrals thus become

$$I_1 = \int_o^{2\pi}\int_o^d \frac{r\sin\theta}{r^2}\, r\, drd\theta \tag{25}$$

$$I_2 = \int_o^{2\pi}\int_o^d \frac{r\cos\theta}{r^2}\, r\, drd\theta \tag{26}$$

It can be seen trivally that both I_1 and I_2 are zero since they are respectively proportional to the integral of $\sin\theta$ and $\cos\theta$ over a 2π interval.

C. THE MAGNETIC FIELD DUE TO THE CURRENT IN THE ELECTRODES

In Figure 24 it will be assumed that the left electrode is fed from the positive output of the generator at the point x=b. The negative output of the generator is connected by the S-cable to the

right electrode at the point x=-a. The two-dimensional, x-directed current at any point in the left electrode is given by

$$I_{x(L)} = - \int_{a}^{x} J_y(x',0)\,dx' \tag{27}$$

where J_y is given by (15). Similarly, for the right electrode, we have

$$I_{x(R)} = - \int_{-b}^{x} J_y(x',0)\,dx' \tag{28}$$

It can be shown that these reduce to

$$I_{x(L)} = - \frac{\sigma CV}{2\epsilon} (x-a), \qquad a \le x \le b \tag{29}$$

$$I_{x(R)} = \frac{\sigma CV}{2\epsilon} (x+b), \qquad -b \le x \le -a \tag{30}$$

The magnetic field at the point (x,y) due to the current in the electrodes is determined by first forming the two-dimensional magnetic vector potential

$$A_x(x,y) = \frac{\mu}{2\pi} \int_{a}^{b} I_{x'(L)} \ln\left(\frac{r_o}{r}\right) dx' + \frac{\mu}{2\pi} \int_{-b}^{-a} I_{x'(R)} \ln\left(\frac{r_o}{r}\right) dx' \tag{31}$$

where r_o and r have been defined in conjunction with (16) and (17). The magnetic field associated with this potential is given by $B_z = -\partial A_x/\partial y$

$$B_z(x,y) = \frac{\mu}{2\pi}\frac{\sigma CV}{2\epsilon}\left[\int_a^b \frac{(x'-a)y}{(x-x')^2+y^2}\,dx' + \int_{-b}^{-a} \frac{(x'+b)y}{(x-x')^2+y^2}\,dx'\right] \tag{32}$$

This expression can be evaluated in closed form to yield

$$B_z(x,y) = \frac{\mu}{2\pi}\frac{\sigma CV}{2\epsilon}\left[\frac{y}{2}\ell n\left[\frac{[(x+a)^2+y^2][(x-b)^2+y^2]}{[(x-a)^2+y^2][(x+b)^2+y^2]}\right]\right.$$

$$\left. +(x-a)\tan^{-1}(\frac{x-a}{y})-(x-a)\tan^{-1}(\frac{x-b}{y})+(x+b)\tan^{-1}(\frac{x+b}{y})-(x+b)\tan^{-1}(\frac{x+a}{y})\right] \tag{33}$$

This is the desired expression.

D. THE MAGNETIC FIELD DUE TO THE CURRENT IN THE S-CABLE

The magnetic field produced by the current in the S-cable can be calculated in closed form from the familiar relation

$$B_z(x,y) = \frac{\mu}{2\pi}\int_{-a}^{b} I_{sc}\,\frac{y}{(x'-x)^2+y^2}\,dx' \tag{34}$$

where I_{sc} is the current in the S-cable. This can be determined from (30) by setting x=-a to obtain

$$I_{sc} = \frac{\sigma CV}{2\epsilon}(b-a) \tag{35}$$

With this substitution, (34) can be evaluated to yield

$$B_z(x,y) = \frac{\mu}{2\pi}\frac{\sigma CV}{2\epsilon}(b-a)\left[\tan^{-1}(\frac{x+a}{y})-\tan^{-1}(\frac{x-b}{y})\right] \tag{36}$$

This is the desired expression.

E. NUMERICAL RESULTS

The two-dimensional solutions presented in the preceding sections have been implemented numerically to solve for the three components of the magnetic field and their resultant or sum over a 1500 foot wide by 750 foot deep rectangle containing the electrodes. Since it is meaningless to calculate the absolute magnetic field levels in the two-dimensional field, only the normalized field has been calculated. Of the three field components, only that produced by the current in the water has not been solved for in closed form. Solution of (19) for this component of the field was implemented by employing the Gaussian quadrature method for numerical integration. The remaining two field components were calculated directly from (32) and (36).

Figures 27, 28 and 29 show, respectively, contour plots of the calculated fields for the current in the water, the current in the electrodes, and the current in the S-cable. The sum of these three field components is shown in Figure 30. It can be seen from these figures that the resultant field is almost everywhere in the same direction as that produced by the current in the S-cable. Thus it can be concluded that the current in the S-cable is the predominant source of the magnetic field. Three-dimensional perspectives of the magnetic fields in Figures 27through 30are shown, respectively, in Figures31 through 34. The vertical height of these plots above the base represents the magnetic field above the arbitrary normalized reference level of -45. The vertical scale is 30 normalized units per inch.

To investigate the effect of the length of the S-cable on the

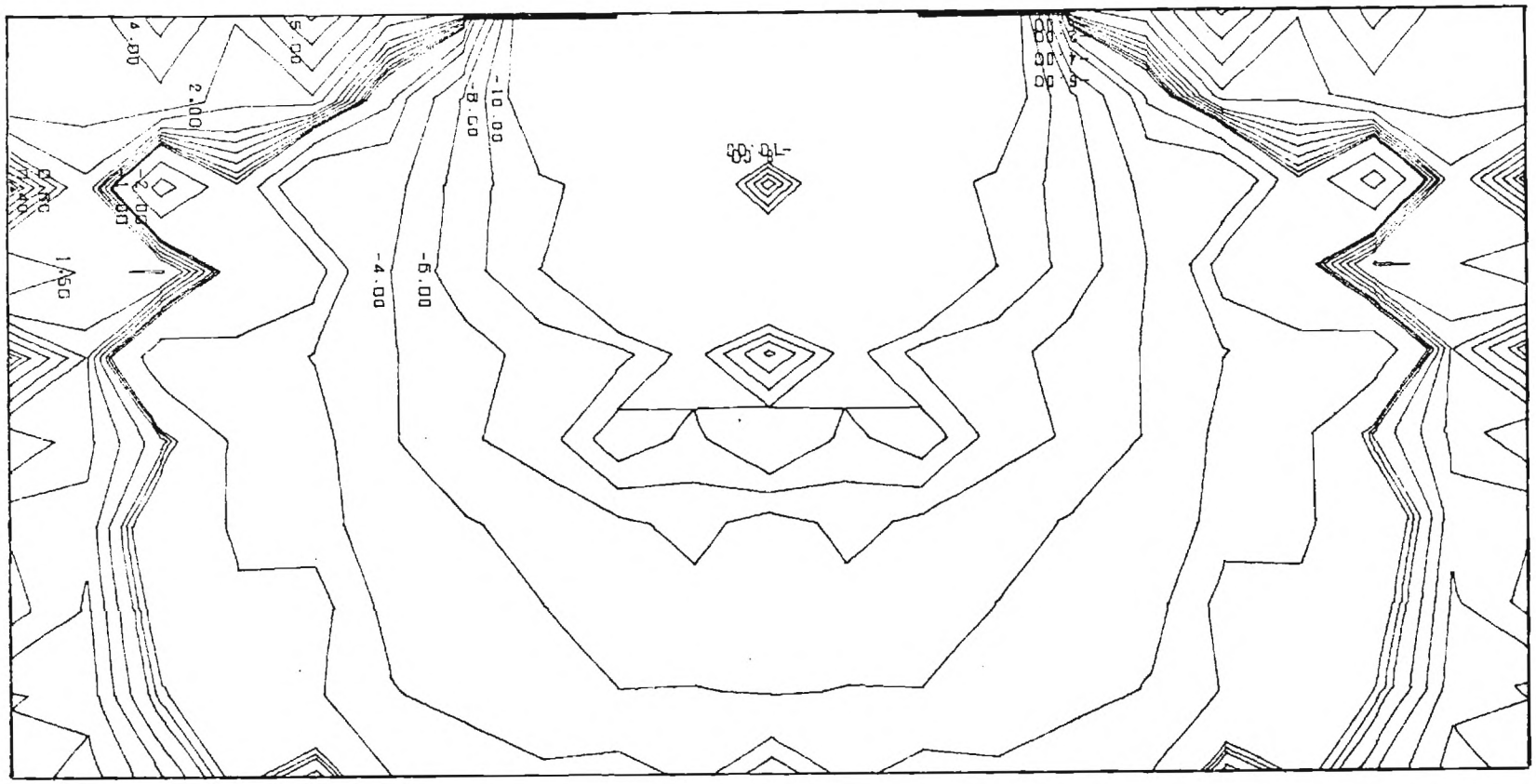

Figure 27. Normalized two-dimensional magnetic field distribution due to the current in the water over a 1500 ft. wide by 750 ft. deep rectangle. 150 ft. electrodes spaced 300 feet apart.

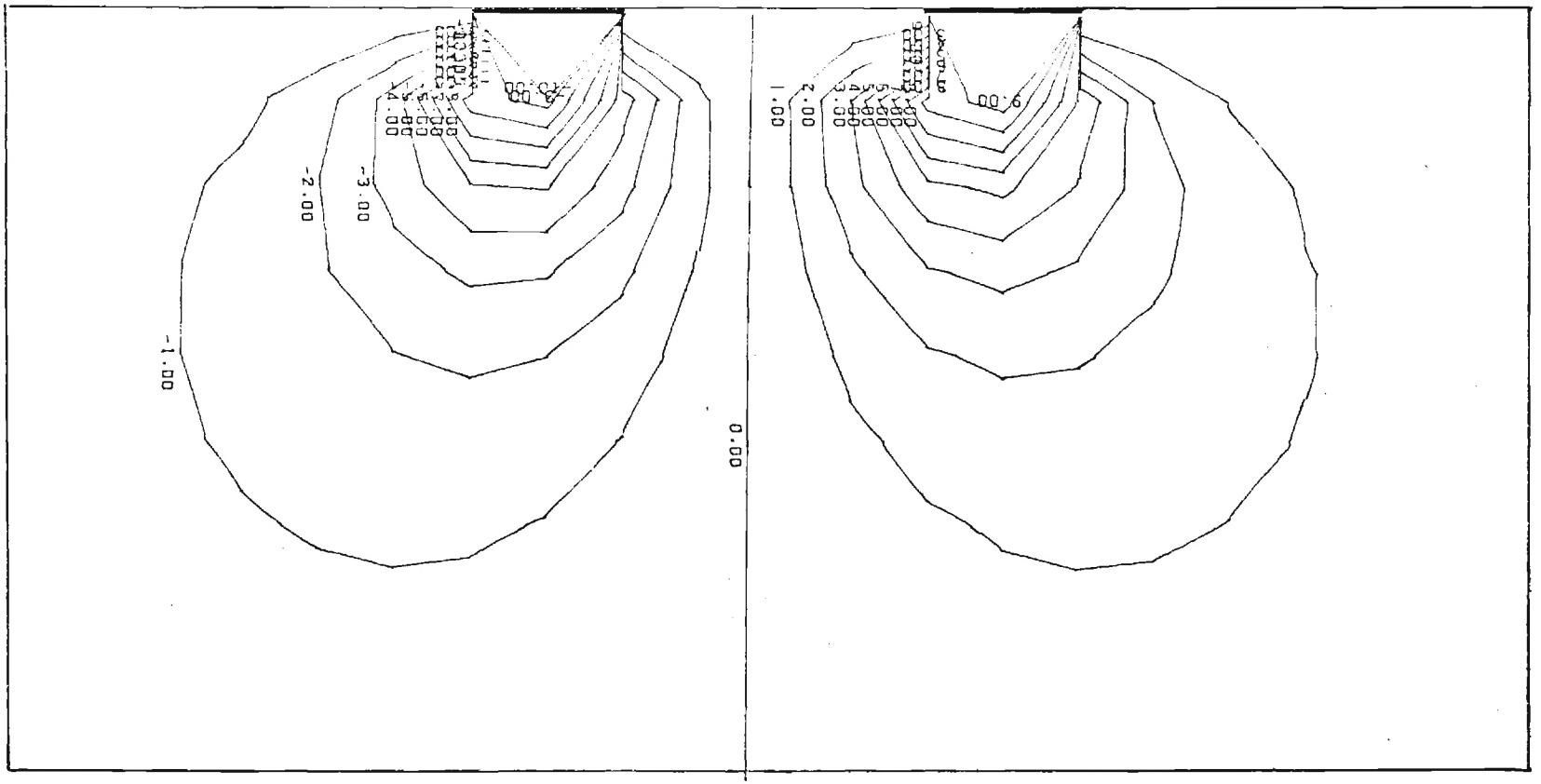

Figure 28. Normalized two-dimensional magnetic field distribution due to the current in the electrodes over a 1500 ft. wide by 750 ft. deep rectangle. 150 ft. electrodes spaced 300 feet apart.

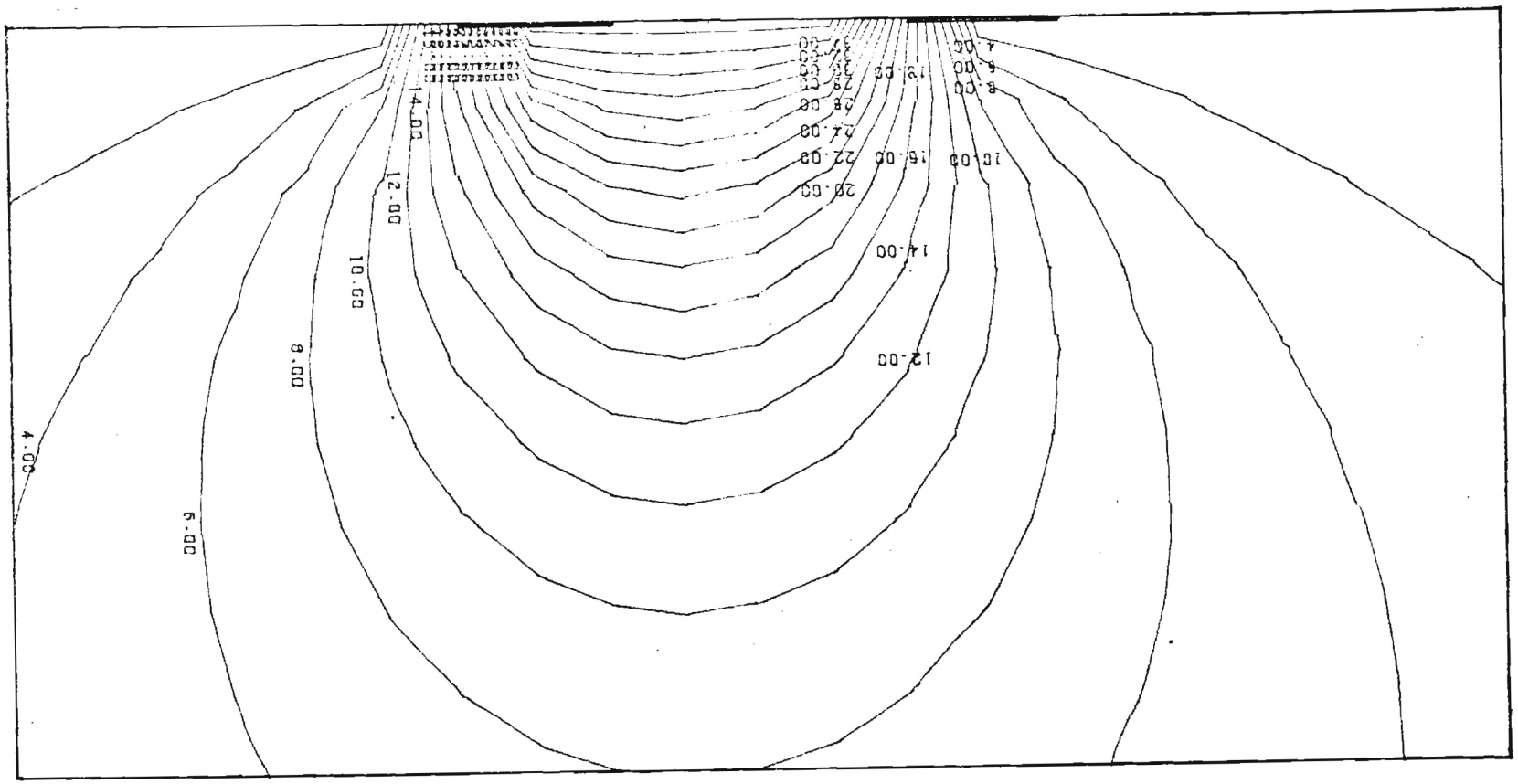

Figure 29. Normalized two-dimensional magnetic field distribution due to the current in the s-cable over a 1500 ft. wide by 750 ft. deep rectangle. 150 ft. electrodes spaced 300 feet apart.

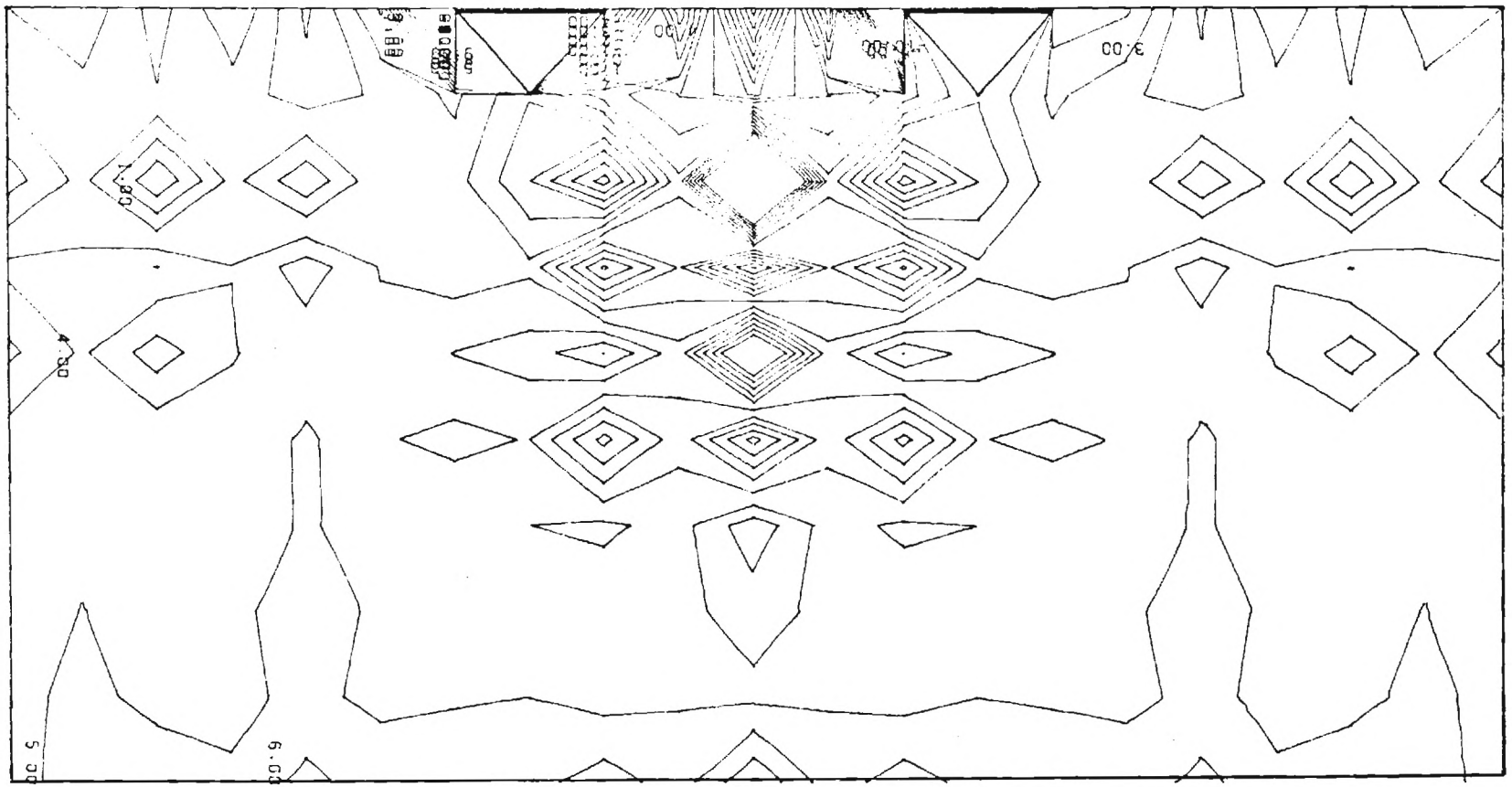

Figure 30. Total, normalized, two-dimensional magnetic field due to the three components of Figures 27, 28, and 29.

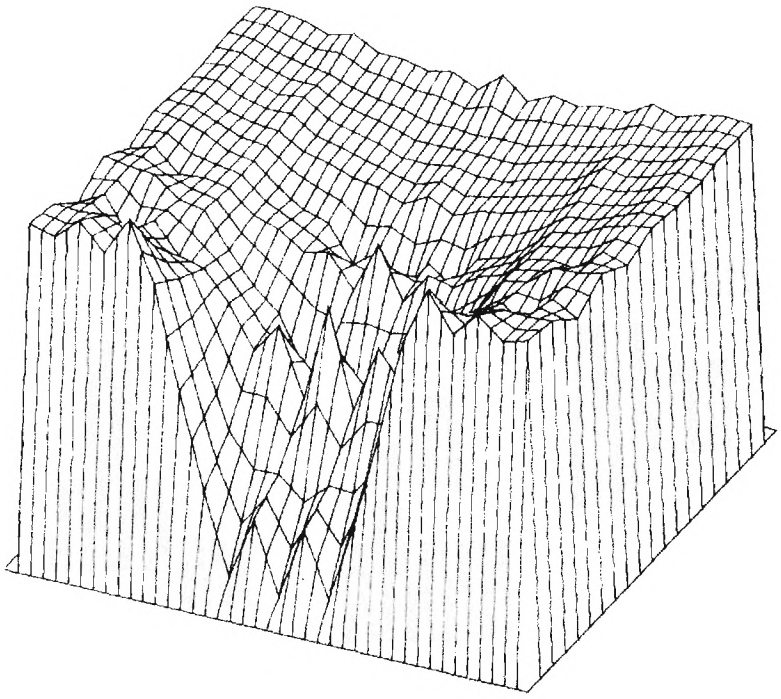

Figure 31. Three-dimensional perspective of the field illustrated in Figure 27.

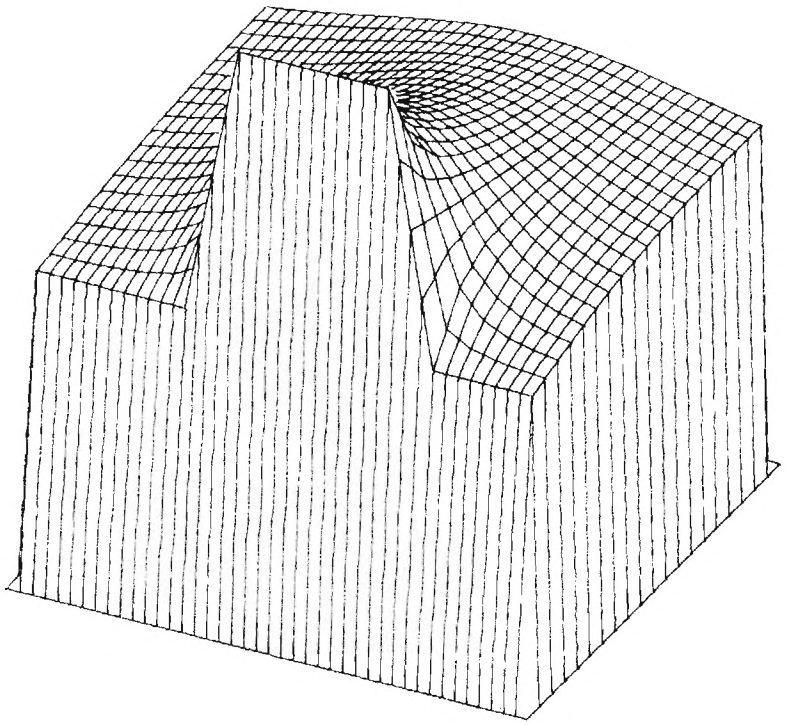

Figure 32. Three-dimensional perspective of the field illustrated in Figure 28.

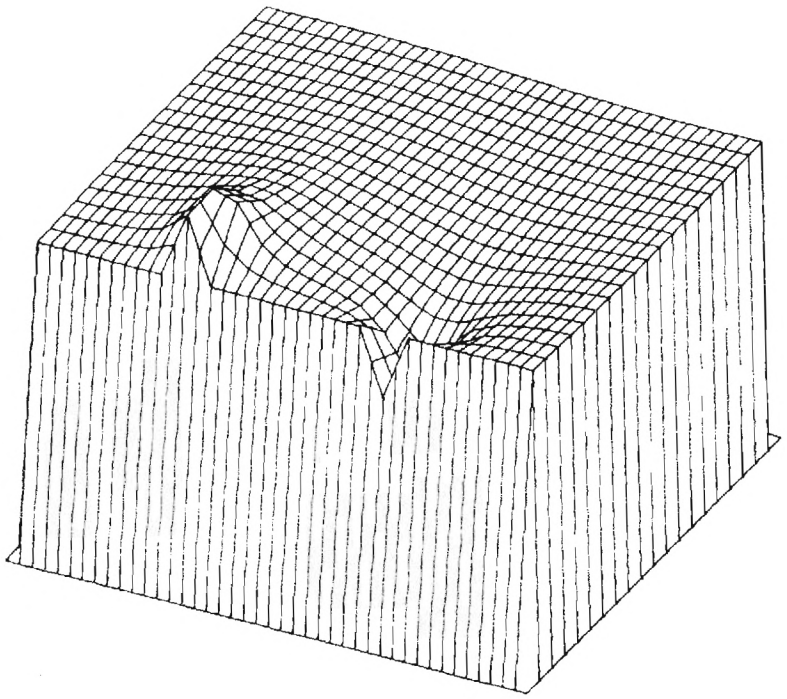

Figure 33. Three-dimensional perspective of the field illustrated in Figure 29.

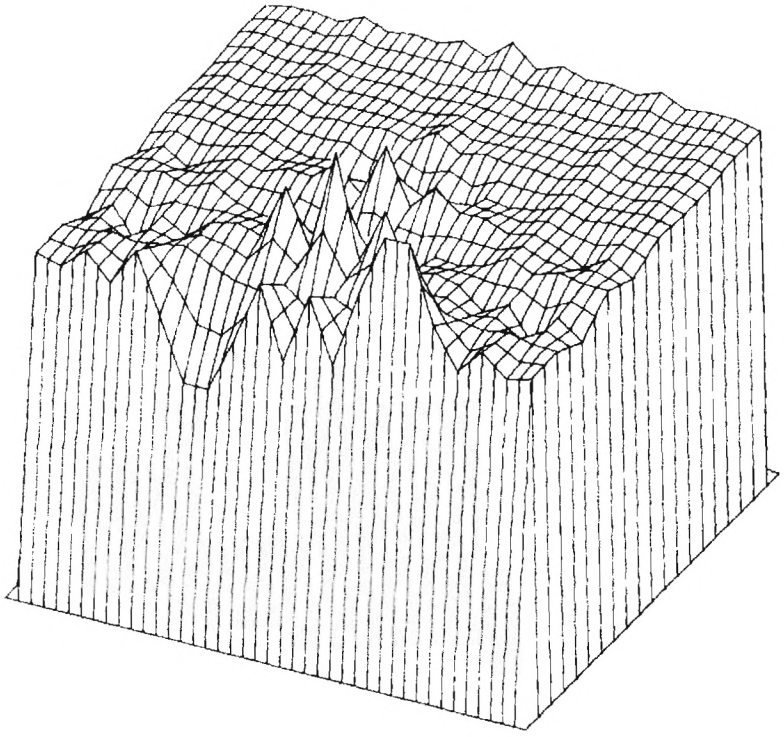

Figure 34. Three-dimensional perspective of the field illustrated in Figure 30.

resultant magnetic field, the calculations were repeated for a 50% increase in electrode separation. The total current was held constant. The results of these calculations are presented in Figures 35 through 38. It can be seen from Figure 38 that the resultant field in the region away from the electrodes has increased by approximately 25%. Whether this conclusions holds for increased distances from the electrodes is not known. However, it will be investigated in more detail with the numerical implementation of the three-dimensional solution derived in the following section.

F. THE THREE-DIMENSIONAL FIELD

Figure 39 illustrates a point source of current at the interface between a conducting and a non-conducting medium. It is desired to calculate the magnetic field produced by the current emitted by this source under the assumption that the current density in the conducting medium is constant over any sphere centered on the source. Once the field associated with a single point source is obtained, superposition can be used to obtain the field of a more complex shaped source by approximating the source with a set of point sources or by integrating over it.

With reference to Figure 39 the current density at the point (x',y',z') is given by

$$\vec{J}(x',y',z') = \hat{r}' \frac{I}{2\pi r'^2} \tag{37}$$

where I is the total current emitted by the source. By symmetry, the current must flow in the radial or $\hat{r}'$ direction. The three-dimensional

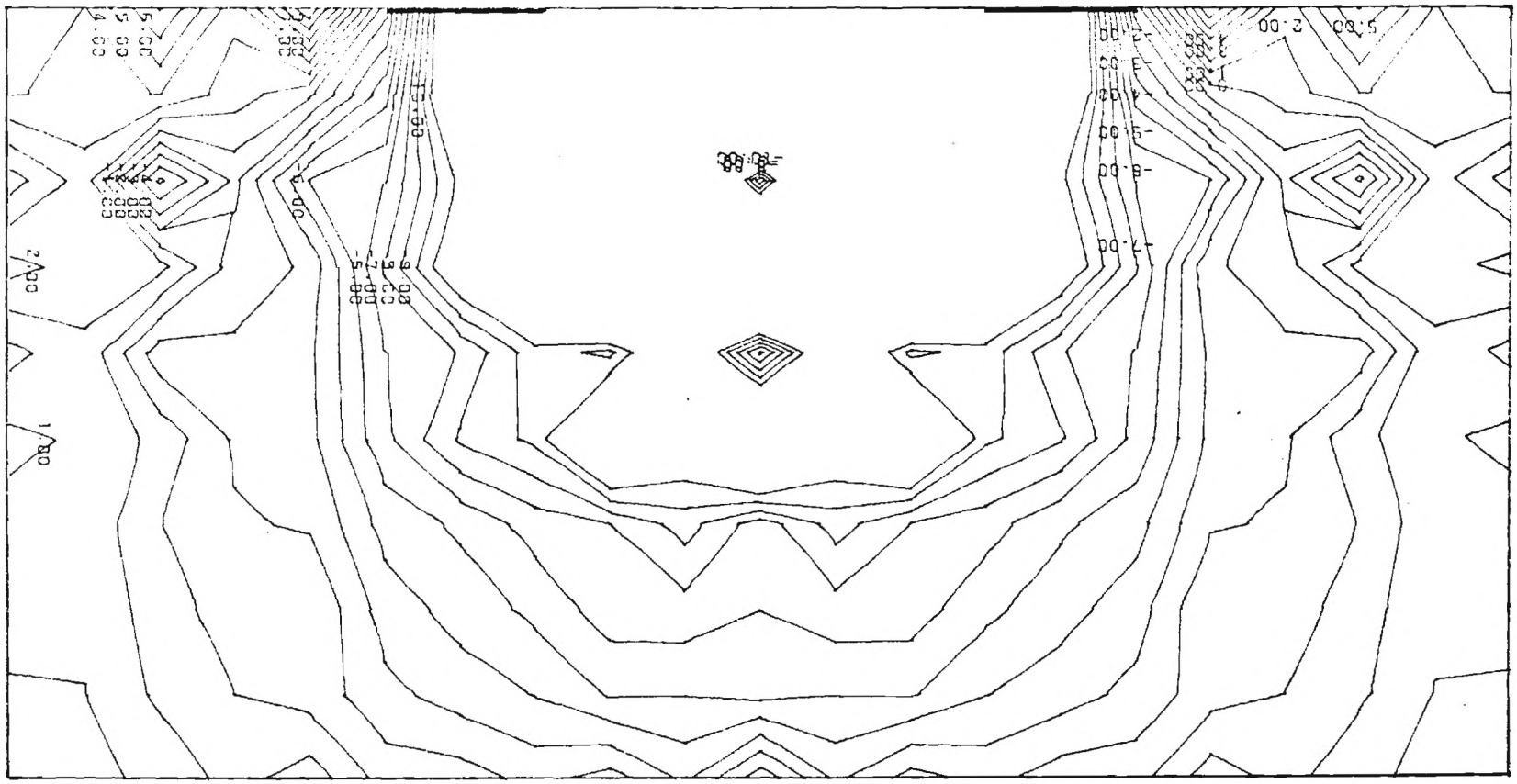

Figure 35. Normalized two-dimensional magnetic field distribution due to the current in the water over a 1500 ft. wide by 750 ft. deep rectangle. 150 ft. electrodes spaced 450 feet apart.

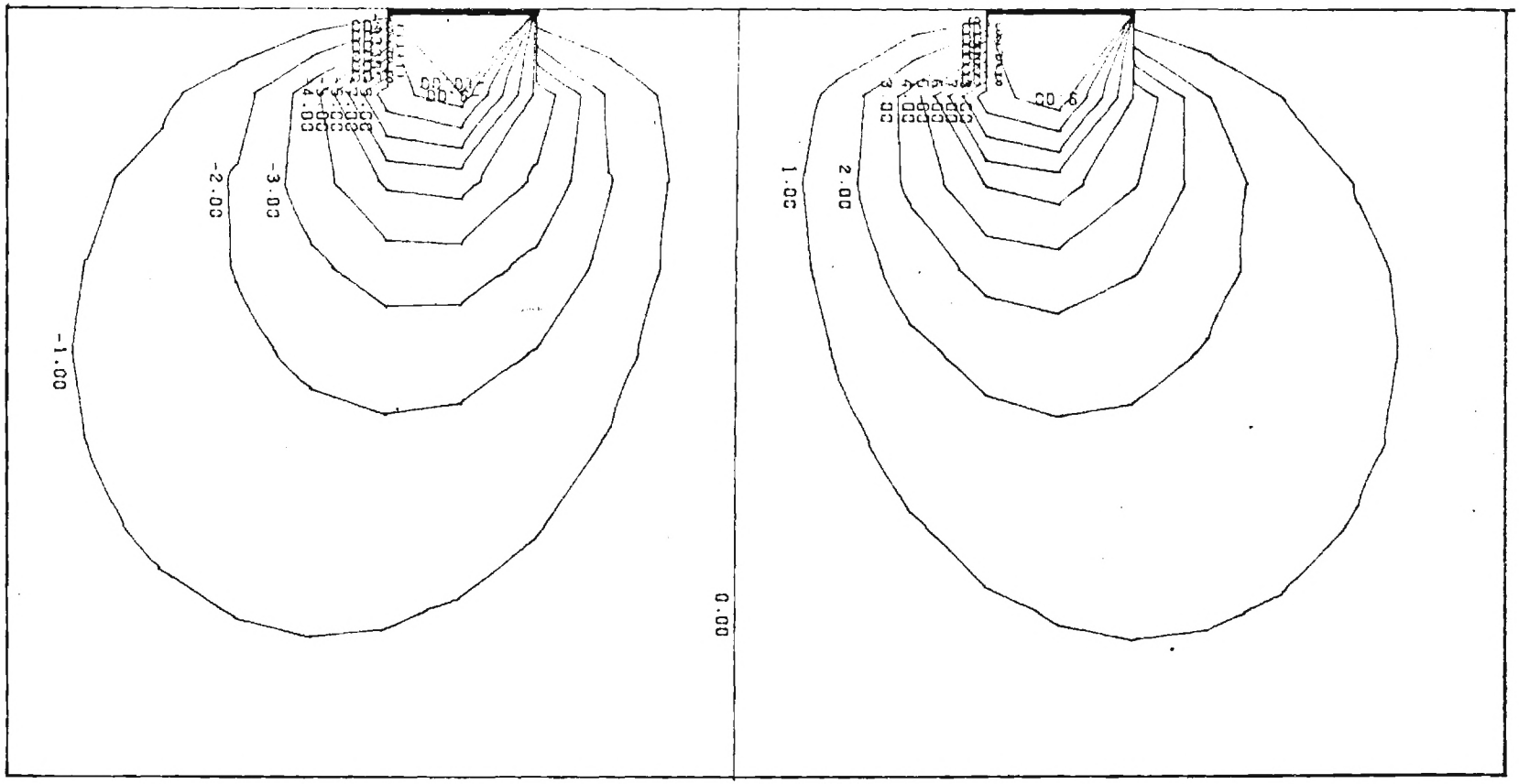

Figure 36. Normalized two-dimensional magnetic field distribution due to the current in the electrodes over a 1500 ft. wide by 750 ft. deep rectangle. 150 ft. electrodes spaced 450 feet apart.

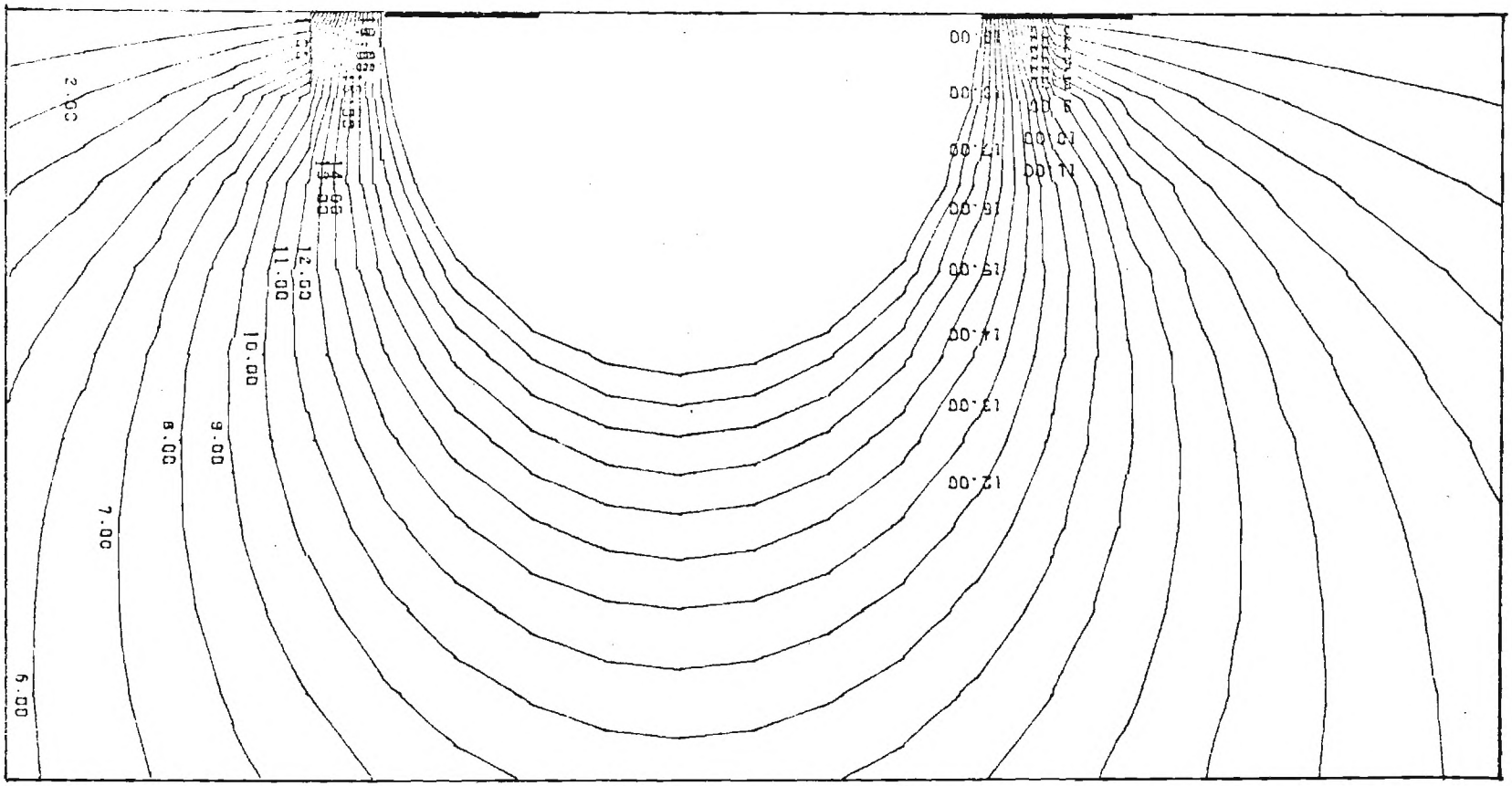

Figure 37. Normalized two-dimensional magnetic field distribution due to the current in the S-cable over a 1500 ft. wide by 750 ft. deep rectangle. 150 ft. electrodes spaced 450 ft. apart.

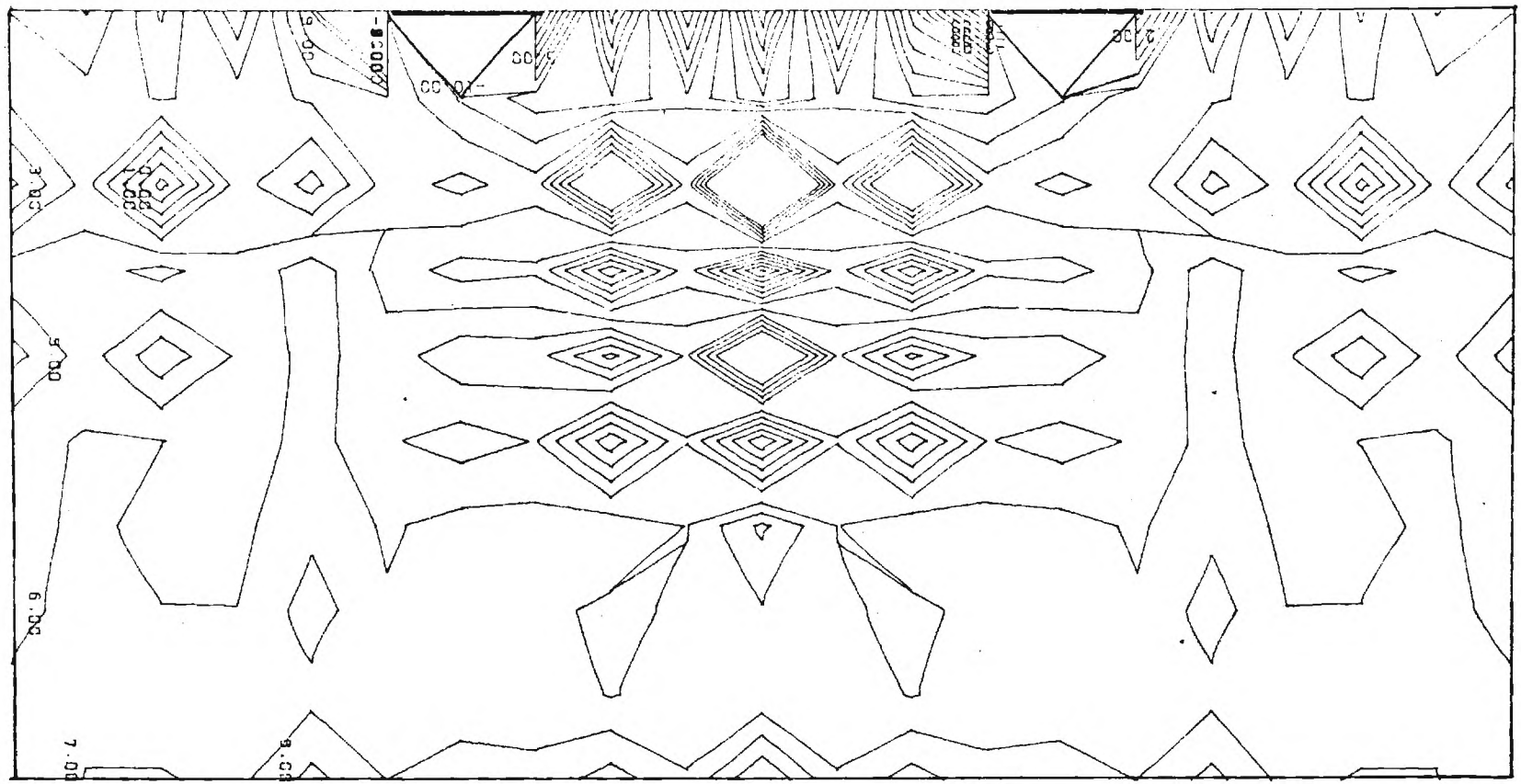

Figure 38. Total normalized two-dimensional magnetic field distribution due to the three components of Figures 12, 13, and 14.

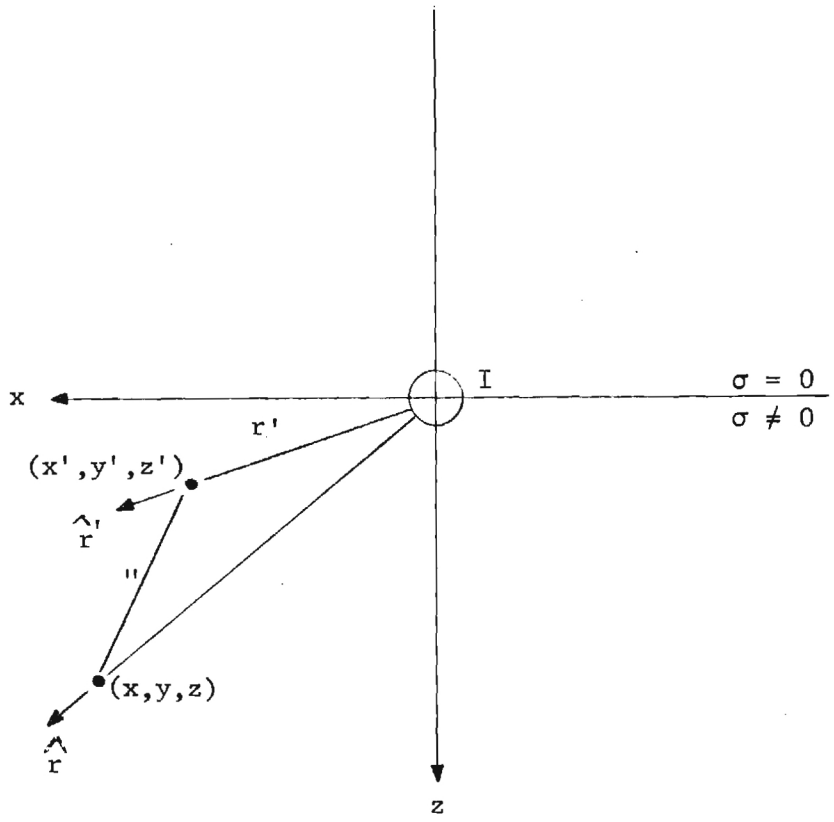

Figure 39. Illustration of the three-dimensional point source geometry.

magnetic vector potential at the point (x,y,z) associated with this current flow is given by [9]

$$\vec{A}(x,y,z) = \frac{\mu I}{8\pi^2} \int_V \frac{\hat{r}'}{r'^2} \frac{1}{r''} dv' \tag{38}$$

where r" is the distance between the points (x,y,z) and (x',y',z'), and V is the volume of the conducting medium. The magnetic field at (x,y,z) is computed from the familiar relation $\vec{B} = \nabla \times \vec{A}$, where the curl operation differentiates with respect to the (x,y,z) coordinates. After a lengthy manipulation, it follows that this is given by

$$\vec{B}(x,y,z) = \frac{\mu I}{16\pi^2} \int_V \frac{1}{r'^3} \frac{1}{r''^3} [\hat{x}(y'z-z'y)$$

$$+ \hat{y}(z'x-x'z) + \hat{z}(x'y-y'x)]dv' \tag{39}$$

The integration in (39) is more conveniently performed after conversion to spherical coordinates with the transformations

$$\begin{aligned} x' &= r' \sin\theta' \cos\phi' \\ y' &= r' \sin\theta' \sin\phi' \\ z' &= r' \cos\theta' \\ dv' &= r'^2 \sin\theta' \, dr' \, d\theta' \, d\phi' \end{aligned} \tag{40}$$

In this case, (39) is transformed into

$$\vec{B}(x,y,z) = \frac{\mu I}{16\pi^2}\int_o^{2\pi}\int_o^{\pi/2}\int_o^{\infty}\frac{1}{r''^3}\,[\hat{x}(z\sin\theta'\sin\phi'-y\cos\theta')$$

$$+\hat{y}(x\cos\theta'-z\sin\theta'\cos\phi')+\hat{z}(y\sin\theta'\cos\phi'-x\sin\theta'\sin\phi')]$$

$$\sin\theta'\,dr'\,d\theta'\,d\phi' \qquad (41)$$

where r" is given by

$$r'' = [r'^2 - 2r'(x\sin\theta'\cos\phi' + y\sin\theta'\sin\phi'$$

$$+ z\cos\theta') + r^2]^{\frac{1}{2}}$$

By symmetry, the field must be symmetrical in ϕ. Thus we may set y=0 to solve for $\vec{B}$ in the x-z plane. When this is done and when the point (x,o,z) is transformed into the spherical coordinates (r,θ,o) with the aid of (40), $\vec{B}$ is given by

$$\vec{B}(r,\theta,o) = \frac{\mu I}{16\pi^2 r}\int_o^{2\pi}\int_o^{\pi/2}\,[\hat{x}\sin\theta'\sin\phi'\cos\theta$$

$$+ \hat{y}(\cos\theta'\sin\theta - \sin\theta'\cos\phi'\cos\theta)$$

$$- \hat{z}\,\sin\theta\sin\theta'\sin\phi']$$

$$\frac{\sin\theta'\,d\theta'\,d\phi'}{1 - \cos\theta\,\cos\theta' - \sin\theta\,\sin\theta'\,\cos\phi'} \qquad (43)$$

where the integration in r' has been performed.

When the integration in ϕ' in (43) is considered, it is obvious that the $\hat{x}$ and $\hat{z}$ components of $\vec{B}$ are zero. Thus the $\hat{y}$ component is the only

non-zero component. Since this component is perpendicular to the x-z plane, it follows then that $\vec{B}$ must be in the $\hat{\phi}$ direction. After a lengthy manipulation, it can be shown that this is

$$B(r,\theta,\phi) = \hat{\phi}\,\frac{\mu I}{8\pi r}\,\frac{1-\cos\theta}{\sin\theta}\,, \qquad 0\leq\theta\leq\pi/2$$

$$= \hat{\phi}\,\frac{\mu I}{8\pi r}\,\frac{1+\cos\theta}{\sin\theta}\,, \qquad \pi/2\leq\theta\leq\pi \tag{44}$$

This is the desired result.

CHAPTER VI

CONCLUSIONS AND RECOMMENDATIONS

A. Conclusions

Anode

1. Platinized niobium is an efficient anode in sea water; it can operate at high current density (0.5A/cm^2, 3.2 A/in^2) and low overvoltage (3.5 to 4.5 volts) with long life expectancy (1,000 hours or more). The low overvoltage reduces demands on the power supply, and the high current density allows considerable flexibility in design.

2. A preliminary design analysis has shown that a workable noble metal minesweeping electrode can be built by adapting the S-cable and using commercially available platinized niobium materials. In the design considered at this time, platinized niobrium strips of 0.5"x0.0625" cross section would be wrapped around an S-cable carrier or similar configuration at frequent intervals to the conductors of the cable. Sealing of the joints would be accomplished by using heat-shrinkable polyethylene tubing and adhesives. Thermodynamic and mechanical analyses have shown that heat distribution and stiffness would be only slightly affected by the niobium strips.

3. A preliminary cost analysis has shown that one noble metal electrode designed for 10,000 A current capacity and life expectancy of at least 1,000 hours can be built for the cost of the S-cable plus $10,000. The cost would be lower in larger quantities.

4. Great care must be exercised to minimize the effects of contact resistance when making conventional electrical measurements to determine the resistivity of conductive polymers.

5. The large overpotentials associated with conducting polymer electrodes in contact with salt water are due to contact resistance on the inner surface of the jacket and high activation overpotential on the outer surface in contact with the salt water.

6. Samples of carbon-impregnated polyethylene cable jacket tested to date have shown high overvoltage and deterioration at the anodic current density considered in the design of a high current minesweeping electrode (70 mA/cm^2, 0.45 A/in^2). It appears that this is a result of oxidation of the carbon because of the high potentials necessary to achieve the desired current.

Cathode

7. Carbon-impregnated polyethylene cable jacket has indicated promise as a cathode in flowing sea water in short-term tests. Further tests are needed to determine the life expectancy of this type of cathode.

8. Platinized niobium is an efficient cathode, allowing operation at high current density and low overvoltage. However, there is no industrial experience with commercial platinized products working in the cathodic regime, and the commonly used substrate materials (titanium and niobium) are susceptible to hydrogen embrittlement; peeling of the platinized layer can also be a problem. Further tests are needed to evaluate the possibility of successful use of platinized materials as cathodes for minesweeping operations. Substrates other than niobium and titanium may offer better performance in the cathodic regime.

9. Our previous studies have indicated an approximate 150 to 200 hours of life for aluminum cathode in the high current system. This has been verified

by calculations, but needs to be established experimentally. If a somewhat better performance, than calculated is experienced, plus the existance of available materials, it is an economic possibility that at least for sea tests and possibly even extended sea trials aluminum cathode could be used.

10. Preliminary results indicate that the computer program developed on this program for the electromagnetostatic analysis of magnetic minesweeping electrode longitudinal and radial currents is accurate. The computer program also calculates electrode and sea path resistances and heat dissipation along the electrodes. This program will play a major role in simulating electrode performance under a variety of electrode configurations and environmental conditions.

11. The two-dimensional magnetic field calculations show that the predominant magnetic field component produced by the electrode/S-cable assembly is due to the return current in the S-cable. A solution for the three-dimensional magnetic field has been obtained from which all components of the true field can be determined by approximating the electrodes by a line a point source current emitters.

B. Recommendations

1. It is recommended that a cable section with platinized Nb strips for test of the electrical and mechanical characteristics be prepared and tested. In this particular phase it is possible to use a section of the proposed "S" cable as a carrier for the system and tests will be made to verify the electrical properties calculated by the EE group.

2. It is recommended that other potential polymer-graphite materials suggested by manufacturers be tested. The results of these tests will indicate if any one or more of these combinations will be better mechanically and electrically than the original carbon loaded material tested.

3. It is recommended that new design concepts be studied and tested if manufacturing techniques are possible. This list of potential electrode jacket materials combines the advantages of a flexible waterproof jacket and the nobility of platinum or a similar noble material.

4. It is recommended that other factors including hydrogen overvoltage, exchange current, maintaining electrochemical reaction on the surface, etc., to provide the best electrical properties available for a graphite-polymer system be evaluated.

5. It is recommended that the cathode characteristics of Pt-Nb and polymer-carbon electrodes be determined and tests on basic cathodic properties be completed and design recommendations of a cathode material be made.

6. It is recommended that final evaluation of aluminum as a cathodic material be made and its possibilities as to cost and life efficiency in the cathodic mode be determined.

7. It is recommended upon the completion of the above and with information from Aerojet General regarding the S-cable, a choice of anode and cathode

be made and anode cathode electrical design established. With this data and design information, potential manufacturers are to be consulted on manufacturing interests concerning engineering and necessary alterations to make production feasible.

8. It is recommended that the electrical-magnetic characteristics of the final anode-cathode design be evaluated under various operational environments. Variables should include sea water conductivity, depth, sea water temperature, etc. In addition, thermal analysis and mechanical analysis of the designs should be evaluated in laboratory and sea test conditions.

APPENDIX I

CALCULATION OF TEMPERATURE DISTRIBUTION IN PLATINIZED Nb ELECTRODES

The three-dimensional Poisson equation for a r, Θ, z coordinate system is:

$$\frac{\partial^2 T}{\partial r^2} + \frac{1}{r}\frac{\partial T}{\partial r} + \frac{1}{r^2}\frac{\partial^2 T}{\partial \Theta^2} + \frac{\partial^2 T}{\partial z^2} + \frac{q'''}{k} = 0$$

To eliminate Θ dependence of temperature T, symmetric geometry is assumed in which the strip is replaced by a Nb tube of the same thickness:

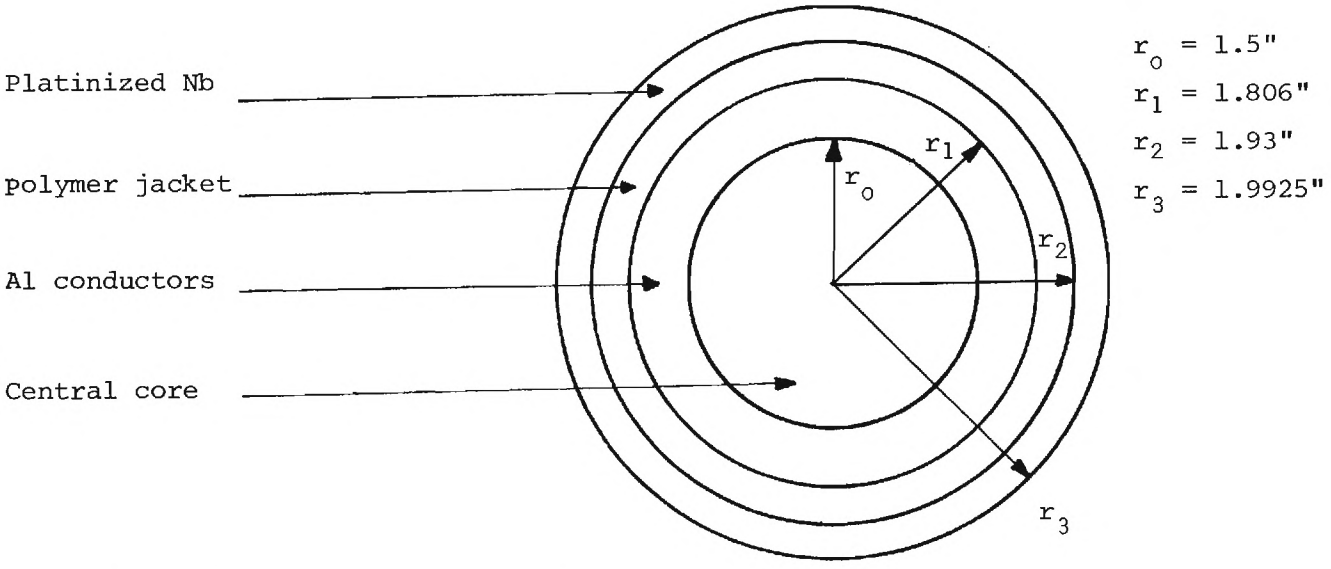

The dimensions given above are accurate, but the drawing has not been done to scale in order to enhance clarity.

The work of the EE group has shown that the current is dispersed into the sea in a non-uniform manner along the length of the anode. The maximum value is 131.5% of the mean and occurs in the first segment. Thus, for a 10^4

amp, ten-segment system, the maximum currents in the Al and Nb conductors are:

$$I_{Al} = 8{,}685 \text{ amp} \qquad I_{Nb} = 1{,}315 \text{ amp} \tag{1}$$

To eliminate z dependence of T, the assumption is made that these maximum currents, which produce maximum heating, are present throughout the electrode, and the Poisson equation thus becomes:

$$\frac{d^2T}{dr^2} + \frac{1}{r}\frac{dT}{dr} + \frac{q'''}{k} = 0$$

A solution to this equation which is valid for all four regions of the cable (central core, Al conductors, polymer jacket, and platinized Nb outer layer) when the appropriate values of q''', k, C_1, and C_2 are used is:

$$T = \frac{-q'''}{4K} \cdot r^2 + C_1 \ln r + C_2 \tag{2}$$

(where C_1 and C_2 are constants).

The thermal conductivities, k, of the various materials are:

$$k_{Al} = \frac{2.36 \text{ watts}}{\text{cm} - {}^\circ\text{C}} \qquad k_{Nb} = \frac{0.523 \text{ watts}}{\text{cm} - {}^\circ\text{C}} \qquad k_j = \frac{3.33 \times 10^{-3} \text{ watts}}{\text{cm} - {}^\circ\text{C}}$$

We do not know the actual value of thermal conductivity for the S-cable jacket; to estimate it we use the value k_j given above which is the average value for the heat-set, cross-linked, carbon-impregnated polyethylene jacket material.

The rates of heat production per unit volume, q''', are:

$$q'''_{Al} = \frac{I^2_{Al} R_{Al}}{V_{Al}} \qquad q'''_{Nb} = \frac{I^2_{Nb} R_{Nb}}{V_{Nb}} \qquad q'''_{core} = q'''_{j} = 0 \tag{3}$$

where R and V respectively denote electrical resistance and volume of conducting material. These quantities are given by:

$$R = \frac{\rho L}{A} \qquad\qquad V = L \cdot A \tag{4}$$

where L = conductor length, A = cross-sectional area of conductor, and ρ = resistivity. The resistivities of the two materials (nelgecting the small temperature coefficients) are:

$$\rho_{Al} = 2.6548 \times 10^{-6} \text{ ohm - cm} \qquad \rho_{Nb} = 12.5 \times 10^{-6} \text{ ohm cm}$$

Actual dimensions are used to calculate q'''_{Al}. The assumption is made that the Nb tube produces the same amount of heat per unit volume as does the strip, so the strip cross-sectional dimensions (0.5"x0.0625") are used in (3). Substitution of (1) and (4) into (3) shows that:

$$q'''_{Al} = 0.4764 \frac{\text{watts}}{\text{cm}^3} \qquad q'''_{Nb} = 531.77 \frac{\text{watts}}{\text{cm}^3}$$

The remaining information necessary to determine the temperature distribution numerically consists of six boundary conditions, three of which involve continuity of temperature:

$$T^{Al} = T^{j} \quad \text{at} \quad r = r_1 \tag{5}$$

$$T^{j} = T^{Nb} \quad \text{at} \quad r = r_2 \tag{6}$$

$$T^{Nb} = T^{s} \quad \text{at} \quad r = r_3 \tag{7}$$

where subscripts Al, j, Nb, and s, respectively, denote the Al conductor region, the polymer jacket, the Nb outer layer, and the sea. Boundary condition (7) is applicable since previous reports have shown that the convective heat flow at the external surface is such that there is a negligible temperature difference between the electrode and the sea.

The other three boundary conditions involve continuity of heat flux across the boundaries between the materials in the electrode. The heat flux, q'', is given by:

$$q'' = -k \frac{dT}{dr}$$

The three additional boundary conditions are:

$$\frac{dT^{Al}}{dr} = 0 \quad \text{at } r = r_o \tag{8}$$

$$k_{Al} \frac{dT^{Al}}{dr} = k_j \frac{dT^{j}}{dr} \quad \text{at } r = r_1 \tag{9}$$

$$k_j \frac{dT^{j}}{dr} = k_{Nb} \frac{dT^{Nb}}{dr} \quad \text{at } r = r_2 \tag{10}$$

Boundary condition (8) indicates that no heat flux exists across the boundary between the central core and the Al conductor. This is because the core temperature is a constant (i.e., dT/dr = 0 in this region). This can easily be seen from the solution (2) since $q'''_{core} = 0$ and the temperature within the core must be finite (i.e., $C_1^{core} = 0$). Thus, from boundary

condition (5) the temperature throughout the central core is equal to the temperature at the inside radius of the Al conductor.

The temperature distribution is determined by substituting the solution (2) into boundary conditions (5)-(10) and solving the resulting six equations for the six unknowns C_1^{Al}, C_2^{Al}, C_1^{j}, C_2^{j}, C_1^{Nb}, and C_2^{Nb}.

The determination of the temperature distribution when the Nb strip is not present proceeds in similar fashion to that outlined above for the solution of the problem where the strip is present. The only differences are that a different value of q'''_{Al} is used, $q'''_{Al} = 0.6315$ watts/cm^3 (since here the Al carries all the current), boundary conditions (7) and (10) are omitted, and boundary condition (6) becomes $T^j = T^s$ at $r = r_2$.

The results of these calculations are displayed graphically in the text of this report.

APPENDIX II

SECOND MOMENTS OF AREA REQUIRED FOR BENDING STIFFNESS CALCULATIONS

The cross-sectional geometry for an electrode consisting of cable "sc" with radius r, plus a platinized Nb strip, "str," with width b and thickness h is shown below. The size of the strip has been greatly exaggerated for clarity of presentation:

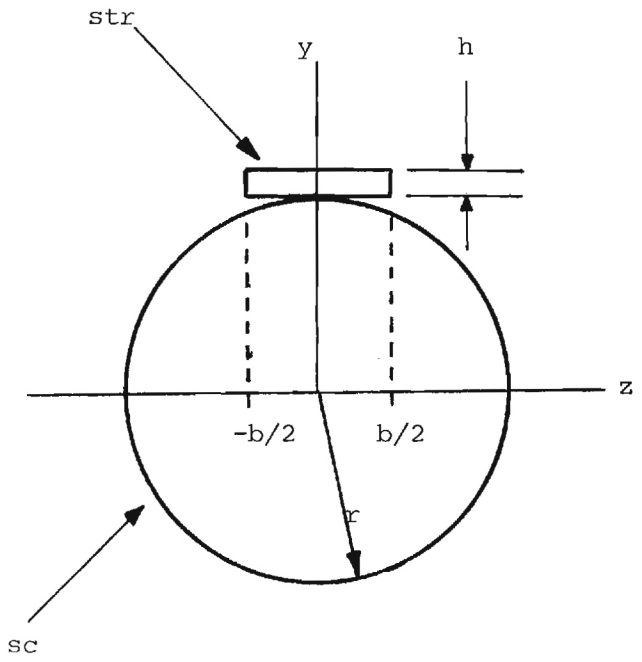

The second moments of area of the cross-sections of the cable and strip about the z-axis are:

$$I_{sc} = \int_{A_{sc}} y^2 dA$$

$$I_{str} = \int_{A_{str}} y^2 dA$$

where A_{sc} and A_{str} are the regions of area occupied by the S cable and Nb strip respectively.

Thus:

$$I_{sc} = \frac{\pi}{4} \cdot r^4$$

$$I_{str} = \int_{-b/2}^{+b/2} \int_{r}^{r+h} y^2 dy dz = br^2h \left(1 + \frac{h}{r} + \frac{1}{3}\frac{h^2}{r^2}\right).$$

The numerical values for b, h, and r in inches are:

$b = 0.5$

$r = 1.93$

$h = 0.0625$

So that the ratio of the second moments is:

$$I_{str}/I_{sc} = 1.10 \times 10^{-2}$$